POLITECNICO DI TORINO

Collegio di Ingegneria Energetica

Corso di Laurea Magistrale
in Ingegneria Energetica e Nucleare

Tesi di Laurea Magistral

Solar chemical looping reforming of methane and H₂O/CO₂ splitting coupled with solid oxide fuel cell

Relatori

firma del relatore (dei relatori)

prof. Massimo Santarelli

Dott. Salvatore Cannone

Candidato

firma del candidato

Muhammad Ishaq

March 2022

Acknowledgment

Abstract

A novel configuration of a polygeneration plant is proposed in this study. Solar chemical looping reforming of methane and simultaneous H_2O/CO_2 splitting cycle is coupled with solid oxide fuel cell to produce syngas, electrical and thermal power. The basis of the study includes the introduction of 1 kmol/hr of CH_4 with the assumption that the suggested plant must operate for 24 hours a day. Two cases, morning and night operations of the proposed system are reported. The dry reforming of fossil fuel (CH_4) with non-stoichiometric ceria is activated in the reduction reactor of chemical looping, while thermochemical dissociation of SOFC off-gas is activated in the oxidation reactor of chemical looping.

The CO_2 emissions carried by the SOFC anode exhaust are also captured using oxy-fuel combustion after burner. The Aspen Plus V11 software is employed for the designed system simulation. Numerous sensitivity studies are undertaken to investigate each subsystem of the proposed CL-SOFC configuration. The performance of chemical looping is assessed by calculating three efficiencies. The overall chemical looping system efficiency (E_1), waste gas efficiency (E_2), and solar to fuel efficiency (E_3) are found to be around 61.9%, 11.4%, and 32.9% respectively. Pinch analysis is conducted to meet thermodynamically feasible energy targets and a heat exchanger network design is proposed for the morning and night operation.

The overall proposed system can generate 102.97 kW of electrical power with an efficiency of 46.6% with carbon capture. The further evaluation demonstrates that the morning plant can generate 52.37 kW of electrical output with an efficiency of 71% with carbon capture and syngas storage while the night operation of the proposed system, can generate 50.6 kW electrical power with an efficiency of 54.7% with carbon capture. During the morning operation, 100% carbon capture is achieved, followed by 49% CO_2 utilization in the CL and 51% CO_2 storage. During the night operation, 100% carbon capture is achieved, followed by 0% CO_2 utilization in the CL and 100% CO_2 storage. As compared to the benchmark SOFC, 61% CO_2 is avoided during the morning and 60% CO_2 is avoided during the night operation of the plant. SPECCA index is reported as 1.14GJ/ton CO_2.

Contents

List of figures

Nomenclature	
C_p	Specific heat (kJ/K)
F	Faraday's constant
LHV	lower heating value (kJ/kg)
$\dot{m}$	mass flow rate (kg/s)
$\dot{En}$	energy rate (kW)
$\dot{N}$	number of moles
P	power (kW)
$\dot{Q}$	heat rate (kW)
T	temperature (°C)
Greek letters	
η	energy efficiency
ρ	density (kg/m^3)
ΔT	Temperature difference (°C)
Subscripts	
0	reference conditions
B	block
Comp	compressor
eq	equivalent
ref	reference
in	inlet
out	outlet
en	energy
fg	flu gas
min	minimum

Acronyms	
AB	Afterburner
AN	Anode
BTU	British thermal unit
CGT	Compressed gas technology
CL	Chemical looping
CCR	Carbon capture ratio
CHP	Combined heat and power plant
C	Component
CATH	Cathode
CYC	Cyclone separator
CL-red	Chemical looping reduction
CL-oxi	Chemical looping oxidation
COMP	Compressor
I.C	Inter cooler
HEXN	Heat exchanger network
SOFC	Solid oxide fuel cell
SCR	Storage carbon ratio
SP	State point
KPI	Key performance indicators
SC	steam to carbon ratio
SIMP-HT	Simple heat transfer
ASU	Air separation unit
HEX	Heat Exchanger
SPECCA	Specific primary energy consumption for carbon capture and avoided
PENG-ROB	Peng Robinson
UCR	Utilized carbon ratio
PDC	Positive displacement compressors

1 Introduction

The year 2020 started with turmoil in the form of COVID-19 and bushfires in Australia. Among these, covid-19 incarnated millions of deaths across the globe. Despite health crises, pandemics not only suppressed the economic activities from 3.4 to 7.6% but also forced humans to change their living style [1]. After increasing gradually for years, worldwide CO2 emissions dropped by 6.4% in 2020 because of limited economic actions. A fall of 6.4% CO_2 is equivalent to almost 2.3 billion tonnes of carbon dioxide[2]. On 12 December 2015, nations that are a member of UNFCCC agreed to mitigate carbon emissions. This agreement is called the Paris agreement. It claims to limit global carbon emissions to well below 2 °C and pursue efforts to restrict it to 1.5 °C[3]. Climate scientists took this opportunity as a beacon of hope in terms of achieving Paris Agreement goals.
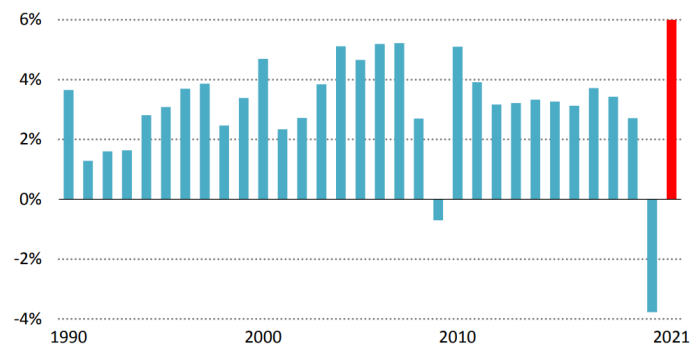
Figure 1.1: Annual rate of change in World GDP 1990-2021[4]
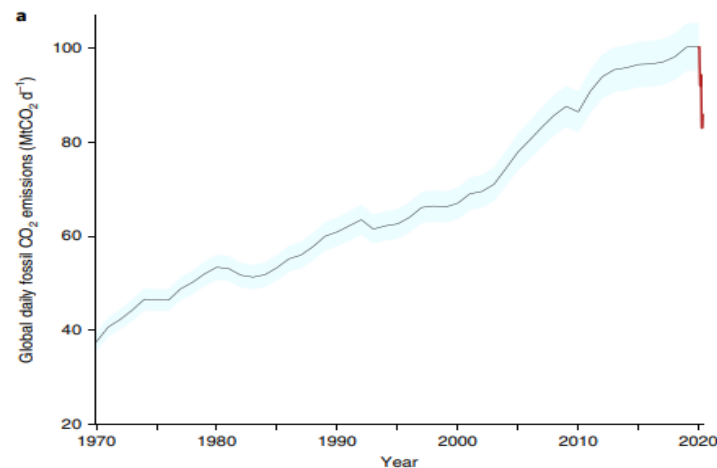
Figure 1.2:Globally daily fossil fuel CO_2 emission [20]

While as the economic activities gained recovery during the start of 2021, the global economy started growing by 6%, more than declining in 2020 has further made carbon emissions to enhance predominantly [4]. Because of anthropogenic carbon emissions into the atmosphere, hydrogen and fuel cells have become a more attractive option and gained more attention from researchers. Solid oxide fuel cell operates efficiently if fed with pure hydrogen.

1.1   Hydrogen as a future fuel

Hydrogen has been considered a source of energy for future generations. It is an energy vector that plays a vital role in chemical industries including pharmaceutical, fertilizers, steel and cement production, textiles, methanol production, and oil refineries. Hydrogen is not only important for the chemical industries but is widely used in Aviation, logistics, shipping, heating homes, public and personal transportation. Liquid Hydrogen has been used as a fuel in the Saturn rockets used by NASA [6]. It can be stored, transported, and can be a sustainable source of energy in near future. Hydrogen storage and transportation methods have been briefly described by Leighty. At Present, the worldwide demand for Hydrogen is 50 million tons per year [7]. and this demand is growing predominantly. Future hydrogen demand is expected to increase to 85 million tons in 2030 [8]. To meet this high demand, currently large production capacity plants including plants of up to 480-ton H_2/day been developed [9].

1.2   Types of hydrogen

Hydrogen is produced by a different process, but generally, these processes are classified based on hydrogen production source and extent of carbon emission. Three major types of hydrogen are named green, blue, and gray hydrogen.

- Grey hydrogen is mainly produced by using fossil fuels. For example, natural gas is a major feedstock for gray hydrogen production. The process is called methane steam reforming, and this is rich in terms of carbon emission. It is responsible for 12 kg CO_2/kg H_2.
- Blue hydrogen is also produced from fossil fuels in the same way as grey hydrogen, but the production process is integrated with carbon capture and storage [9]. Carbon intensity referred to as blue hydrogen is 4 kg CO_2/kg H_2.
- Green hydrogen is produced by using renewable energy sources for example solar and wind. The production process of green hydrogen does not generate carbon emissions. The carbon emission extent related to green hydrogen is 0.6 kg CO_2/kg H_2[10].
- There is also a fourth type of hydrogen that is mainly produced coal gasification process and is called brown or black hydrogen. But it is not of high importance.
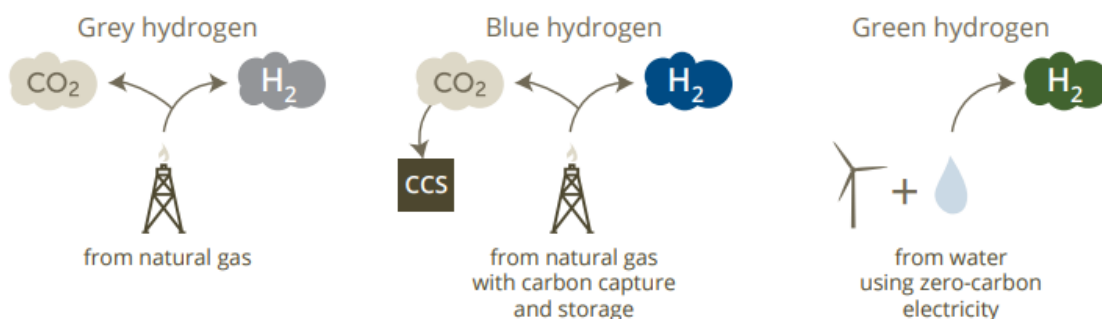
Figure 1.3: Three major types of hydrogen

1.3　Hydrogen production from natural gas

Today most of the Hydrogen production processes are based on fossil fuels due to the reason that fossil fuels are an inexpensive and rich source of hydrogen. Among the fossil fuels, natural gas is generally a preferred feedstock for hydrogen production. Primarily, to synthesize hydrogen, natural gas undergoes a state-of-the-art process that is called steam methane reforming (SMR). A schematic illustration of the SMR process is exhibited in figure 1.4. In this process methane, first of all, undergo a pretreatment section to get removed sulfur contents after that it reacts with the steam (eq 1.1) at 3-25 bar pressure and 700-800 °C temperature in the presence of a suitable catalyst and produces a mixture of hydrogen, carbon monoxide and unreacted methane [11]. Hydrogen quantity is enlarged in a water gas shift reactor (WGS) where carbon monoxide reacts with water and a rich hydrogen stream is achieved along with carbon dioxide [12]. According to Le Chatelier's principle, lower pressure and increased water quantity move reaction equilibrium towards the right to further produce more hydrogen that may lead the process towards high efficiency[13].

$$CH_{4(g)} + H_2O_{(g)} \rightarrow \quad 3H_{2(g)} + CO \qquad \Delta H_R = 206 \text{ kJ/mol} \qquad (1.1)$$

$$CO_{(g)} + H_2O_{(g)} \rightarrow \quad H_{2(g)} + CO_2 \qquad \Delta H_R = -41.1 \text{ kJ/mol} \qquad (1.2)$$
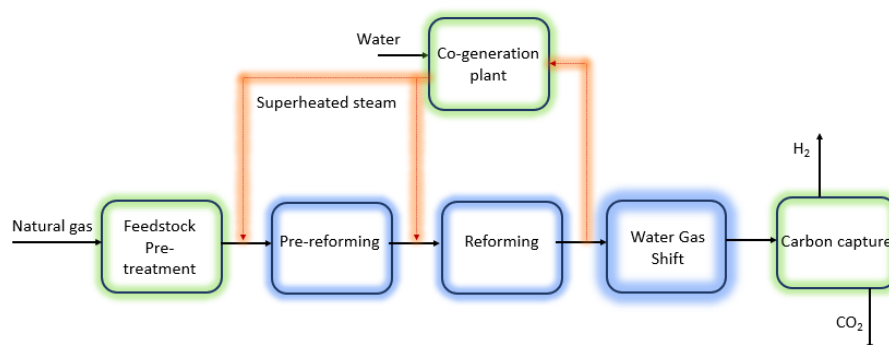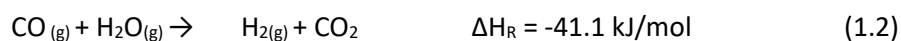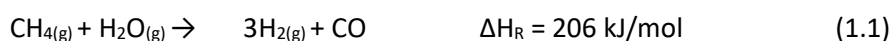
Figure 1.4: Hydrogen production from steam methane reforming.

Steam reforming of natural gas is extensively used to produce hydrogen. Annually more than 32 million tons of hydrogen and 80 million kg per day of hydrogen are produced by using steam methane reforming (SMR) [8].

1.3.1 Advantages of steam methane reforming
Steam methane reforming carries a plethora of advantages.

- ➢ The first and foremost advantage of this process is its high efficiency in the range of 65% to 75%.
- ➢ Steam methane reforming is well established and mature technology.
- ➢ Another key benefit of this process is its high hydrogen yield with 2.4 to 2.7 mol of hydrogen production with every mole of methane.
- ➢ In addition to this SMR is a very cheap source of hydrogen production as the cost of hydrogen production is highly dependent on the cost [12] of natural gas and recently it is considered a very low-priced hydrogen production process.
- ➢ Another key benefit of SMR is its high capacity to achieve excellent energy efficiencies as compared to other hydrogen production technologies for example partial oxidation of fossil fuel feedstock.
- ➢ It can produce hydrogen of high purity around 99.9%.

1.3.2 Disadvantages of steam methane reforming
Although, there are some problems and disadvantages associated with the steam methane reforming process.

- ➢ As this process is highly dependent on the usage of fossil fuels in the form of natural gas, it is responsible for the deep level of greenhouse gas seepage.
- ➢ Because of the endothermic nature of the SMR reaction (eq 1.1), it requires a huge quantity of energy to perform this reaction. This heat is provided with an external furnace by the combustion of extra methane.
- ➢ The operating conditions of the SMR process are very extreme for example achieving 800 ^{0}C presents severe operating conditions.
- ➢ Unfortunately, the process of SMR is still unable to mitigate the release of huge carbon emissions into the atmosphere.
- ➢ Notwithstanding these, SMR is embodied with complex mechanical design, coke deposition, catalyst, and heat and mass transfer.

Despite all the above drawbacks of steam methane reforming, the major problem is a huge quantity of carbon emission during processing. For example, gas discharged during processing extends a considerable amount of 25 tons of CO_2 for 1 MMscf hydrogen production. According to Praxair, the largest hydrogen-producing company, 9.3 kg CO2 is produced for one kg of hydrogen production [15]. This means that SMR offers high hydrogen production efficiency and low carbon capture efficiency.

1.4 Chemical looping combustion
The CO_2 emission penalties incurred by steam methane reforming would therefore compensate for the advantages of hydrogen production. It has opened an opportunity window for researchers to

explore alternative processes for hydrogen production and carbon capture. Thus, to alleviate the catastrophe of carbon emission, other processes have been developed.

Among alternative options, chemical looping combustion (CLC) has been received significant attention. It was first proposed by Ishida [16] and used for hydrogen production and carbon capture. CLC is comprised of two reactors, one acts as an oxidation reactor while the other behaves like a reduction reactor. It was first used by Moghtaderi [17] as an air separation methodology to produce a mixture of CO_2 and H_2O followed by water condensation and carbon capture.

Zerobin et all investigated pressurized chemical looping combustion and found net electrical and carbon capture efficiency of 44% and 90% respectively [18]. Advanced system combination has further made the opportunity to enhance system efficiency and to reduce the energy penalty for carbon capture.

1.5   Chemical looping reforming

After successfully achieving thermochemical splitting of water, many researchers have significantly considered the conversion of CO_2 into CO, as CO can be utilized as a promising chemical for industrial applications including the production of chemicals for example dimethyl ethers, aldehydes, phosgene, acetic acid, methanol, and many other liquid chemicals. One of the possible ways to convert CO_2 into CO is its direct dissociation but it takes place above 2500 °C so it is not a good option for large-scale applications. Another novel technology of CO_2 conversion is its thermochemical dissociation by a process called chemical looping.

Therefore, in recent years, CO_2 dissociation via chemical looping has been taken a specialized focus. If water is split thermochemically hydrogen is produced while if CO_2 is split thermochemically carbon mono oxide is the main product. This elaborates that if water and CO_2 are split at the same time, the product mixture is mainly comprised of syngas is again a potential product for many industrial applications and can be used as an initial fuel for solid oxide fuel cells. Unlike chemical looping combustion (CLC), chemical looping has been conceptualized as the simultaneous splitting of H_2O and CO_2. Like chemical looping combustion (CLC), the setup of chemical looping is consisting of reduction and oxidation reactors with the presence of suitable oxygen mover. These oxygen movers can keep oxygen with them and are called oxygen carriers.

Oxygen carriers play a vital role in the simultaneous splitting of H_2O and CO_2 into a mixture of H_2 and CO [19]. In the process of chemical looping, oxygen carriers must pass through a cycle comprising of two steps, first one is endothermic reduction while the second one is exothermic oxidation. Therefore, sometimes chemical looping is named as two-step cycles.

The first explanation of the chemical looping process has been described now, followed by more reasoning and comprehensive detail on the selection of oxygen carriers in the later stages of the thesis.

1.6   Carbon capture techniques

There are three major methods for CO2 capturing that pre-combustion, post-combustion, and oxyfuel combustion. Among these three processes, the first two are sorption-based techniques

while oxyfuel combustion is a non-sorption technique. Figure 1.5 presents a clear overview of the carbon capture techniques.

1.6.1 Oxyfuel-combustion CO_2 capture technique

In the oxy-fuel combustion technique, first oxygen is separated from the air so that we may have a stream of pure oxygen. In this way, a flue gas stream is obtained that is mainly comprised of H_2O and CO_2. Water is condensed and CO_2 is separated. It is a very mature technology. Currently, the production of pure oxygen from the air requires 200–250 kWh$_{el}$ /tO$_2$ [20].
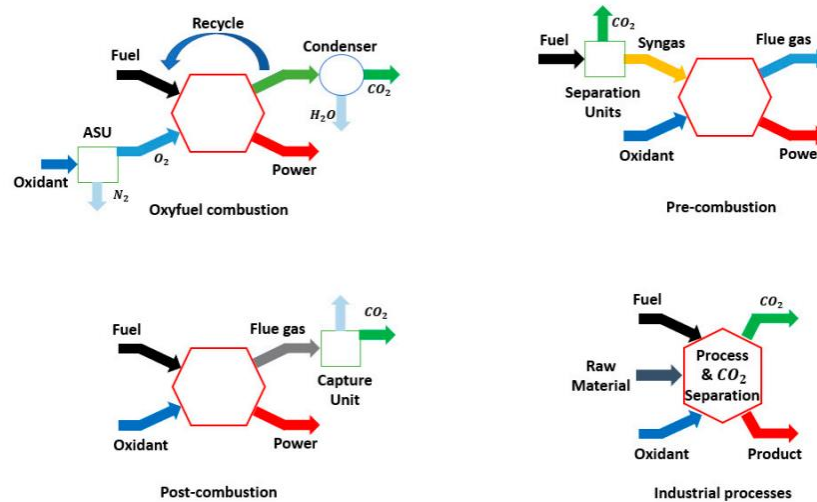
Figure 1.5: Schematic overview of carbon capture technologies including, oxy-fuel, pre-combustion, post-combustion, and a general CO_2 capture in the industry[20].

1.6.2 Post-combustion CO_2 capture technique: High temperature and low pressure.

In the post-combustion technique, we mostly have CO2 in the flu gas stream in the conventional power plants. We burn coal or natural gas with air and a carbon-rich flu gas stream is obtained. This flu gas stream is at the atmospheric pressure and the temperature range is around 1-15 °C. That means we have a hot carbon stream at low pressure and high temperature. The concentration of CO2 in the flu gas stream is very low around 4-14%. Therefore, thermodynamics conditions are no longer feasible for physical absorption. As physical absorption is driven by low temperature and high pressure that is contrary as compared to the situation of post-carbon combustion flu gas stream. Consequently, chemical absorption is favorable for these conditions.

1.6.3 Pre-combustion technique CO_2 capture technique: High pressure and low temperature.

In the pre-combustion CO2 capture technique, physical absorption is advantageous. For example, if in the case of IGCC (integrated gasification combined cycle), the gasifier operates at very high pressure around 30 bar, and CO2 concentration will be very high (around 30-50%) after water gas shift reaction. Due to high concentration, the partial pressure will be very high therefore, thermodynamically physical absorption will be suitable. One of the most important differences between post and pre-combustion is that in the pre-combustion, capture of CO_2 takes place when CO_2 is in the fuel gas mixture, but in the post-combustion, we apply the CO_2 capture technique on the fully oxidized stream.

1.7   Conversion of chemical energy into thermal energy

A plethora of technologies are available for carbon capture that is adopted in commercial power generation plants. Well-known technologies are pre-combustion, post-combustion, and oxyfuel combustion.

In general, oxyfuel combustion technology is considered a promising option when the aim is to burn unreacted hydrogen and carbon monoxide. In the oxy-fuel combustion cycle, fuel is reacted with pure oxygen and a product stream that is purely comprised of H_2O and CO_2 is achieved. The oxy-fuel combustion power plant is characterized by two key parts. First is the air separation unit (ASU) and the second is the combustion chamber. It is more effective in terms of carbon capture as compared to air combustion that diluted the mixture with impurities, especially nitrogen, which further increases the compression power and decreases the carbon capture efficiency. The majority of commercial ASU possess cryogenic air separation processing [21]. There is another pathway to separate air via an ion transport membrane. It is a technique that separates air into oxygen and nitrogen with the help of a ceramic membrane. For example, Park et al. considered ion transport membrane in their proposed plant [22]. The reaction involved in the oxyfuel combustion unit is given as Eq. (1.3) and (1.4).

$$H_2 + \frac{1}{2}O_2 \rightarrow H_2O \qquad\qquad (1.3)$$

$$CO + \frac{1}{2}O_2 \rightarrow CO_2 \qquad\qquad (1.4)$$
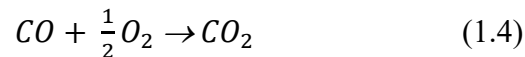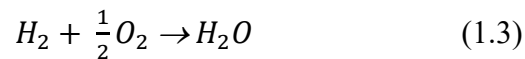
A lot of studies and approaches are considered by the researchers to capture carbon from the solid oxide fuel cell.

- ➤ Sanz et al performed a thermodynamic and economic study of two distinct oxyfuel cycles: the Graz cycle and semi-closed oxy-fuel combustion combined cycle (SCOC-CC). In that study, they found that the Graz cycle has high efficiency due to the large cooling utility. They also concluded that the Graz cycle exhibit less CO_2 capture cost as compared to the SCOC-CC cycle [4].
- ➤ Kuramochi et al. performed a techno-economic study of carbon capture from solid oxide fuel cells. The proposed SOFC plant was coupled with combed heat and power plant (CHP) and the CO_2 capture unit was linked with oxy-fuel and traditional air separation methodologies. In that study, they concluded that SOFC-CHP plants with carbon capture exhibit high costs when the CO_2 price is more than 37 \$/ton CO_2 [7].
- ➤ McLarty et al. proposed a poly-generation plant that is comprised of an air separation unit interconnected with the cathodic compartment of the solid oxide fuel cell. A water gas shift reactor is attached at the anodic exhaust of SOFC to convert unreacted species. In that study, they concluded that ASU is economically suitable for large power plants with a capacity greater than 2 MW [8].
- ➤ Franzoni et al attempted to decarbonize the SOFC-GT system by two different approaches. In the first approach, fuel is decarbonized before introducing the SOFC system and the second approach is focused on water condensation and CO_2 capture. They found that the overall efficiency of the system decreases due to fuel pretreatment, CO_2 capture, and compression [9].

1.8   Syngas storage system

Syngas storage is considered a potential option as it provides many economic benefits at the commercial level. The practical viability and economic attraction of syngas are influenced by the properties of both syngas and their production source. These properties are composition, percentage of hydrogen and carbon monoxide, temperature pressure, and energy density.

In the sense of current study, the syngas storage system allows the chemical looping to activate and operate during the daily operation when plenty of sunlight is available and this stored syngas can be used during night operation when no sunlight is available, so that electricity can be produced twenty-four seven.

- Stored syngas can be utilized to generate electricity when the electricity needs and prices are too high.
- Syngas storage improves resources and economic conceptual terms that are called reliability and availability.

Unfortunately, no literature is available that should encompass a comprehensive raw syngas storage system and most of the existing literature is scattered. However, a few studies are conducted and reported below.

- ➢ Apt et all. conducted a detailed analysis of storing syngas produced from coal gasification. In that report, they addressed all the technical problems associated with syngas storage systems by adopting an economic and engineering approach [2].
- ➢ Newcomer et all. calculated syngas storage systems in the USA and found that syngas storage options increase the net present value and return on investment. Furthermore, they also found that syngas storage decreases the carbon price by up to 25% [3].
- ➢ Newcomer et all studied three cases of syngas storage with 4, 8, and 12h of storage and evaluated the compressor size. They adopted a constant storage pressure of 63 bar [3]. As less literature is available on syngas storage so 63bar is considered as a basis for storing syngas for the present study.

Major technological problems with syngas storage are

- As syngas contains a particular percentage of hydrogen that makes most of the metals brittle and there are chances that hydrogen may diffuse through the walls of pipes.
- Syngas has low energy density.
- Syngas is characterized by low energy density in the range of 150-280 BTU/SCF. This means that larger volumes of vessels are required to store it. On the other hand, methane has a higher energy density, which means smaller volumes vessels are needed to store it.
- Compared to methane, the low energy density of syngas is also considered as a high quantity of syngas is needed to produce the same amount of energy.

There are different storage techniques for syngas gas storage, for instance, compressed gas technology, cryogenic liquid, and solids, such as liquid hydrides are the most common and developing technology nowadays. But in this study, compressed gas technology (CGT) is

conceptualized as a storage option. The main reasons for choosing compressed storage options are given as.

- CGT is a very attractive solution for syngas storage as it is a mature technology, and not very expensive for large-scale storage capacities.
- CGT does not require a very complex equipment range; it is very easy to apply because it just needed a compressor and a storage vessel.
- It is a stationary storage solution.

For storing syngas different types of storage vessels can be used including high-pressure cylindrical bullets, low-pressure gasometers, salt caverns, and excavated rock caverns.

The major drawback of the CGT storage facility is given as.

- It is characterized as low storage density that is influenced by storage operating pressure.
- Low storage density can be enhanced with high pressure but achieving high pressure consumes more power.
- Compressing the syngas requires a lot of compression stages [4].

Compressors are normally used for achieving the storage pressure of syngas. Different compressors are available in the market, for example, centrifugal compressors, rotary screw compressors, axial compressors, reciprocating compressors, positive displacement compressors, and rotary compressors. But the choice is usually made based on the molecular weight and density of the gas mixtures that need to be stored.

Centrifugal compressors increase the pressure by applying centrifugal force on the gas and are used for methane, not syngas or pure hydrogen. Positive displacement compressors (PDC) take a certain amount of gas and compress it in one round and during the second round, it takes the same amount of gas and so on. For hydrogen or syngas, PDC is a suitable choice for compression [2]. Reciprocating compressors can also be used to deal with the diffusive nature of hydrogen.

The characteristic of syngas is to contain low energy density so required pressure increase is achieved in stages and each stage pressure rise is very small with a constant compression ratio of all the compressor stages.

1.9   Carbon capture and compression ratio.

As temperature and pressure are directly proportional to each other, so when the pressure of a gas is increased, its temperature also increases proportionally. This rise in temperature causes many problems in the system, for example, thermal expansion of the components, material degradation, or failure of the equipment system. Therefore, a compression ratio is considered to control the output temperature. Compression ratio is defined as the ratio of discharge pressure to the suction pressure of a compressor.

Practically it is noticed that as the number of stages increases, the cost of the compression systems increases. It also reflects that more cooling media is required to control the temperature. But on the other hand, the greater number of stages suggests a little temperature increase after each stage. Therefore, the final number of stages and compression ratio are developed based on a tradeoff

between several stages and temperature at the outlet. Fina compression ratio is the product of all the compression ratios at each stage. Normally, the compression ratio of all the stages is kept constant.

Biliyok et al. studied natural gas power plants in a post-combustion manner and coupled the CO_2 compression train with the plant and evaluated the power required for effective CO_2 transportation in the pipelines network. CO_2 brought to super critical phase with an outlet pressure of 110 bar. In that study, they observed a 14% decrease in the overall output of the plant beside a 33% increase in the cooling water to control the temperature [30].

1.10 Research objective

The overall objective of the present work is to analyze technically two different scenarios. The first one is the state-of-the-art solid oxide fuel cell. The second case is the plant that is comprised of novel methane-reduced chemical looping coupled with solid oxide fuel cells.

In this thesis, ceria chemical looping is mainly investigated as a substitute for steam methane reforming to produce hydrogen. Methane is reduced in the reduction reactor of chemical looping and a hydrogen-rich syngas mixture is achieved. Besides this, chemical looping technology uses SOFC waste gas in its oxidation reactor to enhance the yield of syngas.

To achieve the overall objective, several sub-objectives are identified that are listed as.

- To explore different oxygen carriers for CO_2/H_2O splitting chemical units based on reduction extent and hydrogen yield.
- To examine the thermodynamic of methane reduction from ceria in the chemical looping unit.
- To develop a model for reduction and oxidation of chemical looping for the simultaneous splitting of CO_2 and H_2O.
- To explore the effect of operating conditions of reduction and oxidation reactors for example effect of temperature, pressure, and feed molar ratio on the hydrogen yield and the performance of the entire chemical looping section and to determine the suitable operating conditions for the chemical looping unit.
- To set limits of temperature, pressure, and flow for efficient operation of CO_2/H_2O simultaneous splitting chemical looping unit based on literature and sensitivity analysis.
- To examine the outcome of combining solar thermochemical simultaneous CO_2/H_2O chemical looping section with a solid oxide fuel cell with a special focus on hydrogen yield on the performance of the proposed system.
- To investigate the performance of chemical looping based on utilizing SOFC waste gas mainly comprised of CO_2 and H_2O.
- To perform a comprehensive analysis of state-of-the-art solid oxide fuel cell and proposed chemical looping unit coupled with solid oxide fuel cell based on electrical efficiency, energy efficiency, SPECCA, carbon capture, and utilization.
- To perform the pinch analysis of the plant during morning and evening operations when chemical looping is available and unavailable respectively.

- Finally, to recapitulate the research conclusion and set recommendations and give way for future research aspects to make the proposed system at an industrial scale.

1.11   Thesis structure

The thesis is structured according to the objectives defined in the above section. Firstly, there is an investigation of state-of-the-art solid oxide fuel cells in ASPEN plus. The scope is to analyze its electrical and thermal and carbon capture performance.

Secondly, there is an investigation of thermochemical simultaneous CO_2/H_2O splitting in methane reduced chemical looping unit. The scope is to evaluate suitable operating conditions and to evaluate the selectivity of syngas produced at optimal operating conditions. The scope also includes determining the efficiency based on methane reduction, solar fuel production, and waste gas utilization in the chemical looping unit.

Then the present work expands the limits towards integrating methane reduced chemical looping unit with the state-of-the-art solid oxide fuel cell to anticipate advantages of generating syngas in both oxidation and reduction reactors of chemical looping. The scope is to determine the electrical, thermal, and carbon capture efficiency of the proposed system. The scope also includes the efficiency gain of carbon capture and utilization achieved in afterburner and oxidation reactor of chemical looping respectively.

In the second part of the thesis, the study extends towards pinch analysis of the proposed system to find the minimum energy requirement of the plant during morning and evening operations.

In chapter 1, a general introduction of the topic is given including hydrogen production and carbon capture technologies.

In chapter 2, a comprehensive overview of the electrochemical energy transformation process is given together with solid oxide fuel cells having a special focus on carbon deposition, its thermodynamics, and its prevention techniques.

In chapter 3, a detailed overview of chemical looping is presented. Different oxygen carriers are discussed that other researchers attempted in the existing literature. Besides this methane reduced ceria chemical looping is encapsulated via comprehensive explanation.

In chapter 4, a detailed methodology adopted during the development of the proposed plant is presented. It also describes which technology is chosen for carbo capture.

Chapter 5 presents a comprehensive description, model development, and assessment of state-of-the-art solid oxide fuel cells and proposed ceria-based chemical looping system coupled with SOFC along with oxyfuel combustion. It includes the working principle of adopted technologies, mechanism, processing reactions, and participating components. The problem of carbon deposition and prevention is well described.

Chapter 6 describes the important discussions of the results generated from this study. It covers several sensitivity analyses, performance assessments of chemical looping in terms of syngas production, electrical and energy efficiency of the proposed plant, and analysis of the system in

terms of carbon capture, utilization, and storage is encapsulated. Furthermore, the design of the plant with minimal energy requirement covering pinch analysis and development of heat exchanger network is reported.

Chapter 7 complies with the conclusions of the performed study and recommendations for future researchers.

2 Energy transformation and electrochemical phenomena

Energy associated with the flow of chemical species is characterized by chemical energy and this chemical energy can be converted into other forms of energy, for example, electrical energy by using the machine. At present, two types of machines are available. One is a thermal machine and the other is an electrochemical machine. Figure 2.1 elaborates the working principle of classical thermal machines and electrochemical machines.

The classical thermal machine works with the transformation of high-temperature heat into work by using thermodynamic cycles of different pathways. High-temperature heat is necessary to feed the thermodynamic cycles. Therefore, chemical energy is first converted into high temperature by heat by combustion. A combustion product in the form of high-temperature heat is introduced to the thermodynamic cycle that generates work in the form of mechanical energy or electrical energy. A specific fraction of low-temperature heat is rejected to the environment as well. Combustion in this process is very primitive and generates entropy within the system that leads towards exergy loss.

Another possible way of converting chemical energy into a different form of energy is to utilize the electrochemical machine or electrochemical generator that is one step transfer motion. It does not include combustion and therefore, it does not generate entropy. So, it transforms directly from chemical energy into electrical energy without combustion or mechanical parts like pistons or blades, etc. It is an alternate option as compared to the classical machine.

If we replace the electrochemical generator, with an electrochemical cell, it will transform energy in both ways from chemical to electrical and in contrary from electrical to chemical energy. In case, the electrochemical cell is operating in a reverse way, which means generating a chemical effect from electrical it is important to empathize that the input to the machine must be electrical in the form of the flow of electrons across the potential gradient.

2.1   Electrochemical cell

An electrochemical machine is a machine that converts chemical energy into electrical energy due to electrochemical reactions. The main output of an electrochemical machine is electrical power and thermal power is achieved as a by-product. This technology is called fuel cell or electrochemical cell.

An electrochemical cell is comprised of three layers. Anode layer, the electrolyte layer, and a cathode layer. On the anode layer, oxidation (releasing electrons) takes place. While on the cathode, reduction takes place. Generally, in a fuel cell, fuel is provided at the anode, and oxygen is supplied to the cathode. The electrolyte layer being in the center of electrodes divides reactant feed and ensures that they do not mix. Electrochemical reactions take place at the surface in both compartments of the fuel cell. Ions are migrated from one compartment to another with the help of electrolytes.

So, an electrochemical cell can drive a series of redox reactions (spontaneous) by organizing it separating into two steps: One step is oxidation at anode, so the release of electrons and the other step is reduction at the cathode, so recombination of electrons. Then we also need a potential

gradient. This potential gradient is also generated by the effect of charge separation, it is analogous to the effect when an electron is separated from the molecules at the anode layer. It generates a voltage gradient. The difference of voltage gradient at the anode and voltage gradient at the cathode is known as the voltage gradient of the whole electrochemical cell. In this way, the whole structure can generate a flow of electrons. Hence, on one side we have a flow of electrons and on the other side, we have a voltage gradient. The final combined effect of these two cases generates electrical power. Power of a fuel cell is the product of current produced and voltage and is given as.

$$W_{el} = \text{current.voltage} = I.V \qquad (2.1)$$
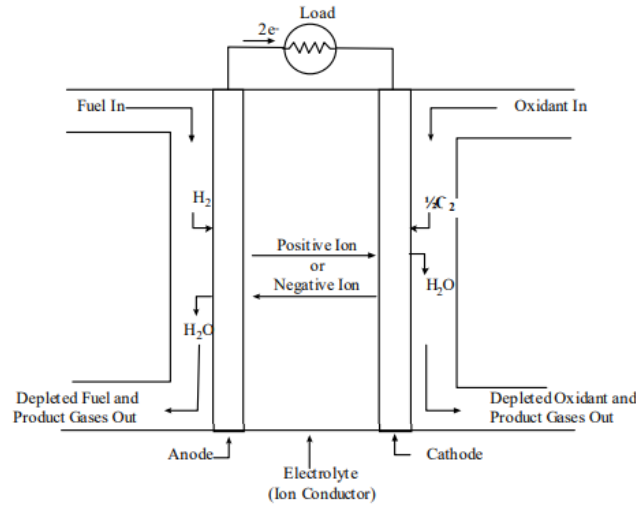
Figure 2.1: Electrochemical processing [31]

In principle, the fuel of electrochemical machines is not limited to hydrogen only, but it is comprised of large categories of molecular families that can be oxidized with sufficient electrochemical reactions which activate at suitable operating conditions. Fuel cell characteristics are changed by changing the type of electrolyte (central layer). So, fuel cell performance is highly dependent on the type of the electrolyte layer. The electrolyte layer is the heart of the electrochemical machine.

Fuel cells are categorized into many types, the type of fuel cell is mainly based on the preference of fuel provided to machine and electrolyte.

Example of reaction for $\Delta \bar{g} < 0$: Chemical energy $\rightarrow$ Electrical energy

Pure hydrogen is introduced at the anode so that the oxidation takes place according to the half-reaction mentioned in Eq. (2.3) and H^+ is produced. If the material of the electrolyte layer is such that it has good mobility with H^+ ions. So, it transports the H^+ ions.

$$H_2 + \frac{1}{2}O_2 \rightarrow H_2O \quad \Delta \bar{g} < 0 \qquad (2.2)$$

$$H_2 \rightarrow 2H^+ + 2e^- \qquad (2.3)$$

$$\frac{1}{2}O_2 + 2e^- \rightarrow O^{2-} \qquad (2.4)$$

$$\tfrac{1}{2}O_2 + 2H^+ + 2e^- \rightarrow \text{H}_2\text{O} \qquad (2.5)$$

$$H_2 + O^{2-} \rightarrow \text{H}_2\text{O} + 2e^- \qquad (2.6)$$
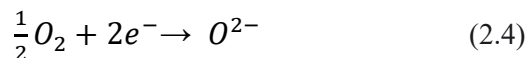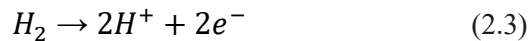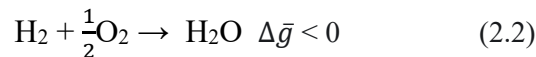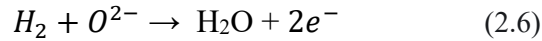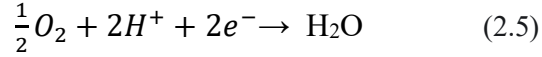
Half oxygen receives two electrons coming from the oxidation of hydrogen in the anode side, and reduction takes place at the cathode, based on half-reaction mentioned in Eq. (2.4). In this way, water is produced at the cathode based on the reaction mentioned in Eq. (2.5). If the material of the electrolyte is such that it has good mobility of O^{2-} ions, in that case, it transports the O^{2-} ions towards the anode side, and water is produced at the anode as mentioned in Eq. (2.6).

So, depending on the type o0f electrolyte, two half-reactions are different based on the types of ions conducted through the electrolyte. Although the same global reactions take place mentioned in Eq (2.2).

2.2   The open and closed electrochemical cell

Sometimes, fuel cells are known as open electrochemical cells as reactants come from the external environment continuously which means fuel is provided to the machine externally to operate the cell. Fuel cells produce power until the fuel is provided. In contrast, batteries are called closed electrochemical machines, as there is no exchange of the reactants from the external environment. That's why batteries have a limit of capacity in terms of exchanging energy. The term 'capacity' is specified for the batteries, not for the fuel cell as the fuel cell does not have a limit of 'energy', but it has a limit of power because power depends on the size of the cell.

In the present research to produce electric power, open electrochemical cells are preferred not the battery or power turbine cycle. Among different fuel cells, solid oxide fuel cell is chosen because of their fuel flexibility.

2.3   Solid oxide fuel cell (SOFC)

For the present study, solid oxide fuel is considered to produce power. The electrolyte in this fuel cell is a solid material, mostly Yttrium oxide (Y_2O_3) stabilized zirconia (ZrO_2). The cell is regarded as high operating temperature in the range of 600-1000 °C. This high operating temperature is coupled with its benefits and drawbacks.

The anode is the electrode where oxidation of the fuel occurred. Catalytic activities of the anode are very critical, it must guarantee the adsorption of hydrogen. Normally, the anode supports the whole cell mechanically and is comprised of Co-ZrO2 or Ni-ZrO2 cermet with a thickness range of 25-500 micrometers.

The cathode is the electrode where reduction of oxygen occurred. Catalytic activities of the cathode must guarantee the adsorption of molecular oxygen. The ceramic cathode is mostly used but, in some cases, ceramic is dopped with LaMnO3.Cathode needs to have a sufficient three-phase boundary. The thickness range of the cathode is 25-35 micrometers. It should not too thin, if it is too thin, there will not sufficient catalytic sites to generate a reduction reaction. But if it is too thick, then the diffusion of oxygen molecules will be impeded too much.

Yttria stabilized zirconia (solid electrolyte) is used in solid oxide fuel cells. The electrolyte layer must be in the range of 5 micrometers, and it should be thin as much as possible to avoid the ohmic drop but it should not be too thin. The electrolyte should be dense to avoid molecular diffusion.

The material for the interconnected plate must show high thermo-mechanical behavior as the machine works at 800, so degradation is not suitable. There are a lot of materials that have this character. CROFER 22 APU is widely used for the interconnected plate. It is stainless steel material with high containing (22%) of chromium that generates the characteristic of good conductivity and at the same time resistance at high temperature and compatibility in terms of volumetric modification with the ceramic.

2.3.1 Advantages of solid oxide fuel cell

- Thanks to the high temperature, the kinetics of the charge transfer are excellent.
- Ni is used as a catalyst that is very cheaper as compared to Pt group metals. This type of catalyst is more benevolent to molecules containing carbon. This is a good advantage from the economic point of view. It has opened doors for an enormous number of hydrocarbon molecules to get oxidized in the machine.
- The advantage of high temperature is the availability of heat at very high temperatures.
- Hybridization of SOFC with other machines is sometimes promising for example gas turbine coupled with SOFC.
- Fuel flexibility is a very good advantage of SOFC, CH_4 and all other hydrocarbons C_xH_y, alcohols, ethers ($C_xH_yO_z$), ammonia, biogas, syngas can be provided to solid oxide fuel cells.
- High temperature is responsible for high electrical efficiency and high global efficiency for a cell. A (state of the art) naked stack has a record of 72% electrical efficiency.
- Because of the high temperature, all the transport processes (charge transfer, ionic conduction, and molecular diffusion) are activated at a very good rate. This generates a lower over voltage.

2.3.2 Disadvantages of solid oxide fuel cell

- Materials with high thermal stability and high tolerance to temperature are required.
- Achieving high temperature is very expensive which also means that the balance of the plant (BOP) is very expensive.
- Because of the higher temperature, higher degradation of BOP is observed that reflects a shorter expected life of equipment (BOP).
- Lower dynamic in general operation. It is not suitable for thermal cycles.
- A high duration of startup and shut down of the machine is required. This shows that there is no continuous switch on and switch off that further reflects that it is impossible to get on and off ten times in a day.
- These are not suitable for transport applications like cars etc., used for trucks but not for power trains. But it is very good for base load and heat recovery.

2.4   Polarization of SOFC.

SOFC is more performing, and its polarization is more characteristic as compared to PEMFC. Due to high temperature:

- Transport phenomena of the machine are improved.
- High kinetic of charge transferrin terms of electrochemical.
- It has a high exchange current density (I_o) and lower activation over voltage.
- Its behavior is mostly resistive and shows the ohmic (so linear) behavior.

In a generic electrochemical cell, electrons are unable to conduct through the electrolyte material, but they are normally conducted and transferred through an external circuit. The condition of the equilibrium is the one when the circuit is open. When we close the circuit, everything is changed, and equilibrium is broken. Therefore, physics is dominated by transport processes. These transport processes are basically of three categories.

Charge transfer: It means that charge (electron) is separated from the original molecule and transferred to an external circuit. When the system is closed, the current starts migrating into the cell. This migration of current generates the process of 'transport process'. This phenomenon is called charge transfer and tends to affect and modify the original voltage as compared to the ideal voltage of cell E. Sometimes it is called activation over-voltage.

Charge migration: This term is interconnected with the ions not electrons. As H^+ ions are completely migrated from anode to cathode by passing through the electrolyte layer, so in this way charge migration modifies the ideal voltage of the cell and is called ohmic affect. This is also called ohmic voltage.

Mass transport: This term is linked with the molecules of H_2, O_2, H_2O, as these molecules are heavy as compared to electrons or ions, so the diffusion process is dominant, and the overall phenomenon is called mass transport. Voltage associated with mass transport phenomena is called diffusion over-voltage.

All these three transport processes generate entropy and affect degradation. Degradation in terms of voltage means voltage compared to the ideal voltage (OCV) decreases.

This affects and modifies the ideal voltage. For the solid oxide fuel cell, the open circuit cell voltage is calculated by Eq. (2.7).

$$V_{id} = E^O + \frac{RT}{2F} \ln \left(\frac{(p_{H_2}.p_{O_2}.)^{0.5}}{p_{H_2O.}} \right) \qquad (2.7)$$

E^O is the ideal voltage for the oxidation of fuel. F is the Faraday's constant equal to 96485 c/mol. R is the general gas constant equal to 8.314 J/mol.k and p is the partial pressure of the species. Eq. (2.7) shows that the ideal voltage of the cell is dependent on the pressure.

2.4.1   Influence of pressure on the operation of solid oxide fuel cell

If less pressure is applied in the solid oxide fuel cell, then there are chances that diffusion over potential or concentration polarization will be decreased. Diffusion over potential appears in a

situation when the concentration of species is lower at the electrode surface as compared to the bulk surface [32]. This situation limits electrochemical processing. This concentration polarization creates entropy within the machine that decreased the overall performance of the system.

Willich et al. conducted experimental work on solid oxide fuel cells at high pressure of up to 8 bar to comprehend their electrochemical and operational behavior. They also studied the pressure dependence on the overall performance of SOFC and found that SOFC system performance increases as the pressure is increased. Furthermore, they concluded that when pressure is increased from 1.4 to 3 bar, around 23% increment in power density occurred [10].

Virkar et al. studied pressure dependency on cathode-supported SOFC and electrolyte-supported SOFC. They found that SOFC performance rises with the rise of pressure particularly for cathode-supported SOFC because of lower diffusion over potential [34].

2.5   Fuel flexibility of SOFC

As SOFC operate at very high temperature in the range of 800 °C so it accepts different types of fuels ranging from liquid hydrocarbons to gaseous fuels methane and syngas. While in contrast PEMFC only works with pure hydrogen as PEMFC operate at low temperature.

Most of the commercial SOFC plants are fed with syngas. In most cases, syngas is produced with the help of steam methane reforming (SMR) where methane and steam react together and produce syngas along with certain proportions of unreacted CH_4 and H_2O. But if syngas is produced by using biomass feedstock (gasification) or catalytic partial oxidation of hydrocarbons then it must contain nitrogen and steam contents as well. Although the steam contents can be recovered by condensing the stream, it will charge an extra amount of energy. So, depending upon the parent fuel feed and processing technology for syngas production, H_2/CO ratio varies accordingly along with the different compositions of unreacted reactants. Thus, it is very imperative to predict the behavior and performance of SOFC with a feed containing alternative syngas composition. Robert J. Kee et al researched SOFC operating conditions, efficiencies, and challenges. They used syngas with different compositions and found that syngas composition has a very slight effect on the performance and conversion efficiency of SOFC [1]. Audasso et al performed modelling of solid oxide fuel cells while considering internal reforming of CH_4. They considered biogas as the main source of SOFC reactants[7].

2.5.1   Reactions in the cathodic compartment of SOFC

On the cathode side, molecular oxygen is supplied. This oxygen is reduced into oxygen ions by absorbing two electrons as depicted by Eq. (2.9). These negative ions are migrated from cathode to anode. The reactions at the cathode will always remain the same, no matter which fuel is used.

$$\tfrac{1}{2}\, O_2 + 2e^- \rightarrow O^{2-} \qquad (2.9)$$
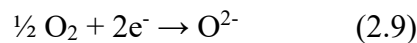
2.5.2   Reactions at anodic compartment of SOFC

On the anode side, fuel is supplied that may lead towards different types of reactions depending on the type of fuel feeding to the anode. Oxidation of fuel takes place at the anode by releasing electrons. These discharged electrons pass through external resistance to produce electrical power.

Electrochemical reactions of hydrogen, carbon monoxide and methane at the anode are represented by Eq. (2.10), (2.11), and (2.12).

Hydrogen: $\qquad H_2 + O^{2-} \rightarrow H_2O + 2e^-$ (2.10)

Carbo monoxide: $\qquad CO + O^{2-} \rightarrow CO_2 + 2e^-$ (2.11)

Methane: $\qquad CH_4 + 4O^{2-} \rightarrow 2 H_2O + CO_2 + 8e^-$ (2.12)
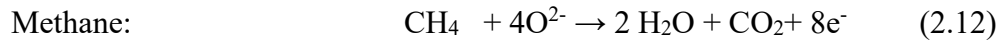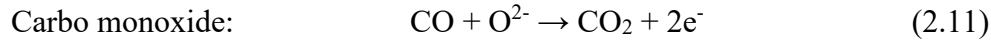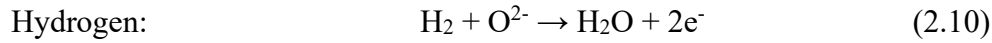
The thermodynamic destination of hydrogen and carbon is always to go towards lower gibs energy while forming H_2O and CO_2. The number of electrons released by the fuel molecules is calculated as a fellow.

- In the case of hydrocarbons like C_xH_y: $Z= 4x+1y$ for example C_3H_8: $Z=12+8=20$
- For alcohols like $C_xH_yO_z$: $Z=4x+1y-2z$.fo example C_2H_5OH: $Z=8+5-4=9$

So, it means that the presence of oxygen generates a reduction in charge number.

We have a mixture of CH_4, H_2, CO, and CO_2 and this mixture is at almost 800 ^0C. So, there are all the conditions to activate the following mechanism of reactions.

Steam reforming-endothermic reaction: $\qquad CH_4 + H_2O \rightarrow 3H_2 + CO$ (2.13)

Dry reforming-endothermic reaction: $\qquad CH_4 + CO_2 \rightarrow 2H_2 + 2CO$ (2.14)

Water-gas shift reaction-exothermic reaction $\qquad CO + H_2O \rightarrow H_2 + CO_2$ (2.15)

Direct electrochemical oxidation of methane $\qquad CH_4 + 4O^{2-} \rightarrow 2H_2O + CO_2 + 8e^-$ (2.16).

What happens, in the end, depends on thermodynamics and kinetics. Reaction (2.13) prevails because of faster kinetics especially compared to reaction (2.16). But mostly reaction of steam methane reforming take place and molecule of hydrogen and CO are produced. It is observed from the above reactions that the molecules that perform the electrochemical reactions and deliver the electrons are the following.

$$H_2 + O^{2-} \rightarrow H_2O + 2e^- \qquad (2.17)$$

$$CO + O^{2-} \rightarrow CO_2 + 2e^- \qquad (2.18)$$
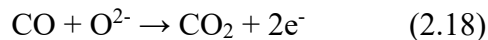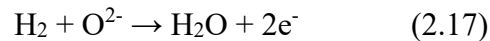
This shows that real molecules that deliver the electrons are not directly the original molecule (CH_4) but are the molecule coming from the reforming of the original molecule. So, we can say that real electrochemical fuel is H_2 and CO.

Comparing Eq. (2.13) and (2.16) it is observed that the number of electrons released in both reactions is the same. In the steam methane reforming, we have three molecules of hydrogen and

one molecule of CO, so the total number of electrons from hydrogen will be 6 and from CO will be 2. In this way cumulative number of electrons in Eq. 2.13,) and (2.16) are identical.

2.6 Kinetics of electrochemical oxidation of hydrogen.

As the number of electrons plays a vital role in the performance of solid oxide fuel cells. If the number of electrons provided by the fuel is more, it means there is extra charge flow in the external circuit that reflects an additional quantity of electrical power.

It is noted that both molecules, H_2 and CO deliver the same number of electrons but the kinetics of both these molecules is different. The kinetic of the hydrogen molecule is faster as compared to the kinetic of CO.

$$\text{Exchange current density} = i_{0,CO} = 1/8^{th} \text{ of } i_{0,H2}$$

This shows that the kinetic reaction of hydrogen is 8 times faster as compared to the kinetic reaction of the CO molecule even though H_2 and CO give the same number of electrons.

2.7 Carbon deposition in solid oxide fuel cell

For the smooth operation of SOFC, it is advantageous that methane must be converted into hydrogen and carbon monoxide and suppress the formation of undesirable species like atomic carbon. Therefore, a perfect internal reforming of fuel is desirable so that carbon formation within SOFC must be minimized. Generally, some design concepts prefer the external reforming of methane as it maximizes hydrogen production and lowers carbon growth inside the system [2]. As explained earlier, among different hydrogen generation processes, steam reforming is highly suitable as it offers the highest hydrogen generation yield. Though, internal reforming is embodied with carbon formation and deposition at specified operating conditions in the anodic compartment of SOFC. This leads to the damaging of the SOFC system. Carbon deposition is very dangerous for the soft operation of SOFC, it suppresses the catalytic activities of catalyst and covers the anode porous structure.

2.7.1 Negative reactions in the anodic compartment of SOFC

Fuel in the form of methane and carbon dioxide is introduced in the anodic region, loaded with Ni catalyst in the presence of high temperature. There are conditions to activate negative reactions in the anodic compartment. These reactions are given below.

$$CH_4 \rightarrow C + 2H_2 \qquad (2.19)$$

$$2CO \rightarrow C + CO_2 \qquad (2.20)$$

$$CO + H_2 \rightarrow C + H_2O \qquad (2.21)$$
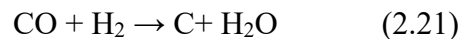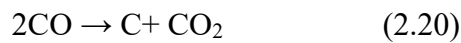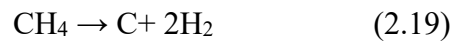
There are three reasons for carbon deposition that are methane cracking, Boudouoard reactions, and Reversed Syngas Formation.

The first reaction Eq. (2.19) is characterized by methane cracking. It is an endothermic reaction and is activated at a high temperature. One molecule of methane is cracked into one atomic carbon in solid form and two molecules of hydrogen. Thermodynamically it has been observed that

methane decomposition into carbon and hydrogen started when the anodic temperature goes beyond 300 °C. The second reaction Eq. (2.20) is considered the Boudouoard reaction. In this reaction, carbon mono oxide is decomposed into carbon dioxide and atomic carbon. The third reaction is named reverse syngas formation reaction. In this reaction syngas combined and converted into negative products in the form of water and atomic carbon.

From the above reactions, it has been observed that carbon is produced in atomic form. This is not in gaseous form, but it is solid carbon in the form of graphite. This process is called carbon deposition. This solid carbon deposits on the surface of electrodes and catalyst.

As the fuel is introduced in the anode, carbon deposition on the surface of the catalyst starts, and catalyst pores are occupied with carbon. Methane molecules cannot be reduced anymore. Meanwhile, the cathodic compartment delivers O^{2-} ions that did not find any oxidizing species on the surface of the catalyst. The result is that it oxidizes nickel catalyst and forms N_2O. In this way, pores of the catalyst block and phenomena are called pore blocking. So incoming CH_4 cannot pass through the pores due to blockage and the cell stops working due to cutting off the fuel. So, in this way cells will break and reoxidation of the catalyst takes place. And degradation of the cell happened.

Carbon deposition enhances the barrier of activation energy and results in a lower reaction rate and reduced kinetics. Even in the presence of a catalyst, a favorable conversion cannot be achieved at a high temperature.

2.7.2 Thermodynamics of Carbon deposit.

Phenomena of carbon deposit take place due to feasible conditions of thermodynamics. So, the mixture containing carbon is thermodynamically in line with conditions of carbon deposit. Girona et al performed detailed analysis and thermodynamic calculations to investigate the connection between carbon deposition and fuel cell operating conditions. In that study, they developed a ternary thermodynamic diagram determining the limits and safe area for carbon deposition [3].

Figure 2.2 shows the equilibrium triangle or thermodynamic ternary diagram explaining the limitations and boundaries of operating conditions of carbon formation. It is divided into two subsections. The upper portion is called the carbon deposition region indicating that carbon quantity is more than 1 part per million (ppm), this is the area of risk as it is poor in terms of H and O. While the lower portion is called the carbon-free region demonstrating that carbon quantity is less than 1 parts per million (ppm). This area is well protected because of the presence of H and O. On the three sides of triangles, the ratio between respective atoms is marked, it represents mole fractions of carbon, hydrogen, and oxygen at different temperatures. For example, CH_4 is marked at 0.2, CO_2 is marked at 0.66 while H_2O is marked at 0.67. Slanting lines within the triangles show the temperature at different levels and portrait threshold limits of carbon deposition. The Gray area inside the triangles shows the mixture of CH_4, CO_2, and H_2O. SOFC will be carbon-free if the C-H-O ratio is below the operating temperature line.
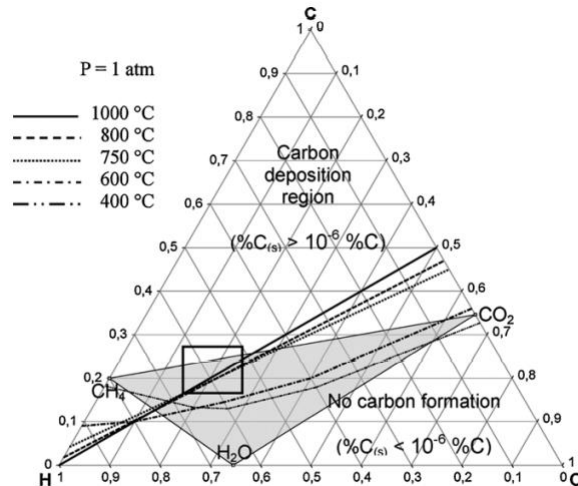
Figure 2.2: Thermodynamic ternary diagram of carbon deposition within SOFC

As steam reforming is an endothermic process means it demands heat, so it acts like a thermal sink inside the stack. So,

2.7.3   How to prevent carbon deposition?

Several approaches have been adopted to limit the carbon formation in the anode of solid oxide fuel cells. For example, anode material, design specification, or operating conditions can be searched.

➢ The first approach is to put some additives with the catalyst so that the kinetics of carbon formation is limited. This approach is also reported in the literature. For example, Laycock et al investigated dry reforming of methane and carbon dioxide in the presence of ceria doping with Nickle. In that study, they found that ceria doping plays a vital role in suppressing the kinetics of carbon deposition and supports the reverse Boudouoard reaction Eq. (2.20) at high temperatures [4]. Stephanie et al investigated solid oxide fuel cells with two different categories of anodes, ceria doped nickel and gadolinia cermet over a range of temperatures from 550-700 °C. In that study, they found that both additives anode exhibited good methane reforming and lowered the mechanism of carbon formation [5].

➢ The second approach is to add excess water to the reactant mixture. It is observed that if SOFC is worked with excess water then reactions Eq. (2.19) and (2.20) are hindered. Because adding water can modify the equilibrium putting the mixture in a situation of a safe area. A lot of researchers considered water as an oxidant agent during SOFC performance. For example, Dogdibegovic et al investigated the performance of solid oxide fuel cells by using different fuels, hydrogen, ethanol, water blend ethanol. In that study, they found that a high power density of 1 W/cm^{2-}is achieved with water blend ethanol at 650 °C and 1.4 W/cm^{2-} at 700 °C respectively. They also confirmed that carbon formation did not take place[6]. The reaction of water and methane is given as Eq.(2.22). This reaction shows that if excess water is used as an oxidant, then the direction of the equilibrium will be towards the right and thus producing more and more hydrogen and carbon monoxide.

$$CH_4 + H_2O \rightarrow 3H_2 + CO \qquad (2.22)$$
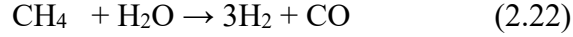
It is observed from Eq.(2.22) that adding water generates a mixture of syngas that is consisted of an H_2/CO ratio of 3.

> ➤ The third approach is to add excess oxygen O_2 in the mixture, it will activate the partial oxidation within the anode. The reaction of partial oxidation is given as Eq. (2.23).

$$CH_4 + 1/2O_2 \rightarrow 2H_2 + CO \qquad (2.23)$$
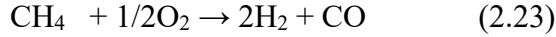
This will generate a mixture of syngas with an H_2/CO ratio of 2. So here mixture performance is less as compared to steam reforming.

> ➤ Another comprehensive approach to alleviate carbon formation and deposition is to add a bit extra quantity of oxidant along with other reactants. Adding CO_2 also acts as an oxygen carrier. It will activate the dry reforming. As dry reforming of fossil fuel is mainly comprised of CH_4 and CO_2 so it is proposed to add an excessive quantity of CO_2 with the methane so that carbon formation can be avoided. The reaction of dry reforming with excess carbon dioxide is given as Eq.(2.24).

$$CH_4 + CO_2 \rightarrow 2H_2 + 2CO \qquad (2.24)$$
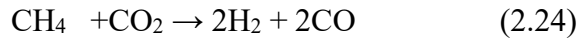
This will generate a mixture of syngas with an H_2/CO ratio of 1. And this reaction is more endothermic as compared to steam reforming. This is good agreement with the literature as well, as several researchers have adopted this approach. For example, Gaddalla et al conducted experimental work on the dry reforming of methane by using the excess quantity of CO_2. In their study, they considered a carbon dioxide to methane (CO_2/CH_4) ratio of 2.64 and found 100% conversion after 51 hours of operation[8]. It is also predicted that carbon formation initiates when low CO_2/CH_4 ratios are considered. Another aspect is that if a high CO_2/CH_4 ratio is used, then it will dilute the fuel and the result will not only be a lower extent of reforming but a lower SOFC power and its efficiency. Therefore, it is important to predict an efficient CO_2/CH_4 ratio which results in the minimum chances of carbon deposition.

Based on the above discussion and reaction equations it can be concluded that if water is used as a source of oxygen, then a higher quality syngas is produced at the output, and it suppresses carbon formation. Consequently, it is considered that water is a good oxygen carrier to avoid carbon deposits. For the present study, above mentioned anodic additives are not considered. But fixed steam to carbon ratio is utilized (SC=2), which will guarantee enough quantity of water inside the reformer, thus avoiding carbon deposition inside the reactor is achieved.

2.8   Thermal balance on SOFC

As solid oxide fuel cell operates at very high temperature, therefore there is a thermal exchange between the cell and the external environment. So, thermal balance on the SOFC is applied based on the first law of thermodynamics. This balance considers all the heat sources and heat sink caused by electrochemical reactions within the stack.

$$Q_{Produced} = \delta H_{reaction} - W_{electrical} \qquad (2.25)$$

$$Q_{Produced} = Q_{Air} + Q_{Reformer} \qquad (2.26)$$

$$Q_{Air} = Q_{Produced} - Q_{Reformer} \qquad (2.27)$$

$$Q_{Waste} = Q_{Air} = \delta H_{reaction} - W_{electrical} - Q_{Reformer} \qquad (2.28)$$

$$W_{electrical} = V. I_{total} \qquad (2.29)$$

Equation (2.25) is purely based on the first law of thermodynamics. δH is the enthalpy change across the anode; this is not all going into heat. But this goes partially into electricity production and the remaining part will go to heat as described in equation (2.25). Now, the total heat produced is the combination of heat removed by air and heat required by the reformer as depicted in equation (2.26). To know how much heat is removed by air, we need to know total enthalpy change across anode, electric power produced, and heat requested by reformer illustrated by equation (2.28). The heat removed by air is also called waste heat.

Therefore, the air is supplied to remove the waste heat from the SOFC stack. The mass flow rate of air supplied is stoichiometrically calculated as

$$Q_{air} = m_{Air}. c_{p\ Air}. (T_{out,\ air} - T_{in,\ air}) \qquad (2.30)$$

$$m_{air} = \frac{Q_{Air}}{c_{p,air} * (T_{out,air} - T_{in\ air})} \qquad (2.31)$$

$c_{p\ Air}$ is the heat capacity of air that is equal to 1005 J/kgk. $T_{out,\ air} - T_{in,\ the\ air}$ is the temperature difference of air. Another useful piece of information is that heat that is currently removed by the air is the heat of the Cathode heat exchanger.

As solid oxide fuel cell operates at high temperature, temperature control is achieved by providing air to the cathode in excess quantity. In most practical cases, an air utilization of around 20% is adopted.

$$m_{AIR\ stoich} = \lambda. m_{AIR\ real} \qquad (2.32)$$

$$\lambda = \frac{Stoichiometrically\ calculated\ air}{Real\ amount\ of\ air\ entered\ in\ cathode} \qquad (2.33)$$

$$C_{total} = N_{fuel} \times FU \times F \times Z_{fuel} \qquad (2.34)$$

$$N_{O_2} = \frac{C_{total}}{Z_{O_2} \times F} \qquad (2.35)$$

λ is the air excess ratio or also called air utilization. Stoichiometric air is calculated by using Faraday's law as per Eq. (2.35). Therefore, in this way, the air excess ratio with respect to stoichiometric air is determined from the thermal balance of the SOFC system. It is worthful to emphasizing that the main objective of sending air is to remove heat that is remained after supplying the endothermic reforming reaction.

2.9   Literature review on SOFC.

Serval researchers devoted their effort to studying the phenomena of solid oxide fuel along with other power generation systems. These are given as.

➢ Sung et al proposed a plant configuration that is the combination of SOFC-gas turbine-oxyfuel combustion hybrid system along with carbon capture and compression unit. They operated SOFC at 7.904 bar pressure, 900 °C temperature and 0.7 as fuel utilization factor. They preheated the incoming air to 700 °C and pressurized it until 8.57 bar. At these operating conditions, SOFC voltage was found to be 0.752V. They concluded the system efficiency was around 69.2% and an efficiency penalty of around 6.1% was reported [42].

➢ Takeshi et al performed the techno-economic analysis of SOFC-combined heat and power plant (CHP) and CO_2 capture was achieved by utilizing an oxyfuel combustion unit with an air separation section. They operated SOFC at 1000 °C temperature, 1.3 bar pressure, and 0.85 fuel utilization. The incoming fuel and air temperature and pressure were set to be 800 °C and 1.3 bar pressure. On these operating conditions, SOFC voltage was calculated to be 0.659 V [43].

➢ Spallina et al proposed a configuration of a polygeneration plant consisting of solid oxide fuel cell and steam power plant integrated with chemical looping combustion process (CLC) together with fluidized bed reactor for the oxidation of unreacted species present in the anode exhaust. They operated solid oxide fuel cells at 800 °C temperature, pressure 1.13 and 0.8 as fuel utilization. The incoming air and fuel temperature was set to be 735°C and 600 °C and pressure for both were set to be 1.13 bar. Cell voltage was used to be 0.8V. They varied several parameters in their study and reported the carbon capture ratio to be 100% [44].

➢ Done et al devoted their effort to the combination of solid oxide fuel cell with the gas turbine, steam turbine co-generation system and optimized the exergy efficiency of the proposed plant configuration. In that study, they operated the solid oxide fuel cell at 1000 °C temperature, 15 bar pressure, and 0.9 as fuel utilization. SOFC fuel temperature was set to be 673K and the incoming air temperature was set to be 853K. They utilized cell voltage to be 0.69V. They reported the efficiency of the combined proposed pant system to be in the range of 60-70% [45].

➢ Xiaosong et al studied the coupling of methane fueled SOFC with the chemical looping combustion with the aim of hydrogen production. They set operating conditions of the SOFC as 1.1 bar pressure and 910 °C temperature and found the operating voltage of the SOFC to be 0.6332V [46].

➢ Musa et al studied SOFC- gas turbine combination and performed a parametric study on operating conditions of the proposed system to achieve suitable SOFC performance [47].

3 Hydrogen production and CO_2 utilization via chemical looping

Fossil fuels and hydrocarbons are rich sources of Hydrogen, but these fuels are responsible for anthropogenic carbon emissions which is a huge problem humanity is facing. Due to the disadvantages of fossil fuels, other modes of hydrogen production have been researched widely. Electrolysis is used for water splitting into hydrogen and oxygen with the reaction $2H_2O$ ---------> $2H_2 + O_2$, but the process is highly endothermic and requires a huge input of electricity. The main advantage of electrolysis is it is a renewable source for hydrogen production without any dangerous byproduct and it can easily integrate with the electricity storage option. But due to its low overall efficiency and high capital cost, it is considered the least preferred option for the commercial application.

Consequently, there is a demand to develop novel hydrogen production methodologies from hydrocarbons with the focus to lower production cost and CO_2 emissions along with comparable process efficiencies and H_2 yield. Recently, the development of methods to produce H_2 and CO has been reported. This involves the utilization of H_2O and CO_2 and to use of the stored lattice oxygen in the metal oxides as an oxidant for the process of steam methane reforming. This process is called chemical looping steam methane reforming.

3.1 Electrochemical process and chemical looping

Electrochemical processes have happened in the electrochemical cell that requires the input of some reactants and produces certain products. Electrochemical processes usually need input in the form of electricity. As electricity is already a transformed form of energy so the input of the electrochemical process is the secondary form of energy. There is an alternative to this process by using another form of energy as a driver for the transformation of reactants into products. This alternate option is named Chemical looping. To remain in the domain of renewables, it is possible to consider solar concentrated energy (CSP). In the case of chemical looping, we are considering solar energy as a driving force for the reactions, and solar energy is not a transformed or secondary form of energy like electricity. Therefore, it may become even more efficient than other electrochemical processes. So, the input of the chemical looping is not a secondary but a primary form of energy.

3.2 Chemical looping processes.

Loop closed of chemical reactions done to obtain some transformation of reactants into valuable products. This loop develops at different temperature levels. Some transformations happen at a low-temperature level while other reactions take place at high-temperature levels, depending on the thermodynamics of reactions at specified operating conditions. Transformation of reactants into products results in modification in enthalpy. This modification in enthalpy generates processes like endothermic or exothermic. This means that chemical looping processes can work in both directions.

3.2.1 Working principle of chemical looping cycle

Chemical looping is nothing but comprised of a loop of reactions. In most cases, this loop exploits the characteristics of some materials to assume different oxidation states of materials.

- These materials can exchange oxygen in a series of reactions or a loop of actions.

- In some steps, these materials lose oxygen, this is called reduction.
- In other steps, these materials recombine oxygen which is oxidation.

So, in the end, chemical looping is a sequence of redox reactions of specified materials that can exchange oxygen because they can be assumed to have different oxidation states of the materials. For example, splitting of H_2O and CO_2 can take place via reduction into H_2 and CO. This is not an electrochemical process, but it is a chemical looping process driven by high-temperature solar heat. The flow of mixtures of chemical species containing carbon can be de-carbonized using chemical looping reactions. One more example of the simplest two-step chemical looping is given below.

In the first step, there is a situation that metal oxide is at a high level of oxidation. This metal oxide with a high oxidation level is ready to develop reduction reactions in the presence of high temperature (CSP). After the reduction step, the metal oxide comes out with a lower oxidation state. Important thing is that this lower oxidation state metal has already another set of oxygen with a different oxidation state. The lower oxidation state is ready to accept oxygen. At this point, the question is, where does this oxygen come from to absorb and to dive into lower oxidation state metal. There are two possibilities for that. One possibility is to provide water molecules and the result is the delivery of hydrogen molecules. Another possibility is to offer it a CO_2 molecule so that it may exchange oxygen with metal oxide and provide us CO. Metal oxide at a lower oxidation state move back towards a higher oxidation state after accepting oxygen molecule. The result is that we get a mixture of hydrogen and CO that is at high Gibbs energy. The above discussion concludes that everything in the chemical looping is based on the exchange of oxygen.
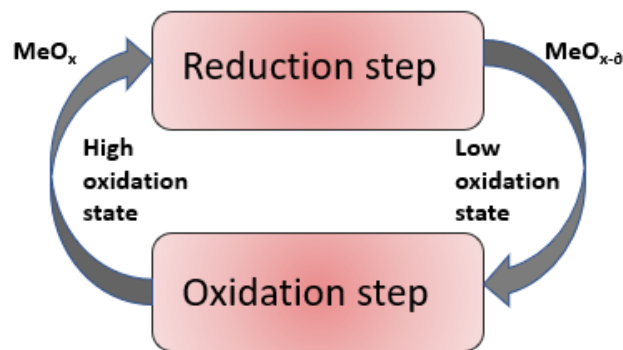
Figure 3.1: Most simple concept of two step chemical looping

Metal oxide at a higher state of oxidation

Reduction step: $$MeO_x \rightarrow MeO_{x-\delta} + 0.5\delta O_2 \qquad (3.1)$$
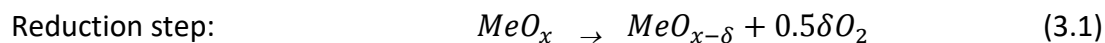
Metal oxide at a lower state of oxidation

Oxidation step: $$MeO_{x-\delta} + \delta H_2O \rightarrow MeO_x + \delta H_2O \qquad (3.2)$$

Oxidation step $$MeO_{x-\delta} + \delta CO_2 \rightarrow MeO_x + \delta CO \qquad (3.3)$$
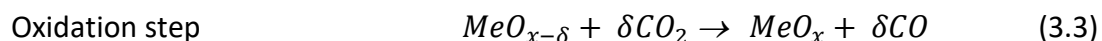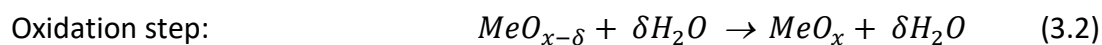
3.3   Materials used for chemical looping.

The process of chemical looping can be operated with different types of materials. The class of such materials is classified into two categories.

3.3.1   Volatile materials.

It is comprised of a group of materials that are volatile during the high-temperature reduction step. These materials undergo a phase change from solid to liquid during the reduction step. The reduced metal is usually in the vapor phase and has a lower boiling temperature as compared to the corresponding metal oxide. So, it needed rapid cooling so that released oxygen may not recombine with the reduced metal. One of the advantages of volatile materials is that their reduction is stoichiometric which means such material loses all the oxygen during the thermally driven reduction step. While drawback of such materials is that the thermal reduction of such oxides takes place at very high temperatures making the process highly endothermic so that it may become volatile. For example, ZnO reduces stoichiometrically at almost 2000°C. Due to high-temperature requirements, this increases the cost of expensive and special materials for the reactors.

Reduction at 2000°C $\hspace{3cm}$ $ZnO \rightarrow Zn + \frac{1}{2}O_2$ $\hspace{2cm}$ (3.4)

Another disadvantage associated with volatile materials is the risk of the recombination process in which released oxygen reconnect back to the reduced metal. To avoid this, fast cooling is a requisite step for volatile oxygen carriers. After the reduction step, separation of reduced metal is very difficult due to different phases that enhance the complexity of the whole cycle.

3.3.2   Non-volatile materials

These materials operate at a lower temperature as compared to volatile materials and do not change the phase (either thermally or chemically) during the high-temperature reduction step. As these oxygen carriers do not undergo phase transformation and remain solid during the whole thermochemical cycle so there no rapid cooling is mandatory.

Separation of the reduced metal is not very difficult due to the absence of phase transformation, so it makes the whole cycle less complex as compared to volatile metal oxides.

The operating temperature range for such materials is 1200-1500°C. The negative aspect of these materials is that reduction is performed non stoichiometrically and these materials lose less oxygen as compared to the previous class of materials. This behavior is very interesting for the researchers.

3.4   Cerium oxide CeO$_2$.

Ceria is the type of oxygen carrier that undergoes reduction step without phase change and releases oxygen non stoichiometrically. It is partially reduced during the high-temperature reduction step. But the extent of reduction depends on the temperature as well.

Cerium dioxide also called ceria since 1980 is a redox material with different oxidation states and has been widely used as catalysts in chemical industries, especially for energy and Hydrogen production processes. It has two oxidation states 4^+ and 3^+ depending upon the temperature. The catalytic performance of ceria is highly dependent on the extent of easiness of changing its oxidation state among these two oxidation states. This shifting of oxidation states is interconnected

with its capability to discharge and gain oxygen called oxygen storage capacity. Ceria is one of the most interesting and potential materials because of its

- minimal sintering effects and high coalesce resistance
- good kinetics and high cyclic efficiency.
- Mechanical resistance

Research conducted by Abanades stated that at thermal reduction temperature of 2000 °C cerium oxide (with oxidation state 4^+) reduced stoichiometrically into cerium (with oxidation state 3^+). But at a temperature less than 2000 °C, cerium oxide reduced non stoichiometrically and generated products that have an oxidation state between CeO_2 and Ce_2O_3. It can also be explained that at 2000 °C, ceria exhibits stoichiometric reduction but at the same time it offers problems of sublimation, high volatility, and high cost to attain an excessive temperature of 2000 °C coupled with high thermal resistive reactor material. On the other hand, at a thermal reduction temperature less than 2000 °C, ceria shows non-stoichiometric reduction along with minimizing the risks of sublimation and costly material properties. It has made researchers attribute their effort towards lower reduction temperature, around 1300-1500 °C, instead of material modification. This interesting behavior of ceria has been demonstrated by Eq 3.5-3.6 showing both stoichiometric and non-stoichiometric characteristics respectively. While Eq. 3.7-3.8 shows the oxidation step of reduced ceria comprised of water and carbon dioxide splitting.

Stoichiometric reduction $\qquad 2CeO_2 \; \rightarrow \; Ce_2O_3 + 0.5O_2 \qquad$ (3.5)

Non-stoichiometric Reduction $\qquad CeO_2 \; \rightarrow \; CeO_{2-\delta} + 0.5\delta O_2 \qquad$ (3.6)

Water splitting $\qquad CeO_{2-\delta} + \delta H_2O \; \rightarrow \; CeO_2 + \delta H_2O \qquad$ (3.7)

CO2 splitting $\qquad CeO_{2-\delta} + \delta CO_2 \; \rightarrow \; CeO_2 + \delta CO \qquad$ (3.8)
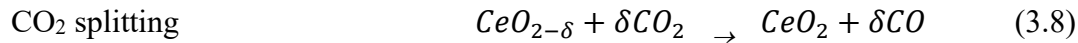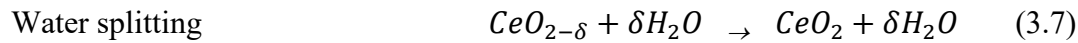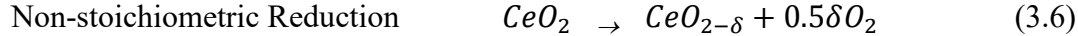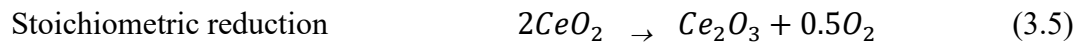
3.4.1 Methane reduced chemical looping in the presence of ceria

As explained that two-step cycle can be first ignited by the reduction step. In most cases, the endothermic reduction step is conducted at a very high temperature in the range of 1400-1600 °C. On the other hand, the exothermic oxidation reaction is driven at a low temperature (900-1100 °C) as compared to the previous reduction step. It represents a huge temperature difference between these two reactors that shifts the process towards complexity in real plants. So, minimizing the reduction temperature is crucial and a huge challenge for researchers. Therefore, to drive the reduction step, there are two possible options: the first one is focused on thermochemical cycle driven by solar, which means to reduce the metal thermally by applying direct heat from concentrated solar power, is not favorable way as it requires a huge temperature and specialized mechanical design of the reactor: the second one is focused on methane operated thermochemical redox cycle means to reduce the metal chemically by utilizing chemical energy embodied in methane.
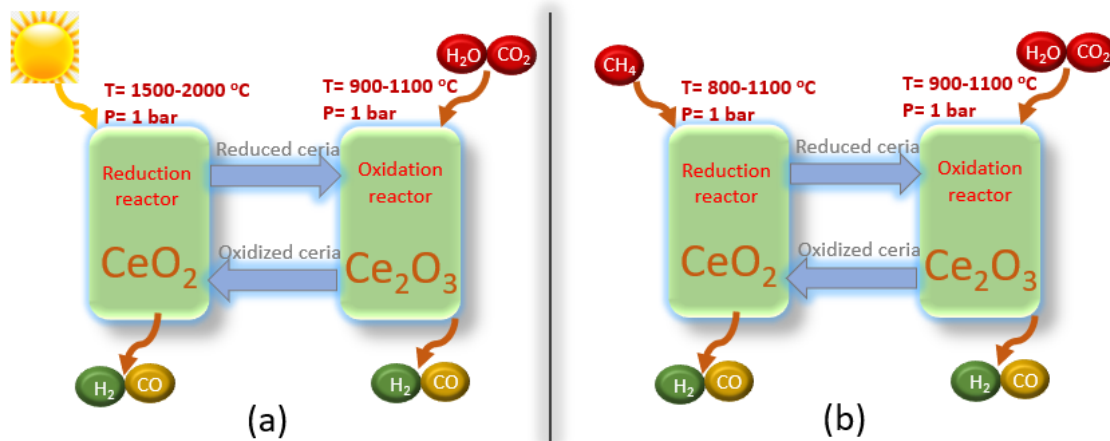
Figure 3.2: Schematic of chemical looping with simultaneous splitting of H2O and CO2 (a) Ceria reduction in the presence of solar energy-requiring high temperature (b) Ceria reduction in the presence of methane requiring less temperature.

The option of coupling a two-step cycle with methane seems intriguing perspective as it only reduces the reduction temperature but is also benevolent to reactor material, generates less temperature difference between reactors and temperature control is less difficult. This approach of combining thermochemical reduction and methane reduction has been verified in the literature. Welte et all conducted an experimental approach and used a thermal solar reactor of 2kW. The main objective was to reduce the ceria [48]. In that study, they adopted the same approach of combining thermochemical redox reduction of ceria and methane reforming and found products in the form of syngas having a molar ratio of 2. Farooqui et all followed the same approach and coupled chemical-looping with the oxyfuel-fired power plant. In his study, they investigated the kinetics of ceria reduced with methane by using different concentrations of methane [19]. Figure 3.2 depicts the ceria reduction with thermochemical redox cycle and methane-driven redox cycle.

3.4.2 Literature review on ceria based thermochemical cycles

Several other researchers devoted their effort to solar fuel production and adopted many approaches to produce the most popular solar fuel, syngas.

For example, Krenzke et al. studied syngas production methods by combining two different pathways that are methane reduction via ceria and partial oxidation of methane. In that research, they found that coupling of ceria cycle with partial oxidation of methane (POM) tends to reduce the endothermic ceria reduction temperature as below as 950 °C. Furthermore, they also considered the non-stoichiometric nature of ceria in the oxidation phase and determine the performance of the ceria- POM system as a function of concentration temperature and non-stoichiometric nature [49].

William et al. studied thermodynamic and kinetic assessment of the ceria redox cycle particularly for hydrogen production. They found that ceria undergoes endothermic reduction step at a temperature range of 1500-1600 °C and exothermic oxidation step at around 800 °C. Although

due to the non-stoichiometric style of ceria, they concluded that hydrogen is produced in the range of 8.5-11.8ml per gram of ceria introduced to cycle [50].

Welte et al conducted an experimental study and utilized a $2kW_e$ solar reactor to produce solar syngas. In their experiments, they coupled the ceria redox cycle with methane reforming. They concluded that at maximum solar flux, 89% methane conversion is achieved at a reduction temperature of 1300 °C. Furthermore, they found the maximum non-stoichiometric ceria reduction extent to be 0.25 [51].

Abanades et al. conducted experimental work on hydrogen production by using ceria thermochemical redox cycle and water splitting. Ceria reduction was achieved in a solar reactor at operating conditions to be temperature, 2000 °C and pressure, 0.1-0.2 bar. Ceria oxidation step was developed in a fixed bed reactor at a temperature range of 400-600 °C. It must be noted that they did not use methane to facilitate ceria reduction [52].

Warren et al. studied the influence of partial oxidation of methane on the ceria thermochemical redox cycle by adopting kinetics assessment of the ceria-POM system. Endothermic ceria reduction was performed at a temperature range of 750-1100 °C in the presence of methane. In that study, they found that the reaction rate is directly proportional to the methane partial pressure [53].

3.5 Perovskites and double Perovskites.

Perovskites are calcium and titanate-based oxide materials comprised of calcium titanate having a crystal structure. The general formula for the perovskites is $A_1B_1O_3$. Here A belongs to alkali-earth metals while B belongs to transition materials in the periodic table. For example, $Ln_{0.6}Sr_{0.4}Mn_{0.6}Al_{0.4}O_3$ and $Ln_{0.625}Ca_{0.375}Mn_{0.5}Cr_{0.5}Al_{0.4}O_3$. In these examples, manganese is doped with aluminum and chromium, respectively. The general formula for the double perovskites is $A_1B_1O_6$. In this case, we have six atoms of oxygen. One of the examples of double perovskite materials is $Sr_2FeNi_{0.4}Mo_{0.6}O_6$.

4 Methodology

The current study evaluates a comparative technical analysis of the state-of-the-art solid oxide fuel cell and proposed solid oxide fuel cell with its off-gas utilization and carbon capture coupled with chemical looping plant along with simultaneous splitting of H_2O and CO_2. Figure 4.1 shows a simplified process flow diagram of the proposed CL-SOFC system by recirculating a fraction of anode exhaust towards the oxidation reactor of chemical looping and by utilizing an oxyfuel afterburner. The syngas storage system has been employed so that the proposed plant may operate 24 hours a day. Based on the literature reported CeO_2 has been chosen as a source of oxygen.
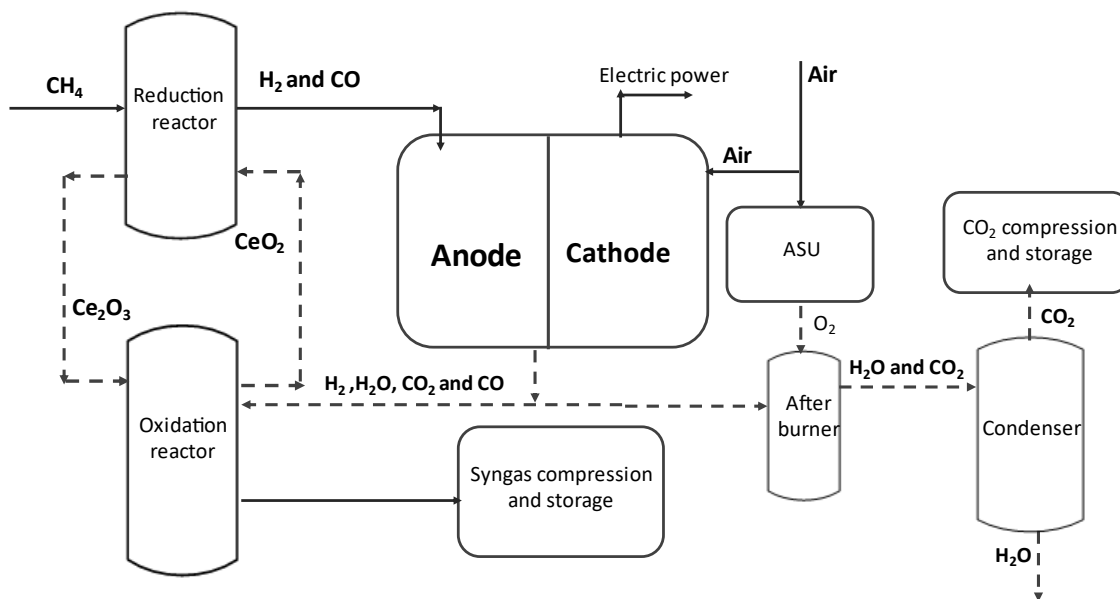
Figure 4.1: Simplified process flow diagram of CL-SOFC system with syngas storage and CO_2 capture

To investigate the proposed plant with the benchmark solid oxide fuel cell, methane reduction in the presence of ceria has been studied as a substitute option for thermal reduction. As explained earlier, ceria undergoes stoichiometric reduction thermally at very severe operating conditions of temperature around 2000-2500 °C and pressure around 0.1-0.2 bar [54]. Besides this at a low temperature of less than 2000 °C in a range of 1300-1500 °C, ceria is reduced in a non-stoichiometric manner. Although ceria reduction is not stoichiometric, it tends to reduce fully at suitable operating conditions. Currently, Warren et al. conducted an experimental study on the kinetics of ceria reduction and found that ceria can reduce stoichiometrically at a temperature more than 900 °C [55]. Although very little literature is available on the experimental research claiming stoichiometric ceria reduction, therefore this assertion needs more insight investigations and deep research.

In the present research, a redox pair of cerium oxide and cerium dioxide for the reduction of ceria has been considered to predict the performance of the proposed plant. Consequently, the chemical looping cycle comprising of methane ceria reduction and its consecutive oxidation with SOFC off-

gas mainly comprising of water and carbon dioxide splitting are conceptualized with the following reactions.

$$2CeO_2 + CH_4 \rightarrow Ce_2O_3 + 2H_2 + CO \qquad (4.1)$$

$$Ce_2O_3 + H_2O \rightarrow 2CeO_2 + H_2 \qquad (4.2)$$

$$Ce_2O_3 + CO_2 \rightarrow 2CeO_2 + CO \qquad (4.3)$$
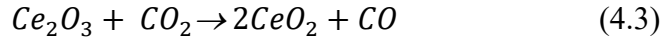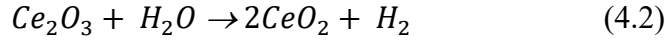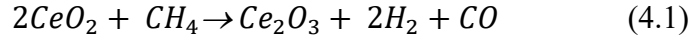
During the first step of chemical looping Eq. (4.1), metal oxide being at a higher oxidation state is reduced by methane and approaches to a lower oxidation state. While during the second step of chemical looping, reduced ceria is oxidized back to a higher oxidation state by receiving oxygen from H_2O and CO_2 and providing CO and H_2 as described by Eq. (4.2) and (4.3) reactions. The oxidized ceria at a higher oxidation state is sent back to the reduction reactor to complete the loop. In this way, syngas with varying composition is produced in both steps of chemical looping. Operation of the proposed plant and benchmark SOFC is initiated with the fuel of 1 kmol/hr. CH_4 as a basis of the current study. A specified amount of syngas is introduced to the SOFC system, remaining part is sent to the syngas storage section. An oxyfuel afterburner is inserted into the plant to facilitate carbon capture. Based on the choices made, the technical performance of the proposed chemical looping-SOFC combination is proceeded as per the methodology shown in figure 4.1.

It must be emphasized that several alternate options for plant configurations, varying in design, methods, operating conditions, coupling of chemical looping unit and further usage, and storing of syngas produced from both reduction and oxidation reactors of chemical looping were scrutinized. Although all possible options of curiosity could not be explained within the range and limitations of the current thesis research. The modelling of proposed CL-SOFC and state-of-the-art SOFC are presented in Aspen plus simulation software and compared the performance of both systems. An excel worksheet was created exclusively for evaluation and interpretation of the data within the scope of the present work.

The electrical performance of the solid oxide fuel cell is examined by Eq. (4.4).

$$Electrical\ Efficiency = \eta_{el} = \frac{W_{net}}{m_{fuel}LHV} \qquad (4.4)$$

4.1   Chemical looping sensitivity analysis and performance calculation

The process assessment, technical performance, and sensitivity analysis of chemical looping operating parameters are encapsulated within this thesis. To predict the performance of the chemical looping system, three efficiencies (overall CL system efficiency E_1, waste gas splitting efficiency E_2 and solar to fuel efficiency E_3) are calculated as per Eq. (4.5), (4.6), and (4.7).

$$E_1 = \frac{LHV_{H_2}(\dot{m}_{red,H_2}+\dot{m}_{oxi,H_2})+ LHV_{CO}(\dot{m}_{red,CO}+\dot{m}_{oxi,CO})}{(\dot{m}_{CH_4}LHV_{CH_4}+\dot{Q}_{Red}+\dot{Q}_{CH_4}+\dot{Q}_{H_2O+CO_2}+\dot{Q}_{ceria,1})_{need}-(\dot{Q}_{oxi}+\dot{Q}_{syngas}+\dot{Q}_{ceria,2})_{release}} \tag{4.5}$$

$$E_2 = \frac{\dot{m}_{CO}LHV_{CO}+ \dot{m}_{H_2}LHV_{H_2}}{(\dot{m}_{CH_4}LHV_{CH_4}+\dot{Q}_{Red}+\dot{Q}_{CH_4}+\dot{Q}_{H_2O+CO_2}+\dot{Q}_{ceria,1})_{need}-(\dot{Q}_{oxi}+\dot{Q}_{syngas}+\dot{Q}_{ceria,2})_{release}} \tag{4.6}$$

$$E_3 = \frac{LHV_{H_2}(\dot{m}_{red,H_2}+\dot{m}_{oxi,H_2})+ LHV_{CO}(\dot{m}_{red,CO}+\dot{m}_{oxi,CO})-\dot{m}_{CH_4}LHV_{CH_4}}{Q_{sol}} \tag{4.7}$$

The first efficiency E_1 considers the amount of syngas produced parallel in both reactors based on 1 kmol of CH$_4$ introduced initially, $\dot{m}_{CH_4}$ is the mass flow rate (kg/sec) of methane introduced initially: $\dot{m}_{red,H_2}$ and $\dot{m}_{oxi,H_2}$ is the mass flow rate (kg/sec) of hydrogen produced in both reactors: $\dot{m}_{red,CO}$ and $\dot{m}_{oxi,CO}$ is the mass flow rate (kg/sec) of CO produced in both reactors: $\dot{Q}_{Red}$ is the heat (kW) required for activating the endothermic reduction reaction; $\dot{Q}_{CH_4}$ and $\dot{Q}_{H_2O+CO_2}$ is the amount of heat (kW) required to preheat the methane and waste gasses: $\dot{Q}_{oxi}$ is the heat released from the exothermic oxidation reactor of the CL system: $\dot{Q}_{ceria,1}$ is the amount of heat needed for the pre-heating of fresh ceria that is introduced to the reduction reactor. $Q_{syngas=}$ $\dot{Q}_{red,syn} + \dot{Q}_{oxi,syn}$ is the amount of heat recovered from the exit syngas produced from both reactors: $\dot{Q}_{ceria,2} = \dot{Q}_{red,Ce_2O_3} + \dot{Q}_{CeO_2}$ is the amount of heat recovered from reduced ceria, before it enters into the oxidation reactor and oxidized ceria before it recirculated back towards the reduction reactor. Furthermore, heat losses are not considered in the efficiency calculation.

The second efficiency E_2 considers the only amount of syngas produced in the oxidation reactor by using a specified amount of SOFC off the gas. This efficiency shows the performance of the ceria CL cycle based on the thermochemical splitting of waste gas.

The third efficiency (E_3) considers syngas production based on solar energy and therefore it is called solar-to-fuel efficiency. It can be defined as the ratio of the difference between the lower heating value of fuel produced and CH$_4$ to the total solar energy required to activate the thermochemical cycle.

To evaluate optimal operating conditions of the chemical looping section, a comprehensive sensitivity analysis is conducted. This analysis is mainly based on temperature, pressure, and feed molar ratio applied on the endothermic reduction and exothermic oxidation reactor.

For the reduction and oxidation reactor of chemical looping, three parameters are varied, and the equilibrium composition of the product stream and three performances discussed above in Eq. (4.5), (4.6), and (4.7) are examined. Table 4.1 illustrates the range of varying parameters. Furthermore, it must be considered that the present study is mainly emphasized the theoretical thermodynamic calculation with no focus on the kinetic studies.

Table 4.1: Range of varying parameters employed in a sensitivity analysis.

Varying parameter	range	Constant parameter
T_{red}	500-2000°C	$P_{red} = 1$ bar; $\dot{n}_{red} = 0.8,$
P_{red}	0.1-2 bar	$T_{red} = 800 \ °C; \dot{n}_{red} = 0.8,$
$\dfrac{CH_4}{CeO_2}$	0.1-2	$T_{red} = 800 \ °C; P_{red} = 1$ bar
T_{oxi}	500-2000°C	$P_{oxi} = 1$ bar; $N_{oxi} = 0.62,$
P_{oxi}	0.1-2 bar	$T_{oxi} = 800 \ °C; N_{oxi} = 0.62$
N_{oxi}	0.1-2, kmol/hr.	$T_{oxi} = 800 \ °C; P_{oxi} = 1$ bar

4.2 Key performance indicators

There are certain parameters for the assessment based on carbon abatement and energy performance and retrofit ability in plant designing. These parameters are called key performance indicators KPI. A wide range of parameters including SPECCA (specific primary energy consumption for carbon capture and avoided), CO_2 captured ratio, CO_2 utilized ratio, CO_2 avoided ratio, is chosen to make a comparison of the proposed plant with a state-of-the-art SOFC system. Although it is worthy important to note that the proposed system does not consider the retrofitting of the current state-of-the-art solid oxide fuel cell model. Certain KPI parameters are identified and explained below.

4.2.1 SPECCA

It is a parameter that is widely used for the assessment of energy penalty and is called Specific Primary Energy Consumption for CO_2 Avoided (SPECCA). It is used to compare different CO_2 capture technologies based on energy consumption. It calculates the amount of primary energy required to avoid CO_2 emission into the atmosphere. It is the ratio of the ''difference of equivalent primary energy consumption of proposed CL coupled SOFC with CO_2 capture and benchmark SOFC without CO_2 capture'' to the ''difference of equivalent CO_2 emissions from the benchmark SOFC without CO_2 capture and proposed CL coupled SOFC with CO_2 capture''.

SPECCA can also be defined as an increased quantity of equivalent primary energy consumption for equivalent CO_2 emission avoided. It is defined in Eq. (4.8).

$$SPECCA = \frac{HR_{eq} - HR_{eq,ref}}{e_{CO2,eq,ref} - e_{CO2,eq}} \qquad (4.8)$$

Equivalent specific primary energy consumption is comprised of direct and indirect specific primary energy consumption. The Direct specific primary energy consumption is the amount of

energy (LHV) directly obtained from the fuel in the form of methane multiplied with its mass flow rate.

$$HR_{eq} = HR_{direct} + HR_{indirect} \qquad (4.9)$$

$$HR_{direct} = \dot{m}_{fuel}.LHV_{fuel} \qquad (4.10)$$

4.2.2 CO2 captured ratio (CCR)

CO_2 captured ratio is a very important KPI for plants involving CO_2 captured processes. It is defined as the ratio of CO_2 mass flow rate (kg/sec) captured $\dot{m}_{CO_2}$ to the mass flow rate of total CO2 $\dot{m}_{CO_2}$ (kg/sec) generated within the system. Eq. (4.11) represents the carbon captured ratio.

$$CCR = \frac{(\dot{m}_{CO_2})_{capture}}{(\dot{m}_{CO_2})_{generated}} \qquad (4.11)$$

CO_2 generated is the total flow rate of CO_2 achieved after oxyfuel combustion of the anode exhaust. It is the amount of CO_2 that is obtained after condensing water and in general, it is originating from the fuel used in the reduction reactor of chemical looping. While on the other hand, CO_2 captured represents the total amount of CO_2 captured.

4.2.3 CO2 utilized ratio

Another KPI is introduced in the present study that is called CO_2 utilized, because during the morning operation around 49% of generated CO_2 is recirculated back towards the oxidation reactor of CL and split thermochemically. It is the ratio of CO_2 mass flow rate (kg/sec) utilized in CL $\dot{m}_{CO_2}$ to the mass flow rate of total CO_2, $\dot{m}_{CO_2}$ (kg/sec) generated at the anode output. It is given as Eq. (4.12)

$$UCR = \frac{(\dot{m}_{CO_2})_{CL}}{(\dot{m}_{CO_2})_{generated}} \qquad (4.12)$$

4.2.4 CO2 storage ratio (SCR)

Another important KPI is the CO_2 stored. It is the ratio of CO_2 mass flow rate (kg/sec) obtained at the outlet of oxyfuel combustion to the mass flow rate of total CO_2, $\dot{m}_{CO_2}$ (kg/sec) generated at the anode output. The remaining amount of CO_2 is forwarded towards the compression section, where it is pressurized to 150 bar and stored permanently. It is given below as Eq. (4.13).

$$SCR = \frac{(\dot{m}_{CO_2})_{CL}}{(\dot{m}_{CO_2})_{generated}} \qquad (4.13)$$

4.2.5 CO2 avoided

The CO_2 avoided from the anode off-gas examines the amount of directly emitted CO2 from the anode exhaust. It is given below as Eq. (4.14).

$$AC_{fg} = \frac{e(fg,ref) - e(fg)}{e(fg,ref)} \qquad (4.14)$$

where, $e(fg, ref)$ is the specific CO_2 emission in the benchmark reference SOFC model without CO2 capture and $e(fg)$ represents the specific CO2 emission from the proposed plat SOFC anode off-gas.

The plant proposed in this study incorporates the following benefits.

- Fossil fuel CH_4 generates syngas with a larger fraction of hydrogen that is fueled to solid oxide fuel cells.
- In the proposed system, fuel is not directly in contact with the air, so the production of pollutant gases NO_X, SO_X is avoided.
- The introduction of CH_4 reduces the reduction temperature of ceria.
- The plant can separate and capture CO_2 while generating electrical power.
- Syngas storage system enables the plant to operate 24 hours a day.
- The performance of the system is significantly enhanced when a portion of anode off-gas of SOFC is refluxed to the oxidation reactor of the CL system.

5 Model description, system development, and analysis

This section describes the model description and development of state-of-the-art- solid oxide fuel cells followed by a detailed description of the proposed system.

5.1   Benchmark SOFC system description

Description of the benchmark SOFC refers to figure 5.1. Biogas is applied in the SOFC benchmark system with a composition having 60% methane and 40% CO_2. Peng-Robinson's (PENG-ROB) equation of state has been chosen as the base method that is suitable for modeling thermochemical gas and liquid processes at certain operating conditions within the SOFC system. Flowsheeting options in Aspen PLUS contain two useful tools that are design specifications and calculators. Four calculators have been adopted for proceeding calculation of air flow rate, current produced, efficiency. Two design specifications are employed for the precise calculation of steam to carbon ratio and required air flow rate. Fuel in the form of methane and carbon dioxide is introduced in the anodic region, loaded with Ni catalyst in the presence of high temperature. There are conditions to activate negative reactions of carbon depositions in the anodic compartment. These reactions are given as Eq. (2.19), (2.20), and (2.21) and the preventions for carbon deposition are given as Eq. (2.22), (2.23), and (2.24)

The first explanation of each process elucidated has been described, followed by a more comprehensive detail on every single component based on input-output, operating conditions, and constraints considered for the model. The simulation model has been divided into five distinct parts, which are the compressions section, heating section, internal reforming, solid oxide fuel cell, and heat recovery section.

- The compression section is mainly considered to increase the pressure of biogas and air with the help of BIO-COMP and AIR-COMP compressors respectively.

- The heating section is adapted to preheat the fuel and air by using BIO-HX and AIR-HX. After that fuel will be moved towards further processing and air will move towards the cathodic compartment of SOFC.

- Biogas fueled SOFC system has been considered that consists of 60% CH_4 and 40% CO_2 and are supposed to be internally reformed within SOFC. However, in the modeling, a separate component REFORMER has been adopted. Reactions involved in the reforming are given below.

- SOFC section is the heart of the proposed system. It is comprised of the anode, cathode, and a SOFC heat exchanger and is demonstrated by components SOFC-AN, SOFC-CATH AND SOFC-HX respectively.

- The heat recovery section is embodied with a burner and a couple of heaters. These components are represented by blocks named BURNER, BIO-HX2, AIR-HX2, and HRU.
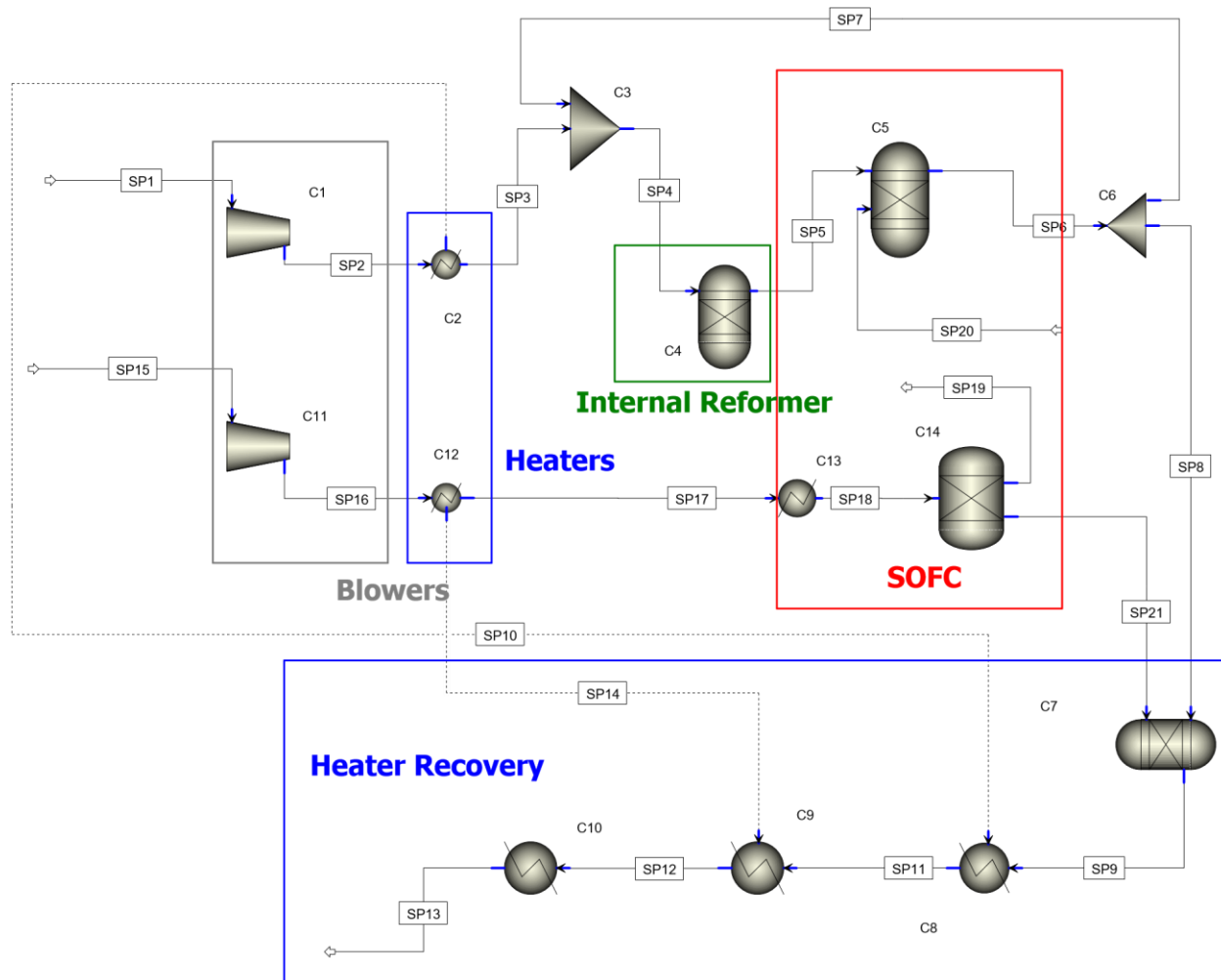
Figure 5.1: Process flowsheet of the solid oxide fuel cell simulation model in Aspen Plus

Figure 5.1 shows the Aspen plus simulation flowsheet of benchmark SOFC integrating all components. This section presents the state-of-the-art solid oxide fuel cell in detail. Organic waste is first processed through anaerobic digestion and converted into biogas. The resulting biogas is contaminated and moves further towards the cleaning section. As the scope of the present study is limited to biogas processing, therefore biogas production and cleaning are not considered in the modeling environment. Consequently, it is assumed that cleaned biogas enters the stream SP1 at ambient operating conditions.

For the smooth operation of SOFC, it is advantageous that methane must be converted into hydrogen and carbon monoxide and suppress the formation of undesirable species like atomic carbon. Therefore, a perfect internal reforming of fuel is desirable so that carbon formation within SOFC must be minimized. Generally, some design concepts prefer external reforming of methane as it maximizes hydrogen production and lowers carbon growth inside the SOFC system. As explained earlier, among different hydrogen generation processes, steam reforming is highly suitable as it offers the highest hydrogen generation yield. Though, internal reforming is embodied with carbon formation and deposition at specified operating conditions in the anodic compartment of SOFC. This leads to the damaging of the SOFC system. Carbon deposition is very hazardous

for the soft operation of SOFC, it suppresses the catalytic activities of catalyst and covers the anode porous structure.

As is demonstrated in figure 5.1 that stream SP1 containing biogas is an input to the compressor C1 with an isentropic efficiency of 90% and exit with a discharge pressure of 1.2 bar. Air at ambient conditions reaches the compressor C11 through stream SP15 which increases air pressure until 1.2 bar. The pressurized biogas reaches the heater C2 through stream SP2 which increases its temperature until 650 °C. The pressurized air reaches heater C12 via stream SP16 that preheats the air until 650 °C. Preheated air approaches SOFC cathode heat exchanger C12 through stream SP17 that increases its temperature until 800°C. The output of the cathode heat exchanger enters the separation block C14 via stream SP18 which separates oxygen from the air.

Heated biogas reaches the mixture C8 through stream SP3 and recirculated species reach the mixer through stream SP7. The product from the mixer reaches the reformer C4 that is operated at 800°C. The reformer is characterized as an isothermal GIBBS reactor. In the reformer, steam methane reforming (SMR) reaction occurs according to Eq (1). and it converts the incoming biogas into a thermodynamic mixture of H_2, CO, and unreacted CH_4. As SMR requires water so it is provided with stream SP7 through a recirculation loop. Syngas mixture enters the SOFC anode C5 and pure oxygen reaches the anode through stream SP20. Reactions take place in SOFC anode according to Eq. (2.17) and (2.18) and electric power is produced. Besides that, a mixture mainly comprised of H_2O and CO_2 is achieved.

Product of SOFC anode reaches splitter C6 through stream SP6 which splits its input into stream SP7 and SP8 based on the results of Design Specs. Stream SP7 containing certain fractions of anodic products ($H_2O/CO_2=2$) is recirculated back to avoid carbon deposition where it is introduced with incoming heated biogas. Stream SP8 reaches burner C7 and air with depleted oxygen reaches through the stream SP21. Burner is modeled as an adiabatic reactor that converts all the chemical energy into temperature increase. The product from the burner reaches the cooler C8 and C9 through SP9 and SP10 respectively. Part of the heat is utilized to preheat the biogas and ambient air through stream SP10 and SP14 respectively. The output of the cooler C9 is still at a high temperature that can be further utilized for useful purposes.

5.1.1 Benchmark SOFC model development
The present system consists of a benchmark SOFC module that is mainly comprised of two main components, anode, and cathode. The recovered heat from the system is gained as a thermal output and used in any other part of the designed system. To perform modeling of the steady-state solid oxide fuel cell, Aspen PLUS V11 software has been considered by adopting internal build-in functions, components, and thermodynamic database. These widespread databases offer a variety of physical and chemical properties of species and mixtures over a broad range of operating conditions [23]. Numerous assumptions have been made to carry out the modeling of complex phenomena incarnated in electrochemical reactions associated with the SOFC system. These assumptions are given below.

- Air feed to the cathodic compartment consists of 21% oxygen and 79% nitrogen.

- All components of input fluids involved in the SOFC system behave as ideal species.

- Contact resistance and pressure drops across the components have been neglected.

- Chemical reactions involved in the system are characterized by decreasing trends of Gibbs free energy.

- The proposed ASPEN model is considered zero-dimensional.

- Internal reforming of the fuel gains chemical equilibrium.

- Heat exchangers implicated in the SOFC model are taken ideal.

- Stack of fuel cell operates at normal operating conditions.

- Among all other species, only H_2 is electrochemically oxidized.

Reactions in the cathodic compartment of benchmark SOFC

On the cathode side, molecular oxygen is supplied. This oxygen is reduced into oxygen ions by absorbing two electrons as depicted by Eq (2.4). These negative ions are migrated from cathode to anode. The reactions at the cathode remain the same regardless of which fuel is used.

Reactions at anodic compartment of SOFC

On the anode side, fuel is supplied that may lead towards different types of reactions depending on the type of fuel feeding to the anode. Oxidation of fuel takes place at an anode by releasing electrons. These discharged electrons pass through external resistance to produce electrical power. Electrochemical reactions of hydrogen, carbon monoxide and methane at the anode are represented by Eq. (2.10), (2.11), and (2.12).

In the anodic compartment of the SOFC, there is a mixture of CH_4, H_2, CO, and CO_2, and this mixture is at almost 800 ^{0}C. So, there are all the conditions to activate the mechanism of reactions depicted in Eq (2.13), (2.14), (2.15), and (2.16).

Design constraints for the Aspen PLUS simulation model are tabulated in Table 1. Eq. (2.34) and (2.35) are adopted in the calculator block for the calculation of oxygen flow rate, current, power produced, etc.

Table 5.1: Design constraints for the Aspen plus simulation model for benchmark SOFC

Parameters	Values
Ambient temperature (°C)	25
Ambient pressure (bar)	1.013
Methane contents in fuel	60%
Fuel flow rate (kmol/hr.)	1.0

Faraday's constant (C/mol)	96485
No of electrons offered by fuel	8
SOFC anode operating temperature (°C)	800
SOFC operating pressure (bar) [24]	5
SOFC cathode heat exchanger temperature, °C	800
Minimum fuel inlet temperature, °C	650
Minimum air inlet temperature, °C	600
Voltage of single cell (V)	0.8
Steam-to-carbon ratio [25]	2
LHV of CH_4, kJ/kg	50085.1875
Air c_p, kJ/kg. k	1.005
Air compressor isentropic efficiency	0.9
Compressor mechanical efficiency	0.85
Fuel utilization [26–28]	0.85
Fuel compressor efficiency	0.90
DC/AC inverter efficiency [29,30]	0.95
Air molecular weight (g/mol)	27.2

As SOFC is a high-temperature cell so fuel utilization has been assumed that 85% of the fuel will be converted into respective products. It must be noted that if fuel utilization is considered more than 85%, then it will increase the oxygen quantity within the stack. This increased oxygen will further activate the Nickle oxidation and the cell will stop working. Therefore, the scope of the analysis considered 85% fuel utilization. F is the Faraday's constant, Z_{fuel} is the equivalent number of electrons embodied within the fuel. N_{O_2} is the oxygen flow rate in mol/sec. An efficient modeling environment is built by linking all the calculations with the simulation model. For that purpose, four calculators are considered in the Flowsheeting options of Aspen PLUS.

Calculator C-1 is created to import the molar flow rate of fuel based on initial assumptions (1kmol/hr.) and the input value is exported from to stream SP1 that is overwritten on it. The molar flow rate of fuel is utilized to calculate the total current produced by the SOFC system as mentioned in Eq. (5.11). The molar flow rate of oxygen is calculated based on Faraday's law depicted in Eq. (5.12). Pure oxygen reaches anode C5 through stream SP20. This stream is firstly initialized with 1 mol/sec of oxygen. Then oxygen flow rate determined in calculator C-1 is

exported to stream SP20. After that, a new calculator block C-2 is generated with two variables. One variable (NO2AN) is linked with an oxygen flow rate in-stream SP20 while the second variable (NO2CAT) is correlated with an oxygen flow rate in-stream SP19 which is the outlet stream of separation block C14. Both variables are set equal in the FORTRAN code and operation is executed. In this way required oxygen flow rate is achieved in separation block C14. As described earlier, the reactions in the anode are exothermic and the air is supplied to create thermal balance within the stack. Part of the exothermic heat is consumed in the reforming reactions in reformer block C4 though, the remaining heat is removed through the air. To know how much air is required in the cathode compartment, calculations are performed in calculator block C-3 Air calculations are achieved by using Eq. (2.28) and (2.30).

It is worthful to emphasizing that the main objective of sending air is to remove heat that is remained after supplying the endothermic reforming reaction.

To determine the system performance and identify the scope of development, the efficiency of the system plays a vital role. Therefore, efficiencies calculations are performed in calculator block C-4. These calculations are dependent on the definitions of system performances that are previously explained. Efficiency definitions are calculated as per Eq (4.4).

5.2   Proposed system description

A novel configuration (depicted in figure 5.2) of using fossil fuel methane for power, heat, syngas production, and carbon capture is proposed in this study. Ceria-based chemical looping is used to activate the methane reforming and thermochemical dissociation of waste gas. The PENG-ROB property method is adopted to simulate the proposed systems as it is highly recommended for the systems having solid species in equilibrium with the vapor-liquid system. It is also suitable for the processing of thermochemical processes.

The present study develops a new simulation model for the simultaneous ceria reduction and methane reforming employing ASPEN PLUS software and also performs numerous sensitivity analyses to explore the newly developed system.

This section describes the proposed system in detail. Figure 5.2 displays the schematic layout of the proposed plant. It depicts that there are five major subsystems of the proposed systems. Subsections involved in the entire proposed model are given as:

- ➢ Thermochemical Ceria-CL cycle that is initially activated with sun power, fossil fuel methane, and ceria.
- ➢ Solid oxide fuel cell that is fed with syngas production from the reduction reactor of ceria chemical looping.
- ➢ Oxy-fuel combustion unit that is introduced with SOFC anode off-gas in the presence of pure oxygen generated in air separation.
- ➢ Syngas storage and compression system. A specific amount of syngas is introduced to SOFC, while the remaining quantity is devoted to the storage section.
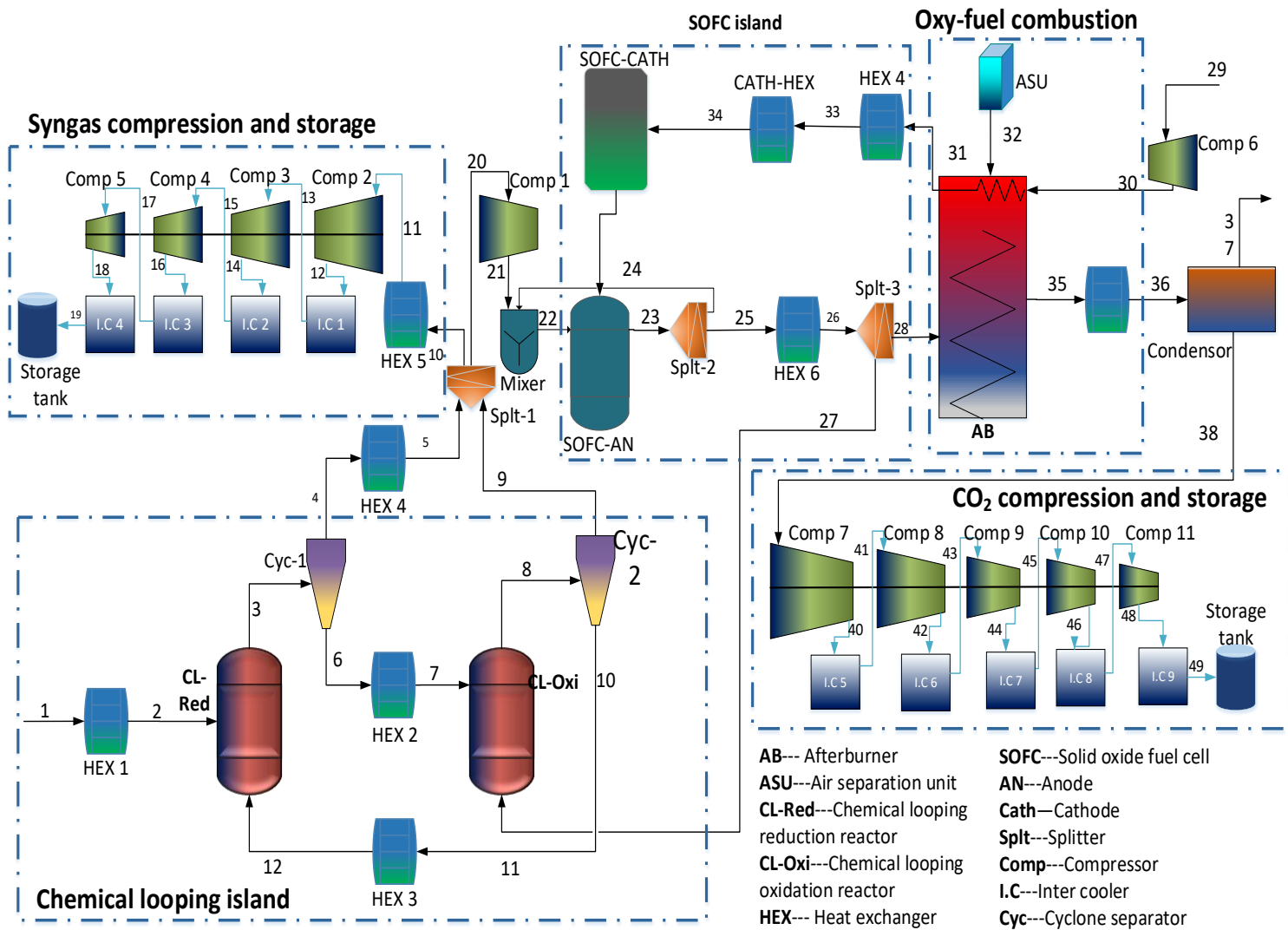
Figure 5.2:Schematic of the proposed two-step chemical looping integrated with solid oxide fuel cell, oxyfuel combustion, syngas, and CO₂ storage system for syngas, electricity, and thermal power generation.

➢ The carbon capture unit is employed pure carbon dioxide that is obtained as one of the products of the oxyfuel combustion unit followed by the cooling and condensing of the mixture.

Figure 5.3 depicts the ASPEN PLUS simulation flowsheet model integrating all the components involved in the proposed system and with the specification of each point accordingly. The proposed system is comprised of the following subsystems.
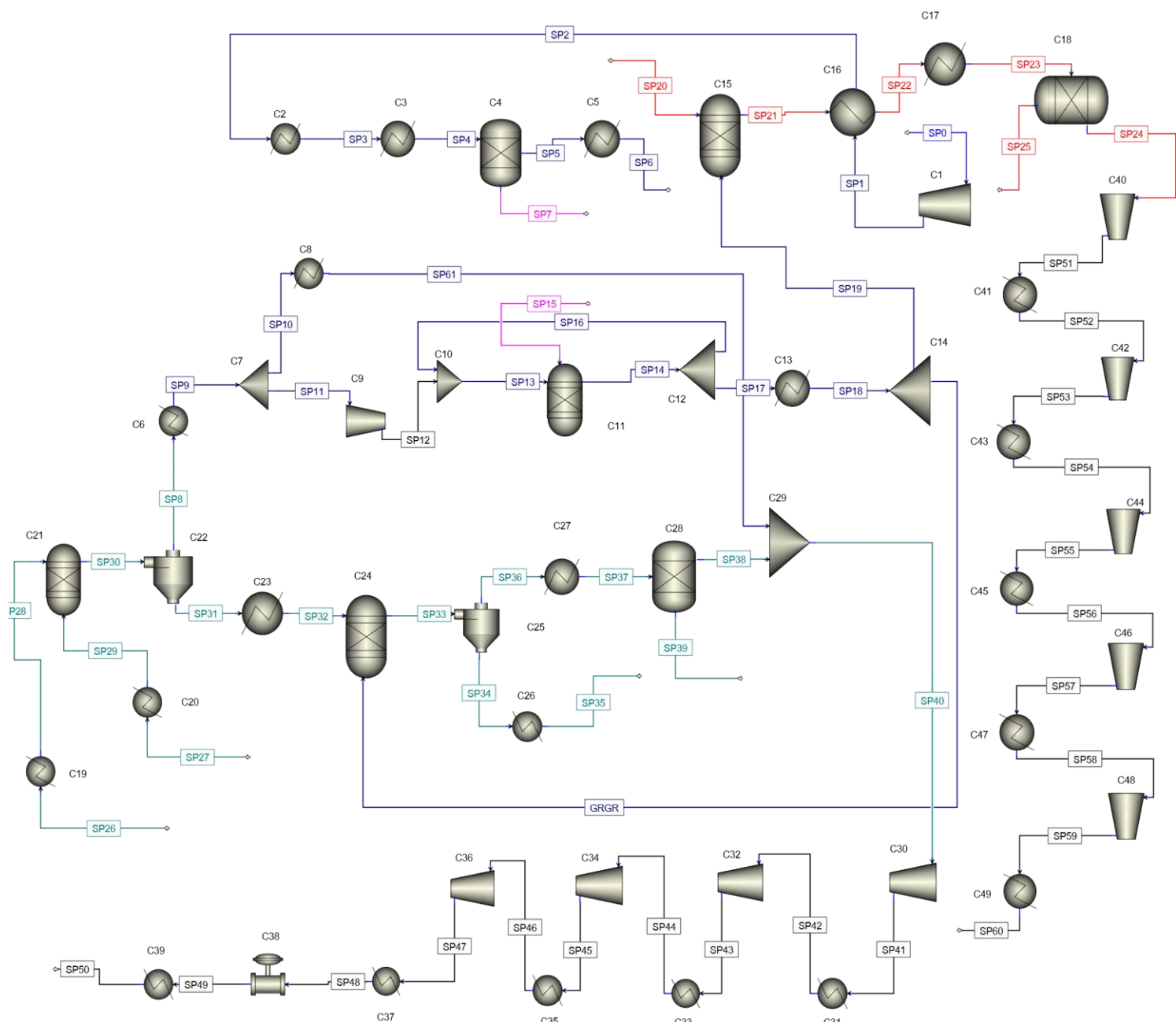
Figure 5.3: ASPEN PLUS simulation flowsheet of the proposed configuration

5.2.1 Ceria based thermochemical cycle

A detailed explanation of the proposed system is now reported and is referred to in figure 5.3.

The fossil fuel methane and ceria are preheated at 650 °C in the heat exchanger blocks C19 and C20. The preheated methane then reaches the chemical looping reduction reactor C21 through stream SP29 and the ceria reaches the reactor through stream SP28.

The product from the CL reduction reactor, mainly comprised of reduced ceria and syngas at around 800°C, reaches the first cyclone C22 through stream SP30 which separates reduced ceria from the reduction output stream from SP31 and leads the syngas to the heat exchanger. The reaction product mixture except reduced ceria reaches the heat exchanger C6 through stream SP8 and cools down until 650°C. The splitter C7 is used to split the incoming syngas mixture via stream SP9. Around 40% of the produced syngas (0.91 kmol/hr.) are allowed to move in the stream SP11 to further enter the SOFC island and the remaining 60% syngas (1.3 kmol/hr.) is dedicated to syngas storage section via stream SP10.

Reduced ceria coming out of the first cyclone through stream SP31 reaches the heat exchanger block C23 to reduce its temperature until 650°C. Waste gas mainly comprising of H_2O and CO_2 at 650°C coming through stream SP61 is entered in the CL oxidation reactor C24 and reduced ceria reaches the reactor through stream SP32. Thermochemical dissociation of the waste gas occurred in the CL oxidation reactor giving out a mixture of oxidized ceria, syngas, and a minute quantity of water contents. The products of the CL oxidation reactor at around 800 °C reaches the second cyclone C25 through stream SP33 that separates the oxidized ceria from the oxidation output from stream SP34 and leads the remaining products towards the heat exchanger.

The oxidized ceria at 800 °C coming out of the second cyclone entered in the heat exchanger block C26 where it is cool down and come out at 650 °C via stream SP35. It is considered that oxidized ceria stream SP35 is recirculated to CL reduction reactor C21 to get reduced again and so that

the thermochemical cycle is completed. CL oxidation reactor product mixture (except oxidized ceria) reaches the heat exchanger C27 through stream SP36 and get reduced its temperature. Cooled syngas mixture is entered in the condenser block C28 through stream SP37 where water contents are condensed and separated via stream SP39, while the syngas is introduced to the storage section through stream SP38.

5.2.2 Solid oxide fuel cell

A portion of the syngas produced from the CL reduction reactor C21 reaches the compressor block C9 with an isentropic efficiency of 90% through stream SP11 and exit with a discharge pressure of around 1.1 bar. Compressed syngas reaches the mixer block C10 through stream SP12 and the recycled species reach the mixer through stream SP16.

The product from the mixer reaches the anodic reactor of solid oxide fuel cell C11 that is operated at 800°C and 1.1 bar pressure. The anodic compartment of SOFC is characterized as an isothermal GIBBS reactor.

Air at ambient conditions reaches the compressor C1 through stream SP0 which increases air pressure until 1.1 bar. The pressurized air reaches SIMP-HT heat exchanger block C16 with four

streams that preheat the air until 380 °C. Initially, preheated air reaches the heater block C2 through stream SP2 and gets heated at 600°C. Preheated air approaches SOFC cathode heat exchanger C3 through stream SP3 that increases its temperature until 800°C. The output of the cathode heat exchanger enters the separator block C4 through stream SP4 that separates oxygen from the air. So, in this way syngas mixture enters the SOFC anode C11 and pure oxygen reaches the anode through stream SP15. Stream SP15 loaded with oxygen is firstly initialized with 1 kmol/hr. But then a calculator block is employed to set equal streams SP7 and SP15.

Reactions take place in SOFC anode according to Eq. (2.10), (2.11), and (2.12) and electric power is produced. Besides that, a mixture mainly comprised of H_2O and CO_2 is achieved. Product of SOFC anode at 800 °C reaches first splitter C12 through stream SP14 which splits its input into stream SP16 and SP17 based on the results of Design Specs. The first output stream of splitter block stream SP16 containing certain fractions of anodic products ($H_2O/CO_2=2$) is recirculated back to avoid carbon deposition where it is introduced with incoming heated biogas in the mixer block C10. While its second output stream leads towards the heat exchanger C13, where it is getting reduced its temperature until 650 °C. The output stream of the heat exchanger reaches the second splitter C14 through stream SP18.

Splitter block divides the incoming anode off-gas mainly comprised of H_2O and CO_2 as per Eq. (2.10), (2.11), and (2.12). Anode exhaust mainly consists of H_2O 60%, CO_2 30%, and unreacted species with around 7% hydrogen and 3% CO. A specified fraction is dedicated to stream SP61 that is introduced to the CL oxidation reactor C24 so that thermochemical splitting of H_2O and CO_2 may take place to oxidize the reduced ceria. The remaining portion of the anode off-gas reaches the afterburner block C15 through SP19, while pure oxygen exiting from the air separation unit reaches the burner through stream SP20.

After the burner reactor is modeled as an adiabatic reactor meaning that net heat duty is kept zero so that all the chemical energy of the unreacted H_2 and CO is converted into thermal energy increasing temperature.

5.2.3   Oxyfuel combustion
After burner products (66.6% H_2O and 33.3% CO_2) at around 1225°C reaches the SIMP-HT heat exchanger C16 through SP21 while the compressed air at ambient temperature reaches the heat exchanger through SP1 and get heated. In this way, after the burner off-gas is cooled until 900 °C. The output of the SIMP-HT heat exchanger reaches another heat exchanger C17 having two streams of which input stream SP22 and output stream SP23 and cooled down to 100°C. The cooled mixture of CO_2 and H_2O approaches the condenser block C18 having two outlet streams, SP24 loaded with pure CO_2 and SP25 containing only H_2O in a liquid state.

5.2.4   Carbon dioxide capture
Pure carbon dioxide enters the carbon compression section through stream SP24. This section contains the compressor train mainly comprised of five compressor blocks named C40, C42, C44, C46, C48, and five intercoolers named C41, C43, C45, C47, and C49. Each intercooler cools the pressurized species until ambient temperature. A compression ratio of 2.79 is employed to compress the CO2 until 150 bar. Compressed CO2 moves towards the permanent storage through stream SP60.

5.2.5 Syngas storage section

Syngas produced from the CL oxidation reactor C24 through stream SP38, and a fixed percentage of the syngas produced from the CL reduction reactor C21 through stream SP61 approached the syngas storage section. The syngas storage section is started with a mixer C29 that accepts the stream SP38 and SP21. This section contains four compressors named C32, C34, C36 C38, and four intercoolers named C31, C33, C35, and C37. A compression ratio of 2.8 is employed to achieve the final syngas pressure around 62bar. During the night operation compressed syngas approaches valve C38 through stream SP48 and it is heated in heater C39 before introducing into the SOFC anodic reactor C11.

5.3 Model development, system analysis, and assessment.

The proposed system employs fossil fuel methane for electrical/thermal power generation, syngas production, and carbon capture. Ceria-based chemical looping is included as external methane reforming and with a special focus on the processing of waste anode off-gas into useful product syngas. The oxyfuel combustion unit is fed with pure oxygen and employed to convert the unreacted H_2 and CO so that pure CO_2 is obtained. A syngas storage section incorporated with the proposed plant based on the assumption that the plant must operate 24 hours a day. So that the dependency of the CL unit is detached during the night operation.

This section describes the operating parameters of involved components, different types of performances of the proposed system.

5.3.1 Ceria based chemical looping thermochemical cycle

The operating conditions of the chemical looping section are selected based on the literature and sensitivity analysis perform against temperature, pressure, and molar ratio. Criteria, selected parameters, and results of the sensitivity analysis are reported in the later section of the present thesis.

As explained in previous sections the chemical looping process is mainly comprised of two reactors, endothermic reduction reactor, and exothermic oxidation reactors. The first component in this process is GIBBS reactor C21 and is characterized to simulate reactions as mentioned in Eq. (2) and (3). The operating conditions of the reduction reactor are established at 1 bar pressure, 800 °C temperature, and 0.8 molar feed ratio. Table 5.1 shows the operating conditions of the proposed plant's chemical looping unit.

It has two input streams and one output stream. Input stream SP27 is loaded with methane at ambient operating conditions, and it is going to be preheated in the heater block C20 at 650°C temperature. After that, it is allowed to pass through the reduction reactor. Second input stream SP28 is constituted by ceria at 650°C temperature and 1 bar pressure. Ceria stream does not consist of gaseous or liquid species rather it is comprised of solid particles. Therefore, particle size distribution is executed in the ASPEN PLUS. While fuel stream SP29 is constituted by 100% methane in gaseous form. Its molar flow rate is assumed to be 1 kmol/hr. and considered as a basis of the present study.

A calculator block has been established and the molar flow ratio of fossil methane/ceria is set 0.8. In this way, the molar flow rate of ceria has been calculated to be equal to 1.25 kmol/hr.

Methane reforming takes place in the reduction reactor in the presence of ceria and the reactants are modified into products comprising of a mixture of H_2, CO, Ce_2O_3 based on Eq. (4.1), (4.2), and (4.3). Furthermore, it has been observed that the product stream SP30 also contains 13% of unreformed methane. As product stream of reduction reactor of chemical looping is coupled with the input of SOFC. SOFC being a high-temperature fuel cell offers a wide range of fuel as its input. Therefore, the remaining methane contents will be reduced within SOFC.

As explained before, one of the objectives of this study is that the plant must operate for 24 hours a day without entirely depending on solar energy. As solar energy does not remain constant because of its intermittent nature. Therefore, a storage system has been considered, that will allow the storage of surplus syngas so that they can be consumed by the plant during the night operation when chemical looping is no longer available.

The difference among operation phases of both chemical looping and SOFC is evaluated as a fellow.

- Operation period of chemical looping during a day = 8 hours
- Operation period of SOFC during a day = 24 hours

CL oxidation reactor C24 is first fed with reduced ceria in the form of Ce_2O_3 present in stream SP32. Another input stream SP61 is consisted of a mixture of H_2O and CO_2 coming from the anodic exhausts of the SOFC.

The operating conditions of oxidation reactor C24 are established at 1 bar pressure, 800 °C temperature and 0.62 km/hr the flow rate of the waste gas. Table 5.2 shows the operating conditions of the proposed plant involving chemical looping.

Table 5.2: Operating conditions od ceria based thermochemical looping cycle

Parameters	Values
Chemical looping	
Fuel flow, kmol/hr.	1
Atmospheric temperature, °C	25
Atmospheric pressure, bar	1
Reduction reactor temperature, °C	800
Reduction reactor pressure, bar	1
Methane to ceria feed ratio	0.8
Reduced ceria flow, kmol/hr.	0.627
Oxidation reactor temperature	800
Oxidation reactor pressure, bar	1
Waste gas flow inlet to an oxidation reactor, kmol/hr.	0.625

5.3.2 Solid oxide fuel cell

Chemical looping is interconnected with the benchmark solid oxide fuel cell as depicted in figure 5.2 with the assumption that external reforming of the fuel takes place in the CL reduction reactor. SOFC island is similar to the benchmark except that a portion of the anode exit gas is sent to the oxidation reactor of chemical looping so that thermochemical dissipation of the waste gas takes place, and the remaining is recirculated to the after-burner section. From the literature review, it is found that the operating conditions of the SOFC coupled with other models are diverse.

In the existing literature, the CL-SOFC combination is not present. However, many other possible SOFC combinations are studied by a lot of researchers with different operating conditions as briefly described in section 2.9.

For the proposed plant in the present study, research conducted by Xiaosong et al is taken as a reference [46]. The SOFC operating temperature, pressure, and fuel utilization are set at 800 °C, 1.1 bar, and 0.85 respectively. The anode inlet fuel and cathode inlet air temperature and pressure are set 650 °C and 1.1 bar respectively. The operating conditions of the SOFC island are given in table 5.2

The operating principle of the system can be summarized as follows: methane and air are compressed up to the SOFC stack operating pressure by the fuel and air compressors.

Table 5.2: Operating conditions of major components of integrated SOFC

Operating parameters	Values
Solid oxide fuel cell	
SOFC anode operating temperature, °C	800
SOFC anode operating pressure, bar [56] [32]	1.1
SOFC cathode heat exchanger temperature, °C	800
Minimum fuel inlet temperature, °C	650
Minimum fuel inlet pressure, bar [56]	1.1
Minimum air inlet temperature, °C	600
Minimum air inlet pressure, bar [56]	1.1
Cell voltage, V [56]	0.6332
Faraday constant, C/mol	96485
DC/AC inverter efficiency [57], [58]	0.95
Steam to carbon ratio, S/C	2
Air compressor isentropic efficiency	0.9
Compressor mechanical efficiency	0.85
Fuel utilization [59]–[61]	0.85
No of electrons offered by CH_4	8
No of electrons offered by H_2	2
No of electrons offered by CO	2

5.3.3 Oxy-fuel combustion

In aspen plus, afterburner C15 is modelled as an adiabatic reactor which means all the chemical energy of unreacted fuel (H_2 and CO) will utilize to temperature increase. To control the temperature at the output, air at the ambient temperature reaches the heat exchanger block C16 through stream SP1.

A comprehensive combustor operating conditions must be evaluated for the complete oxy-fuel combustion of SOFC off-gas. The operating conditions of the oxy-fuel combustion part are given in table 5.3. SOFC off-gas is comprised of H_2O, CO_2, H_2, and CO. Unreacted H2 and CO species in the anode exhaust react with the pure oxygen according to Eq. (4) and (5) and produces H_2O and CO_2.

In the present study simulation model, off-gas composition includes 7% H_2, 3% CO, 60% CO_2, and 30% H_2O but in the large commercial plant, SOFC off-gas contains H_2 and CO with larger mole flow rate. Therefore, it is evaluated that characteristics of SOFC off-gas are such that it contains high moisture contents and low calorific value due to low percentage of H_2 and CO. These special characteristics suppress the flame stability and strength.

Table 5.3: Operating conditions and fuel specification of the oxy-fuel combustion unit

Operating parameter	Values
Oxy-fuel combustion cycle	
Burner heat duty, kW	0
Combustion pressure, bar	1
Inlet oxygen temperature, °C [62]	25
Inlet oxygen pressure, bar [62]	1
Inlet anode off-gas pressure, bar	1.1
Inlet anode off gas temperature, °C	800
Afterburner outlet temperature, °C	900
Fuel	
LHV of CH_4, kJ/kg [63]	50085.18
LHV of H_2, kJ/kg [63]	120039.68
LHV of CO, kJ/kg [63]	10107.142
Air c_p, kJ/kg. k	1.005
Air molecular weight, g/mole	28.96

In the next step, this stream is moved further towards water condensation, and a stream of pure CO_2 is obtained. The captured CO_2 then passed through a series of compressors and heat exchangers that make the captured CO_2 pressurized and purer. In this way, pure CO_2 is captured easily as compared to traditional techniques and moved towards permanent storage. Carbon capture and storage techniques are briefly explained in the available literature [5], [6].

Although oxy-fuel technology is an efficient approach to take pure CO_2, it is linked to the air separation process that is a very energy-intensive task. State-of-the-art ASU requires 0.19 MJ/kg O_2, and commercial ASU unit needs 0.245 kWh/kg O_2 [3] CO_2

It is observed that if an excessive quantity of oxygen is introduced into the combustor, it increases the flame temperature but decreases the CO_2 concentration at the combustor exhaust. This depicts that the extra quantity of oxygen reduces the product of interest that further portraits that extra oxygen requires more power in the ASU.

5.3.4   Syngas storage and carbon capture unit

During the first 8 hours of the day, there is plenty of sunlight that results in a huge production of syngas during the day. While during the night operation, the chemical looping section of the plant will not operate due to the intermittence nature of solar energy and the absence of sun. So, in the proposed plant a syngas storage unit has also been considered. To operate the plant 24 hours continuously, this storage unit plays a crucial role in the whole plant configuration. In addition to this, a storage unit is necessary for the smooth operation and functioning of the solid oxide fuel cell as SOFC is highly affected by load disruptions and fuel cutoff. Based on several moles input (1 kmol/hr. CH_4 and 1.25kmol/hr. CeO_2) to the chemical looping section, it has been figured out that chemical looping is oversized as compared to the SOFC. Thanks to the oversized chemical looping plant, it was possible to store a huge quantity of syngas produced from the reduction reactor of chemical looping. In this way, SOFC was fed with a constant amount of syngas to resolve the issue of intermittence of sunlight and the remaining syngas will be stored in the storage unit to be used during the night.

Unfortunately, in Aspen plus V 11.0 the component for the storage tank does not exist. So, to simulate the storage unit, the proposed plant is integrated with other components in the flowsheet. These components are compressor trains (from C30 to C36) is employed with a constant compression ratio of 2.8 and an inter cooler has been applied to recover the heat from syngas.

In the proposed configuration of the plant, one of the sub-objectives was that

- SOFC must operate 24 hours a day regardless of the unavailability of solar energy.
- During the first 8 hours, the anode should generate a particular amount of exhaust that fully oxidizes the reduced ceria (Ce_2O_3) generated from the reduction reactor of chemical looping.

This sub-objective has been achieved in the following way:

As described in the previous section of chemical looping, the methane and ceria undergo reduction reactions and produce syngas and Ce_2O_3, respectively based on Eq. (5.1) and (5.2). A cyclone separator has been applied to separate the syngas and solid contents of reduced ceria. It has been observed that 0.625 kmol/hr. of reduced ceria has been separated from the cyclone. From Eq. (4.2) and (4.3) it is pragmatic that stoichiometrically, 0.625 kmol/hr. of H_2O and CO_2 is required in the oxidation reactor of chemical looping to fully oxidize the reduced ceria (Ce_2O_3) into respective ceria (CeO_2).

By applying 0.91 kmol/hr. of syngas in the anodic reactor of SOFC that generates the exhaust flow rate of around 1.2163 kmol/hr. An iteration is performed in the Flowsheeting option of ASPEN PLUS so that the splitting operation of the anode off-gas is executed in such a way that

0.624kmol/hr. of the anode of gas is introduced to the CL-oxidation reactor and the remaining is moved towards oxyfuel combustion.

A splitter C7 has introduced between the output of reduction reactor stream SP9 and input of anodic reactor of SOFC stream SP12, which divides the flowrate of syngas into two different streams SP10 and SP11. Stream SP11 is an input to the SOFC anodic reactor. The remaining amount of syngas gas (0.5923 kmol/hr.) is moved towards the storage section through stream SP10 and used when chemical looping is no longer available due to little sunlight or during night hours. Table 5.4 demonstrates the operating parameters of the syngas and carbon dioxide compression unit.

Table 5.4: Operating parameters of syngas, CO_2 storage, and compression system.

Operating parameter	Values
Syngas Storage	
Final syngas storage pressure, bar[27] [28]	60
Final syngas storage temperature, °C [27] [28]	50
Compressor isentropic efficiency	0.90
Compressor mechanical efficiency	0.85
Pressure compression ratio per intercooled stage	2.8
Cooler outlet temperature, °C	25
Cooler pressure drop, %	2
CO_2 compression and storage	
Compressed CO_2 pressure, bar [66]	150
Pressure compression ratio per intercooler stage	2.72
Compressor isentropic efficiency	0.90
Compressor mechanical efficiency	0.85
Cooler outlet temperature, °C	25
Cooler pressure drop, %	2

6 Results and discussion

In this section, all the important results obtained from the present study are reported.

6.1   Chemical looping sensitivity analysis

6.1.1   Sensitivity and thermodynamic analysis on reduction reactor of chemical looping

As briefly explained in the previous section that the reduction reactor of chemical looping takes CH_4 and CeO_2 as reactants. These reactants are processed under endothermic conditions. The product stream of the reduction reactor mainly consists of a gas mixture comprised of H_2, CO, unreacted CH_4, H_2O, CO2, and solid contents of Ce_2O_3 and unreduced CeO_2. This equilibrium composition of the product stream is highly dependent on the temperature, pressure, and feed ratio of reactants. Impact of these parameters, temperature in the range of 500-2000 °C, pressure from 0.1 to 2 bar and reactant feed ratio (molar basis) on the equilibrium composition of H_2, CO, CO_2, H_2O, CH_4, CeO_2, and Ce_2O_3 are explained in this section.

Figure 6.1 (a) depicts the equilibrium composition of the product stream of the reduction reactor as a function of reduction reactor temperature. All the species involved in equilibrium including unreacted fuel (CH_4), solid contents of unreacted CeO_2 are plotted against reduction temperature. From figure 6.1 (a) it is observed that reduction of the input reactants initializes at above 550°C temperature. Reforming of fuel (CH_4), and reduction of ceria suddenly increases at around 600°C and its mole fraction steadily decrease until 0.166 and 0 respectively. So, 84% conversion is achieved at 800 °C, after that mole fraction of CH_4, remains constant even at a higher temperature. A sudden decrease in the mole fraction of ceria is attributed to the fact that no mass transfer limitations are available at that conditions and the activation barrier is minimum due to the high intrinsic reaction rate of ceria, therefore is 100% ceria is reduced. As the concentration of ceria decreases, the mole fraction of Ce_2O_3 rises gradually and its maximum value is attained at 800 °C after that its concentration remains unchanged no matter even at a high temperature. It can also observe that the production of the wanted fuel (H_2 and CO) initiate at a lower temperature of around 500 °C and it suddenly started increasing at 600°C. Both get peaked at 800 °C, while at a high temperature they remain unchanged. It can be observed that the concentration of unwanted species usually H_2O and CO_2 are minimum during the studied temperature range.

The influence of temperature on the thermodynamic yield of the reduction reactor is compared with the work conducted by Warren et al. They conducted an experimental approach towards simultaneous methane reforming and non-stoichiometric ceria reduction in the presence of a packed bed solar reactor and examined the products of reduction reactor [55]. Table 6.1 presents the suitable comparison of the present study with the experimental work of Warren et al at a temperature range of 800°C, 900°C and 1000°C in the presence of 0.25 mol/sec CH_4 and 1 mol/sec CeO_2. According to table 6.1, it is concluded that the result of the present study proves a good agreement with the literature studies. By combining all the factors along with the comparison with the literature, it is recapitulated that the favorable operating temperature of the reduction reactor for simultaneous methane reforming and ceria reduction is in the range of 800-900 °C in the presence of 0.7-0.8 molar ratio of the reactants. But at 900 °C, higher solar input is needed therefore, a suitable reduction temperature is decided to be 800°C.

Table 6.1: Comparison of thermodynamic products yielded by reduction reactor of the present study with the results reported by Warren et al [55].

Temperature (°C)	Mole fraction				
	H_2 (%)	CO (%)	CH_4 (%)	H_2O (%)	CO_2 (%)
800					
[55]	61.0	19.9	0.1	0	0
Present work	56.9	28.4	14.0	0.2	0.1
900					
[55]	65.8	25.6	0.5	0.5	0.1
Present work	65.28	32.7	0.6	0.9	0.3
1000					
[55]	66.0	32.5	0	0.7	0.8
Present work	63.7	32.4	0.03	2.8	0.8

Figure 6.1(b) illustrates the equilibrium concentration achieved at the output of the reduction reactor as a function of pressure. All possible chemical species are considered in this graph. It is desired that at the output of the reduction reactor, there must be a minimum quantity of CH_4, the maximum concentration of wanted species (H_2 and CO), and zero quantity of unwanted species (H_2O and CO_2). It can be seen from figure 6.1(b) that, the concentration of H_2 and CO is peaked at 1 bar pressure, and it drops gradually as pressure rises. It is analogous to desire. On the similar, as the pressure crosses 1 bar, CH_4 quantity decreases at the output as well.

So, at higher pressure, the percentage of wanted species reduces. That is entirely contrary to our objective. Therefore, it can be concluded that a higher level of vacuum or lower pressure of around 1 bar delivers much better results and higher syngas production yield. As no experimental literature is available in which the influence of reduced pressure is examined. But Warren et al keep the pressure of reduction reactor 1 bar. Therefore, based on results of pressure sensitivity analysis and literature reported [55], 1 bar is considered as favorable pressure for the operation of a reduction reactor.

Figure 6.1 (c) demonstrates the equilibrium composition of the endothermic reduction reactor as a function of the molar feed ratio ($mCH_4/mCeO_2$). As observed from the graph the production of H_2 and CO accelerate at a feed mole ratio of 0.1 and it remains maximum in a range of 0.75 and 0.8. CeO_2 gets 100% reduced at around 0.8 and Ce2O3 gets peaked at the same molar ratio. Furthermore, unwanted species remain almost zero even at a higher feed molar ratio.

6.1.2 Sensitivity and thermodynamic analysis on oxidation reactor of chemical looping

The equilibrium composition of syngas achieved in the oxidation reactor of chemical looping is presented now in this segment. This syngas is produced by dissociation of SOFC off species in the presence of reduced ceria obtained from reduction reactor of chemical looping.

Figure 6.1 (d) shows the effect of oxidation temperature on the oxidation extent of reduced ceria and the production of H_2 and CO. A mixture of syngas comprising of 48% H2 and 49% CO is obtained at 900°C, after that at a higher temperature mole fraction of both species decrease

gradually. Composition of unwanted species, H_2O and CO_2 are minimum at a temperature range of 900-950 °C. Additionally, complete oxidation of reduced ceria is achieved at around 900°C resulting in 100 % CeO_2 at the same temperature. From the sensitivity analysis, favorable results are achieved at 900°C but Abanades et al [52]conducted experimental work on hydrogen production by using ceria thermochemical cycle, and they picked the oxidation temperature in the range of 400-600°C, that is less as compared to the favorable results of 900°C, therefore a moderate approach is adopted and 800°C was set the temperature of oxidation reactor.

Figure 6.1 (e) shows the influence of oxidation pressure on the composition of syngas produced in the oxidation reactor of chemical looping. It is observed that pressure of around 1 bar is suitable for an oxidation reactor. Furthermore, a stoichiometric approach is implemented on the input flow rate of the waste gas for the oxidation reactor, as depicted in figure 6.1 (f), with an introduction of 0.625 kmol/hr. of the waste gas, the maximum yield of H_2 and CO is obtained along with complete oxidation of reduced ceria.
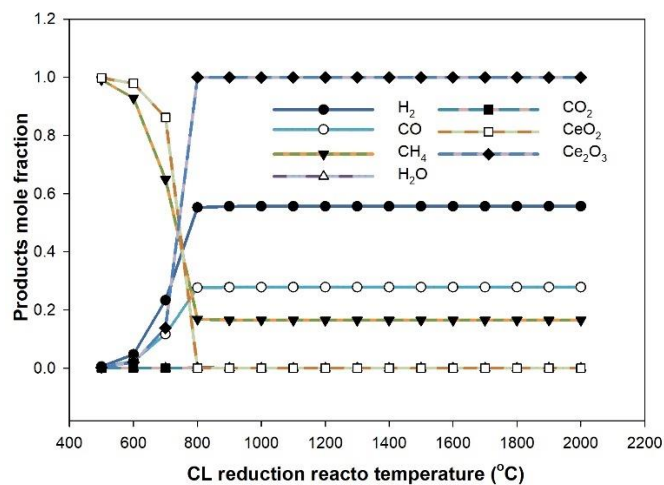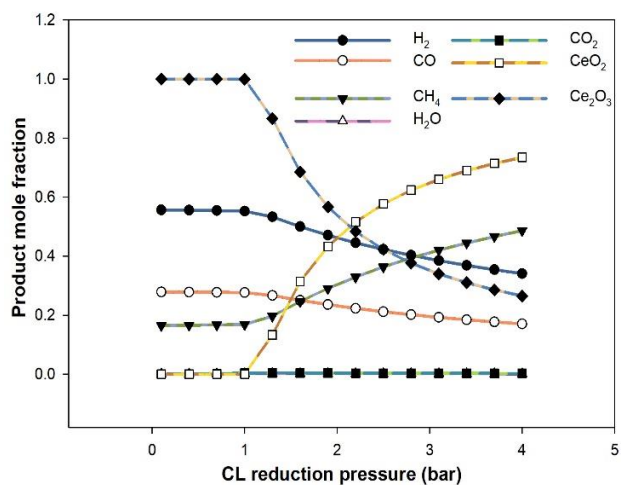
Figure 6.1: Influence of temperature, pressure, and flow ratio on the reduction and oxidation reactor of chemical looping

6.1.3 Dependence of CL system performance on operating conditions.

The efficiency of the chemical looping system plays a vital role in the assessment of the overall performance of the thermochemical cycle. As explained previously, two streams of syngas are obtained from reduction and oxidation reactors respectively, although, syngas produced from the oxidation reactor must be the main focus because it exhibits the performance of thermochemical dissociation of H2O and CO2 gases. Favorable operating conditions of the chemical looping that are discussed previously, resulted in three efficiencies are reported in table 6.2.
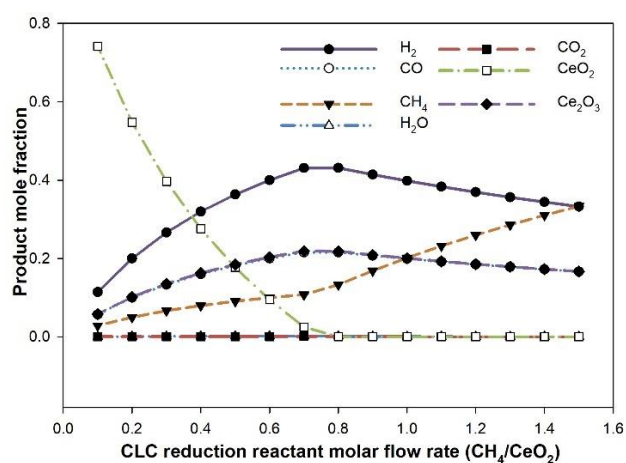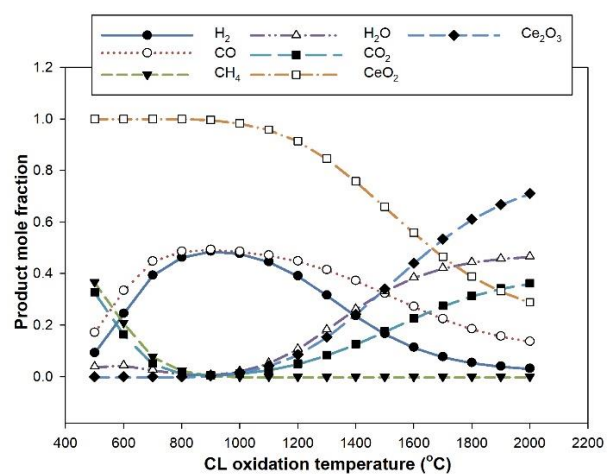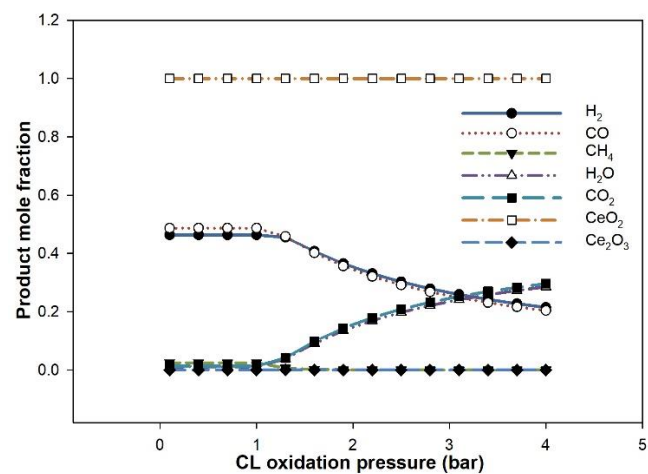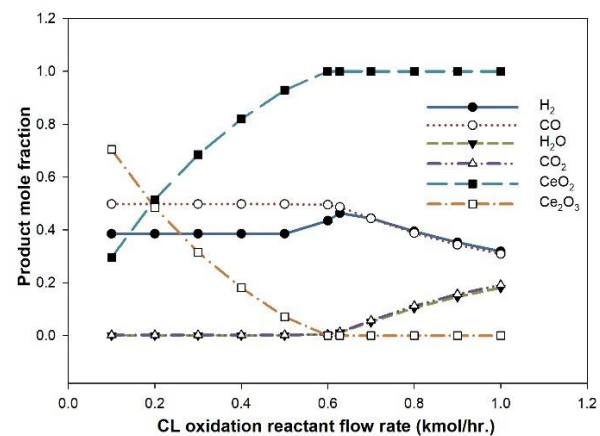
Operating parameters of the chemical looping cycle influence the performances of the CL system that are defined in the previous section and depicted by Eq (5.4), (5.5), and (5.6). In this section the effect of reduction temperature T_{red}, pressure P_{oxi}, the molar flow ratio $\dot{n}_{red}$ and oxidation temperature T_{oxi}, pressure P_{red} and waste gas flow rate N_{Oxi} on the three efficiencies of the thermochemical cycle is described.

In figure 6.2 (a) E_1 (CL overall efficiency), E_2 (waste gas efficiency) and E_3 (solar to fuel efficiency) are plotted against the reduction temperature T_{red} varying between 500-2000°C while keeping $P_{red} = 1$ bar, $\dot{n}_{red} = 0.8$, $T_{oxi} = 800°C$, $P_{oxi} = 1$ bar and $N_{Oxi} = 0.62$. It was assumed that thermochemical splitting of waste gas and oxidation reactions were completed instantaneously without solar input.

As the temperature of the CL reduction reactor is increased, high contents of syngas are generated at the output. Therefore, E_1 started to increase at a temperature of around 550°C and it is maximum (62%) at around 800°C. At higher temperatures around 1400°C, E_1 slightly increased (71%) as compared to the one at 800°C. However, at the same time if E_1 at 1400°C is more, E_3 is minimum at that temperature.

As the reduction temperature is increased from 500°C, $\eta_{solar-to-fuel}$ suddenly increases. At 700°C it is peeked to 77%, after that it is rapidly decreased. But at a lower temperature, between 500°C to less than 700°C, lower efficiency is obtained, as, at a low temperature, a lower yield of H2 and CO is obtained. One of the possible reasons for high efficiency at 700°C is that in the $\eta_{solar-to-fuel}$ formula, heat provided by the solar is in the denominator and at 700°C, less input heat (17.7 kW) is required by the reduction reactor therefore a higher efficiency is achieved, while at 800°C, more heat (70.4kW) is provided by the solar to the reduction reactor.

In figure 6.2 (b) E_1 (CL overall efficiency), E_2 (waste gas efficiency) and E_3 (solar to fuel efficiency) are plotted against the reduction pressure P_{red} varying 0.1 to 4 bar while keeping $T_{red} = 800 °C$, $\dot{n}_{red} = 0.8$, $T_{oxi} = 800°C$, $P_{oxi} = 1$ bar and $N_{Oxi} = 0.62$. It was assumed that thermochemical splitting of waste gas and oxidation reactions were completed instantaneously without solar input.

Looking at figure 6.2 (b), a decreasing trend of overall CL system efficiency E_1 is achieved at high pressure. At $P_{red} = 1$ bar, maximum efficiency of 61.9% is achieved as compared to its minimum value of 32% at $P_{red} = 4$ bar. One of the possible reasons includes that at high pressure, reversible reasons started proceedings and a lower percentage of syngas is produced at the output. While on the other hand, the maximum value of solar to fuel efficiency E_3 is obtained at a reduced pressure

of 2.2 bar. The reason is that as the pressure is increased, syngas contents at the output decrease, unreacted methane increases. Furthermore, a lower solar power (48kW) is required at higher pressure (2.2 bar) as compared to higher solar power (70.4kW) demand at lower pressure (1 bar).

In figure 6.2 (c) E_1 (CL overall efficiency), E_2 (waste gas efficiency) and E_3 (solar to fuel efficiency) are plotted against the reduction reactant molar flow ratio $\dot{n}_{red}$ varying between 0.1-1.5 while keeping $T_{red} = 800$ $P_{red} = 1$ bar, $T_{oxi} = 800°C$, $P_{oxi} = 1$ bar and $N_{Oxi} = 0.62$. It was assumed that thermochemical splitting of waste gas and oxidation reactions were completed instantaneously without solar input.

Stoichiometric conditions of simultaneous methane reforming and ceria reduction as per Eq. (4.1) are that for 2 moles of ceria, 1 mole of CH4 is needed and the product mixture will be comprised of 1 mole of reduced ceria, 2 moles of H2, and 1 mole of CO. This depicts the reduction reactor molar flow ratio $\frac{CH_4}{CeO_2}$ to be 0.5. Therefore, at stoichiometric conditions, a maximum (64.4%) overall efficiency E_1 is reported. Similar value of E_1 is obtained at $\frac{CH_4}{CeO_2} = 0.7$, while a bit higher flow ratio of $\frac{CH_4}{CeO_2} = 0.8$, a bit lower efficiency E_1 is predicted. However, at the same time, at stoichiometric conditions of $\frac{CH_4}{CeO_2} = 0.5$ a lower (28.7%) solar to fuel efficiency E_3 is reported while at $\frac{CH_4}{CeO_2} = 0.8$, a bit higher (32.9%) E_3 is obtained. At a higher molar fuel ratio of more than 0.8, an increasing trend of E_3 is obtained but a decreasing trend of E_1 is predicted.

At the favorable operating conditions ($T_{red} = 800$ $P_{red} = 1$, $\frac{CH_4}{CeO_2} = 0.8$ bar, $T_{oxi} = 800°C$, $P_{oxi} = 1$ bar, $N_{Oxi} = 0.62$) of the chemical looping system, three performances identified in Eq.(4.5), (4.6) and (4.7) are reported in Table 6.4

Table 6.2:Three performances of chemical looping

Efficiency	Value (%)
$\eta_{overall}$ E_1	61.9
$\eta_{waste\ gas}$ E_2	11.4
$\eta_{solar-to-fuel}$ E_3	32.9
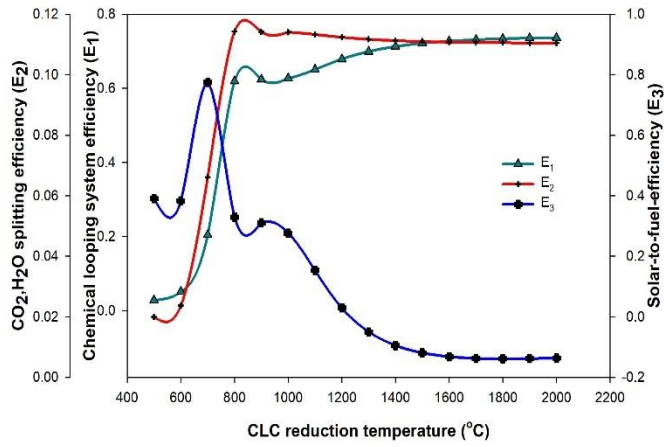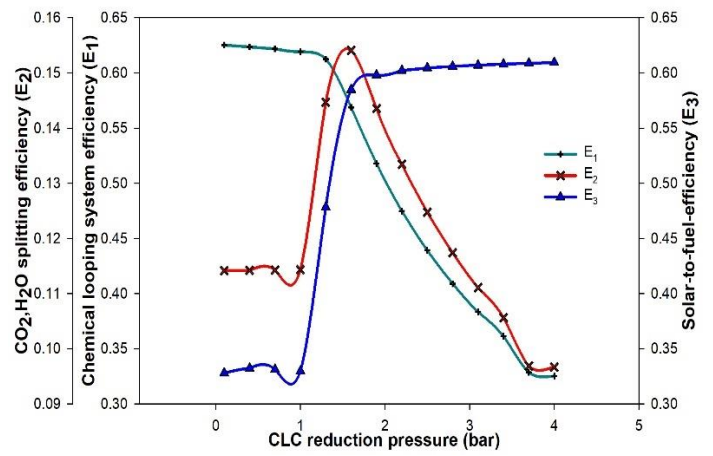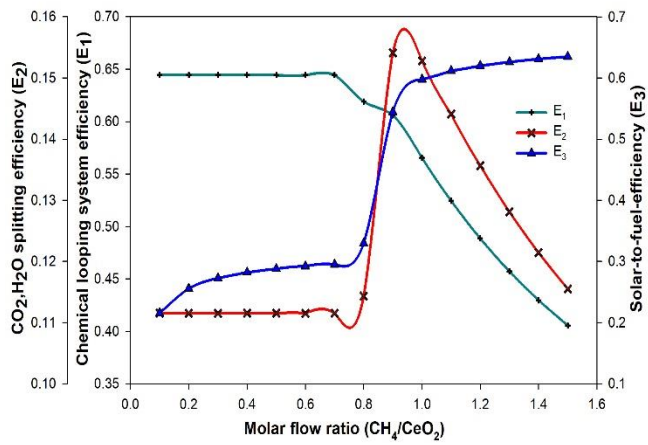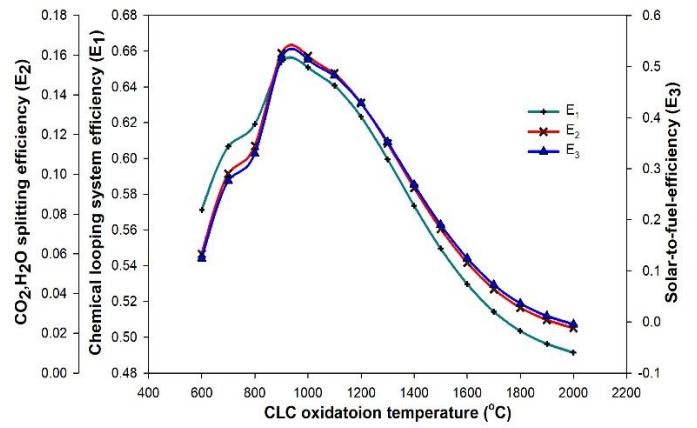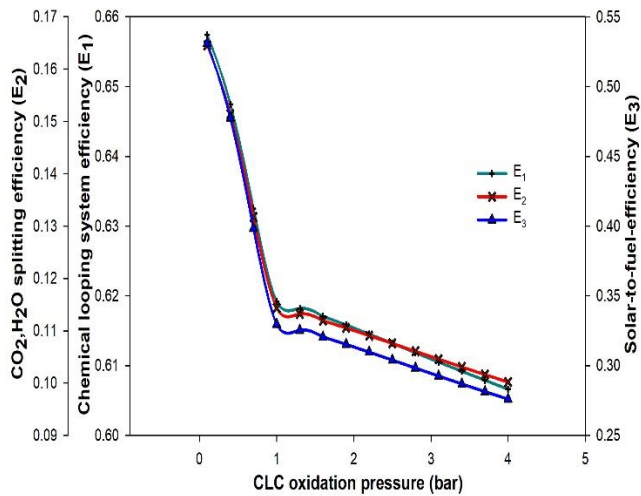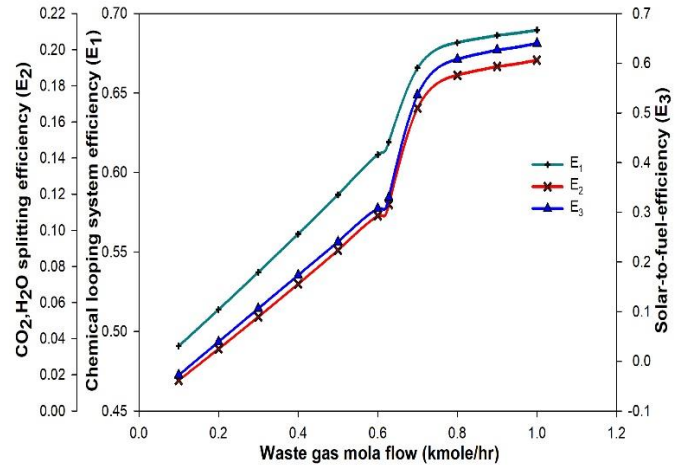
Figure 6.2: Influence of temperature, pressure, and flow ratio on the overall efficiency (E_1), waste efficiency (E_2), and solar-to-fuel-efficiency (E_3).

6.2 Pinch analysis: Design with a minimum energy requirement

Pinch analysis is conducted separately for the two designs of the proposed plant systems (i.e morning operation with CL; night operation without CL). Both designs differ from each other based on the fact that chemical looping is accessible or not.

6.2.1 Definition of constraints and boundary conditions

Before diving into the pinch analysis, it is important to describe the technical constraints and boundary conditions. The constraints considered are given as.

- The temperature of the hot stream must be greater than the temperature of the cold stream.
- In the process of stream coupling, the temperature of the hot inlet stream must be greater than the cold outlet stream and the temperature of the cold inlet stream must be greater than the hot outlet stream. This depicts that in each coupling a minimum temperature difference of 20°C must be considered.

$$T_{Cold_{in}} = T_{Hot_{out}} - 20 \qquad\qquad (6.1)$$

$$T_{Hot_{in}} = T_{Cold_{out}} + 20 \qquad\qquad (6.2)$$

- Heat transfers co-efficient U remains constant.
- The temperature of the syngas and CO_2 in the compression train must be low so that compression work is also minimized.

To achieve the minimum requirement of temperature and during the heat exchanger network design following rules and conditions are respected.

- There must be no external heater on the right side of the grid diagram (below the pinch point, cold streams), this means that cold streams must be brought to pinch point temperature by using hot streams. Furthermore, it must follow the CP rule as depicted in Eq. (6.3).
- There must be no cooler on the left side of the grid diagram (above the pinch point, hot streams), this means that hot streams must be brought to pinch point temperature difference by the heat transfer with the cold streams. Moreover, it must follow the CP rule as depicted in Eq. (6.4).
- No process heat exchanger must be between hot streams on the left side and cold streams on the right side of the diagram.

6.2.2 Pinch analysis of the morning operation

Pinch analysis is implemented on the morning design configuration of the plant with the special focus on creating a suitable heat exchanger network so that the energy requirement of the plant is fulfilled internally by the hot streams and energy requirement from the external sources must be minimum.

6.2.3 Identification and characterization of flows

The first step in applying the pinch analysis is comprised of identifying the streams of the plant that are entering and exiting from the heat exchangers either in hot form or cold form.

In the morning operation of the proposed system, all the five subsections of the plant are activated and in the operation phase. However, the syngas and CO_2 compressions section consist of four and five compressors respectively along with the same number of intercoolers. Intercoolers exchange heat with the water so that required storage conditions are achieved.

Consequently, twenty-three streams are identified during the morning operation of the configured plant. Among these four are cold streams (stream SP2: air entering in the heater C2; stream SP3: air entering the cathode heat exchanger C3; stream SP27: methane entering in the heater C20; CL-reduction reactor C21) are identified. The remaining nineteen streams are recognized as hot streams. Details of these streams covering inlet temperature, outlet temperature, mass flow rate, mass heat capacity, and power heat are reported in table 6.3.

Among the nineteen hot streams, major hot streams are only nine (stream SP31: reduced ceria entering HX C23; stream SP34: oxidized ceria entering in HX C26; stream SP8: syngas entering in HX C6; stream SP10: syngas entering in HX C8; stream SP36; syngas entering in HX C27; stream SP5: oxygen-depleted air entering in HX C5; stream SP22: AB exhaust entering in HX C17; stream SP17: SOFC-AN exhaust entering in HX C13; SOFC anode C11; CL-oxidation reactor C24;) also depicted in table 6.3. The remaining nine hot streams depict the streams (SP41, SP43, SP45, SP47 and SP51, SP53, SP55, SP57) that are coupled with intercooler of syngas and CO_2 compression section.

Table 6.3:Major hot and cold streams involved in pinch analysis of morning operation.

| # Stream pinch	# Stream model	Component	Stream type	T_in(°C)	T_out(°C)	Mass rate (kg/sec)	G*cp (kW/k)	Heat (kW)
1	SP31	Ce_2O_3	Hot	1073.15	933.15	0.0572	0.0278	-3.89
2	SP34	CeO_2	Hot	1073.15	923.15	0.0600	0.0273	-4.10
3	SP8	Syngas	Hot	1073.15	923.15	0.0072	0.0238	-3.57
4	SP10	Syngas	Hot	923.15	298.15	0.0043	0.0124	-7.8
5	SP36	Syngas	Hot	1073.15	298.15	0.0016	0.0046	-3.57
6	SP17	CO_2+H_2O	Hot	1073.18	923.15	0.0084	0.0148	-2.22
7	SP22	CO_2+H_2O	Hot	1173.15	373.15	0.0044	0.0069	-5.54
8	SP5	Air	Hot	1023.15	298.15	0.1066	0.1233	-89.39
9	SP41	Syngas	Hot	431.5	298.15	0.0059	0.0155	-2.07
10	SP43	Syngas	Hot	431.5	298.15	0.0059	0.0156	-2.08
11	SP45	Syngas	Hot	431.70	298.15	0.0059	0.0157	-2.10
12	SP47	Syngas	Hot	431.95	298.15	0.0059	0.0161	-2.16
13	SP51	CO_2	Hot	425.7	298.15	0.0024	0.0022	-0.28
14	SP53	CO_2	Hot	396.1	298.15	0.0024	0.0022	-0.21
15	SP55	CO_2	Hot	396.7	298.15	0.0024	0.0023	-0.23
16	SP57	CO_2	Hot	398.0	298.15	0.0024	0.00313	-0.31
17	SP59	CO_2	Hot	389.7	298.15	0.0024	0.0063	-0.57
18	C11	-	Hot	1073.15	1073.05	-	778.7	-77.87
19	C21	-	Cold	1073.05	1073.15	-	704.75	70.47
20	C24	-	Hot	1073.15	1073.05	-	194.53	-19.45
21	SP27	CH_4	Cold	298.15	923.15	0.0045	0.0146	9.16
22	SP2	Air	Cold	556.5	873.15	0.1080	0.117	37.12
23	SP3	Air	Cold	873.15	1073.15	0.1081	0.123	24.73
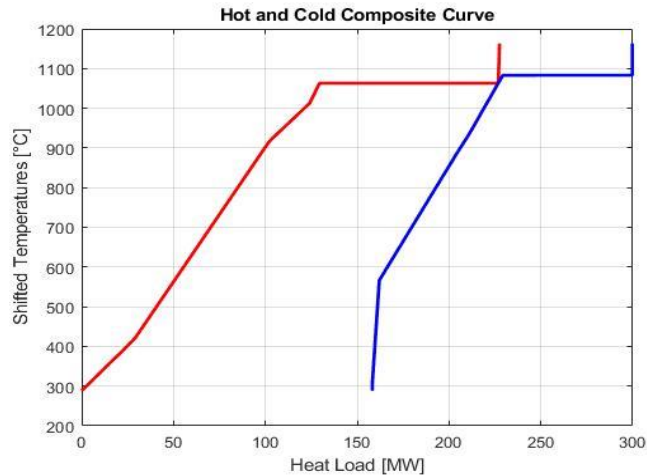
Figure 6.3: Composite curves of morning operation with red line showing hot streams and blue lines showing cold streams.

6.2.4 Calculation of the pinch temperature and minimum energy target.

Based on the thermal data of the morning configuration of the proposed plant mentioned in table 6.3, a minimum energy target is obtained from the pinch analysis. These energy targets are achieved with the help of a useful tool called a composite curve. These curves are comprised of temperature-enthalpy (T-H) profiles of heat availability in the plant (hot composite curve) and heat demands within the plant (cold composite curve)

Figure 6.3 illustrates the construction of the composite curve for the morning operation of the plant which has nineteen hot streams and four cold streams.

From the limitations of the second principle of thermodynamics, all the cold streams (blue line in figure 6.3) must be underneath than that of hot streams (red line in figure 6.3). This also suggests that the hot fluid stream delivers all the heat to the cold stream until the minimum temperature difference is 20°C.

Between the hot and cold composite lines illustrated in figure 6.3 area, A is emphasized. It shows the right side of the pinch diagram (figure 6.3) and depicts that heat embodied in the hot streams can be migrated to the cold streams. While on the other hand, area B demonstrates the left side of the pinch diagram (figure 6.3) and emphasize that part of the heat (0.69kW) required by the cold stream after crossing pinch temperature is delivered by hot streams (SP22) and the remaining heat (1.78kW) is provided by using an external heater (H1). In the last, the point where the minimum difference in temperature is found in the pinch point of the plant. The proposed heat exchanger network (HEN) of the morning operation is given in figure 6.4.

Table 6.5 demonstrates that hot side and cold side pinch temperature is 1073.18°C and 1053.18°C respectively with a minimum temperature difference of 20°C. Cooling duty during the morning operation is 158.260 kW and this heat is recovered by utilizing C1, C2, C3, and C4. as mentioned in figure 6.4. While the heating duty for the morning operation is 72.25 kW is provided by the heater H1 and H2 as mentioned in figure 6.4. Pinch rules defined above are implemented in heat exchanger network (HEXN) design and it is exhibited from figure 6.4 that no heater is present on the right side of the pinch barrier (below the pinch) and no cooler is placed on the left side of the pinch barrier (above the pinch).

Figure 6.4: Heat exchanger network design with minimum energy consumption for the morning operation

Table 6.4: Amount of heat exchanges in each heat exchanger

Heat exchanger	# Stream pinch	kW
A	7--23	1.25
B	20--23	19.45
D	3--23	1.57
E	1--22	3.90
F	8--22	33.23
G	2--21	4.10
H	6--21	2.23
I	8--21	2.84
J	7--23	0.69
H1	23	1.78
H2	19	70.48

Table 6.5: Pinch temperature, heating, and cooling duty of the morning operation

Parameters	Values
$T_{pinch_{hot}}$ (°C)	1073.18
$T_{pinch_{cold}}$ (°C)	1053.18
$Q_{min_{heating}}$ (kW)	72.25
$Q_{min_{cooling}}$ (kW)	158.26
ΔT_{min} (°C)	20

6.2.5 Pinch analysis of the night operation

Figure 6.5 illustrates the construction of the composite curve for the night operation of the plant. It must be noted that during the night operation of the proposed plant chemical looping is not operated. Therefore, part of the anode exhaust is not recirculated. Consequently, the syngas storage system is not activated but storage syngas is utilized during night working hours. The night operation of the plant has eleven streams, among which three are cold streams and eight are hot streams.

Among the eight hot streams, major hot streams are only three (stream SP5: air entering HX C5; stream SP22: afterburner exhaust entering in HX C17; SOFC AN C11). The remaining five hot streams depict the streams (SP51, SP53, SP55, SP57, and SP59) that are coupled with an intercooler of CO_2 compression section blocks (C41, C43, C45, C47, and C49). Three are major cold streams (SP2: air entering in HX C2; SP3: air entering in HX C3 and SP49: syngas entering in HX C39).

It is observed from Figure 6.5 that the behavior of the composite curves follows the limitations of the second principle of thermodynamics, all the cold streams (blue line in figure 6.5) are beneath that of hot streams (red line in figure 6.5). This also suggests that the hot fluid stream delivers all the heat to the cold stream until the minimum temperature difference is 20°C.

Hot and cold composite lines are separated by a considerable space between them, it is highlighted as area A. It shows that all the heat associated with hot streams can get transferred to the cold streams showing the right side of the pinch diagram in figure 6.6. While on the other hand, area B demonstrates the left side of the pinch diagram and emphasizes that part of the heat required by the cold stream after crossing pinch temperature is delivered hot stream (SP59) and the remaining heat is received by using an external heater H1. In the last, the point where the minimum difference in temperature is found in the pinch point of the plant. The proposed heat exchanger network (HEN) of the night operation is given in figure 6.6. Table 6.7 demonstrates the quantity of heat transfer in each heat exchanger while table 6.8 demonstrates that hot side and cold side pinch temperature is 1073.2°C and 1053.2°C respectively with a minimum temperature difference of 20°C. Cooling duty during the night operation is 103.65 kW and this heat is recovered by utilizing C1, C2, and C3 as mentioned in Figures 6.5. While the heating duty for the night operation is 1.781kW which is provided by the heater H1 as mentioned in figure 6.6. Pinch rules defined above are implemented in heat exchanger network (HEXN) design and it is exhibited from figure 6.6 that no heater is present on the right side of the pinch barrier (below the pinch) and no cooler is placed on the left side of the pinch barrier (above the pinch).

Table 6.6: Major hot and cold streams involved in pinch analysis of night operation

# Stream pinch	# Stream model	Component	Stream type	T_in(°C)	T_out(°C)	$\dot{m}$ (kg/sec)	G*cp (kW/k)	Heat (kW)
1	SP5	Air	Hot	1023.2	298.15	0.1066	0.1233	-89.40
2	SP22	CO_2+H_2O	Hot	1173.2	373.15	0.0044	0.0069	-5.54
3	SP51	CO_2	Hot	425.8	298.15	0.0050	0.0022	-0.28
4	SP53	CO_2	Hot	396.1	298.15	0.0050	0.0022	-0.22
5	SP55	CO_2	Hot	396.8	298.15	0.0050	0.0024	-0.23
6	SP57	CO_2	Hot	398.0	298.15	0.0050	0.0031	-0.31
7	SP59	CO_2	Hot	389.8	298.15	0.0050	0.0063	-0.58
8	C11	CO_2+H_2O	Hot	1073.2	1073.05		778.7719	-77.88
9	SP2	Air	Cold	598.5	873.15	0.1080	0.1352	37.13
10	SP3	Air	Cold	873.2	1073.15	0.1081	0.1237	24.74
11	SP49	Air	Cold	292.9	923.15	0.0059	0.0170	10.71
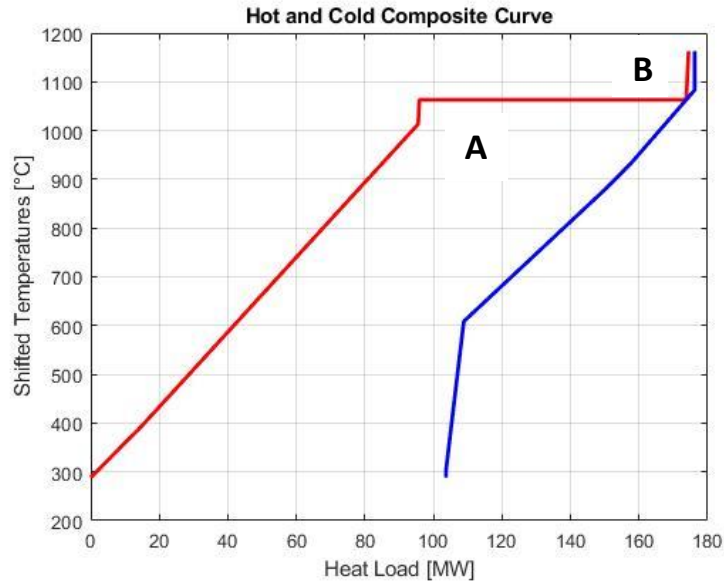
Figure 6.5: Composite curve of the night streams with red line showing hot streams and blue line showing cold streams
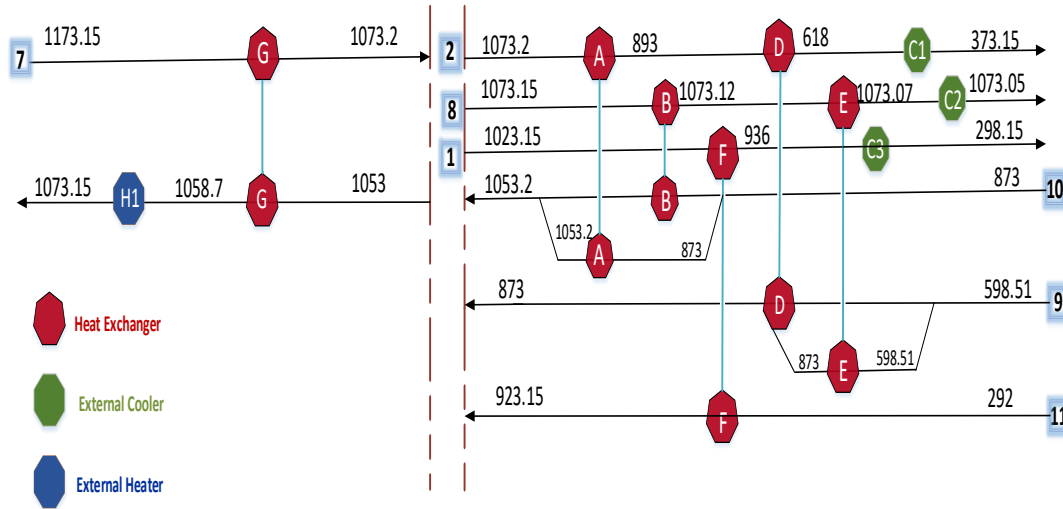
Figure 6.6: Heat exchanger network design with minimum energy consumption for the night operation

Table 6.7: Amount of heat transfers in each heat exchanger

Heat exchanger	# Stream pinch	Q (kW)
A	2--10	1.25
B	8--10	21.02
D	2--9	1.91
E	8--9	35.22
F	1--11	10.71
G	2--10	0.69
H1	10	1.78

Table 6.8: Pinch temperature, heating, and cooling duty of the morning operation

Parameters	Values
$T_{pinch_{hot}}$ (°C)	1073.2
$T_{pinch_{cold}}$ (°C)	1053.2
$Q_{min_{heating}}$ (kW)	1.781
$Q_{min_{cooling}}$ (kW)	103.65
ΔT_{min} (°C)	20

6.3   Carbon capture, utilization, and storage

The CO_2 captured ratio, the CO_2 utilization in the oxidation reactor of CL, the CO_2 stored after oxyfuel combustion unit, the CO_2 avoided from the SOFC anode assess and demonstrate the effect that the CO_2 capture technology execution imparts on the total CO_2 abatement and emission of the proposed power plant. The results of key performance indicators (KPIs) decided previously for the CL-SOFC and the reference SOFC are presented in this section.

For the energy performance, SPECCA is calculated against the reference and proposed CL-SOFC system. The main energy consumers of the CL-SOFC system are the reduction reactor of chemical looping, air separation unit, air, and fuel compression section.

The simulation of the suitable operating conditions of the CO_2 capture unit is mainly focused on the amount of pure oxygen needed by the afterburner to combust unreacted fuel (H_2 and CO), and the amount of air required to remove the waste heat.

Initially, 1 kmol/hr. of fossil, methane is entered in the benchmark SOFC, and 67.4% electrical efficiency is achieved, and after that 1 kmol/hr. CH_4 is introduced to the CL reduction reactor in the absence of syngas storage and CO_2 capture and 40.8% electrical efficiency is attained. One of the possible reasons is that for the benchmark internal methane reforming is considered while in the CL-SOFC system, external reforming of methane is characterized in the reduction reactor of chemical looping. For that CL integrated SOFC requires more air to remove waste heat. Therefore, more compression work is devoted to the excess quantity of air. After that CO_2 capture is implemented on the CL-SOFC system, 0.64kW for syngas compression, 0.95kW for CO_2 compression, and 1.30 for ASU are subtracted from the total power produced, in this way 40.0% electrical efficiency is achieved.

Then, after that whole plant is divided into morning and evening operations. 1.32 kmol/hr. of syngas is devoted to the storage section and the remaining 0.92 kmol/hr. of the syngas is introduced to the proposed CL-SOFC system with CO_2 capture and syngas storage. In this configuration, 73.5% and 71% energy efficiency are reported without and with carbon capture respectively. During the night operation, the same quantity (0.92kmol/hr.) of syngas is introduced to the SOFC and 57.1% and 54.7% overall energy efficiency are achieved without and with carbon capture, which is a bit lower as compared to morning operation. The reason is that during the night operation syngas storage section remains off and syngas compression power (8.34 kW) is saved that making the net electrical efficiency a bit higher. Another possible reason is that more ASU work (0.375kW) is required during the night operation as compared to ASU work (0.245kW) required during the night operation, therefore, this factor is also play role in the difference in the energy efficiency of the morning and evening operation.

As described previously, the proposed plant CL-SOFC is assumed to be operated 24 hours a day. For that, the plant is characterized to have a syngas storage system that stores a certain percentage of the produced syngas during the 8 hours a day when chemical looping is available. In this way, the stored syngas will be utilized during the remaining 16 hours when chemical looping is no longer accessible. Consequently, the CO_2 production is different during the morning and night operations of the plant. As previously reported, one of the key objectives of the CL-SOFC plant is

to achieve the maximum CO_2 captured ratio. During the morning operation, 0.0048 kg/sec of CO_2 is produced as shown in table 6.9. Among these, around 0.00236 kg/sec of CO_2 is recirculated back towards the oxidation reactor of chemical looping, where it is utilized and split thermochemically. In this way, during the morning operation of the CL-SOFC, 49.0% of CO_2 utilization is achieved based on Eq. (4.12) The leftover 0.00246 kg/sec CO_2 is pushed in the direction of the compression unit, where it is compressed to 150 bar and stored permanently. In this way, 51.1% of the CO_2 stored ratio is achieved as per Eq. (4.13) also mentioned in table 6.9. The combination of CO_2 utilized in CL and stored leads towards a 100% CO_2 capture ratio.

During the night operation, almost the same quantity of CO_2 (around 0.0049kg/sec) is produced and chemical looping is no longer accessible. Therefore, the 0% CO_2 utilization ratio is determined as per Eq. (4.12). Accordingly, all the produced CO_2 (0.0049kg/sec) is driven towards the compression section followed by permanent storage, and a 100% CO_2 storage ratio is accomplished based on Eq. (4.13). Consequently, a 100% CO_2 capture ratio is achieved based on Eq. (4.11). The CO_2 avoided for the morning and the night operation is calculated to be 61% and 60.0% based on Eq. (4.14).

SPECCA value is highly dependent on the equivalent amount of carbon emission from a power plant, despite this it is also dependent on the carbon capture and electricity production technology. Because the reason is that the electricity production plant is supposed to deliver electrical power to the selected carbon capture technology. Therefore, the SPECCA index plays a vital role in determining the electricity generation efficiency of a power production plant. For the present proposed system, oxy-fuel consumption is employed as carbon capture technology, where a major part of the electrical power consumption is associated with air separation unit and compression. The value of the SPECCA index for the proposed configuration is reported as 1.141 GJ/ton CO_2 which is in good agreement with the values reported in the literature.

Table 6.9: Result summary of Carbon capture, utilization, and storage associated with proposed CL-SOFC system.

Key performance indicator (KPI)	Benchmark SOFC	Morning CL-SOFC	Evening CL-SOFC	Daily operation
Net electrical efficiency (without CO_2 capture)	67.4%	73.5%	57.1	48.3
Net electrical efficiency (with CO_2 capture)	60.0%	73.1%	54.7%	46.6%
CH$_4$ consumption (kmol/hr)	24	-	-	8
$\dot{m}_{CO_2}$ (kg/sec)	0.012	0.0048	0.0048	0.0096
CO_2-utilized in CL (kg/sec)	0	0.00236	0	0.00236
CO_2-stored (kg/sec)	0	0.00224	0.0045	0.00674
CO_2 utilized ratio (%)	0	49	0	24
CO_2 storage ratio (%)	-	51	100	76
CO_2 captured ratio (%)	-	100	100	100
CO_2 avoided (%)	-	61	60	21
SPECCA (GJ/ton,CO_2)	-	-	-	1.141

7 Conclusion

In this study, a novel ceria-based chemical looping process and its integration with the reference SOFC is proposed for syngas generation and storage, electrical and thermal power production, and CO_2 capture and storage. The entire system is modelled in the ASPEN PLUS simulation environment.

External reforming of the fuel is substituted with a novel ceria-based chemical looping cycle for syngas production. The proposed plant is examined from the perspective of morning and evening operations. A syngas storage system is employed so that the plant may operate during the night when chemical looping is not accessible. During the morning operation, a fraction of anode-off gas is devoted to the oxidation reactor of chemical looping so that thermochemical dissociation of the waste gas may take place, and the remaining waste gas is moved towards oxyfuel combustion followed by carbon capture and compression system. A number of sensitivity analyses are conducted to evaluate the effect of operating conditions on the yield and performance of the chemical looping cycle. Following are the significant conclusions of the present study.

- According to the basis (1 kmol/hr. CH_4) considered for this study, ceria based chemical looping can best operate at $T_{red} = 800$ °C, $P_{red} = 1$ bar, $\dot{n}_{red} = 0.8$, $T_{oxi} = 800$°C, $P_{oxi} = 1$ bar and $N_{Oxi} = 0.62$
- At these operating conditions, overall efficiency E_1, waste gas efficiency E_2 and solar-to-fuel efficiency E_3 of the chemical looping system are obtained to be $\eta_{overall} = 61.9$, $\eta_{waste\ gas} = 11.4$ and $\eta_{solar-to-fuel} = 32.9$ respectively.
- Based on the pinch analysis, morning operation requires 158.2 kW and 72.2 kW as cooling and heating utilities respectively.
- Based on the pinch analysis, night operation of the proposed system requires 103.65 kW and 1.780 kW as cooling and heating utilities respectively.
- Benchmark solid oxide fuel cell with 1 kmol/hr. of biogas generates 150.4 kW of electrical power with an efficiency of 60% with no CO_2 capture and utilization.
- The proposed system can generate 102.97 kW of electrical power with an efficiency of 48.3% without carbon capture.
- The proposed system can generate 102.97 kW of electrical power with an efficiency of 46.6% with carbon capture.
- During the morning operation of the proposed system, 52.37 kW electrical power is generated with an efficiency of 71% with carbon capture and syngas storage.
- During the night operation of the proposed system, 50.6 kW electrical power is generated with an efficiency of 54.7% with carbon capture.
- 100% carbon capture is achieved during the morning operation, followed by 48% CO_2 utilization in the CL and 52% CO_2 storage during the morning.
- 100% carbon capture is achieved during the night operation, followed by 0% CO_2 utilization in the CL and 100% CO_2 storage during the night operation.
- As compared to the benchmark SOFC, 54% CO_2 is avoided during the morning and 51% CO_2 is avoided during the night operation of the plant.
- SPECCA index is reported as 1.141GJ/ton CO_2.

References

[1]   J. K. Jackson, R. M. Nelson, K. M. Sutter, and M. D. Sutherland, "Specialist in International Trade and Finance Specialist in Asian Trade and Finance," 2021.

[2]   J. Meinhardt *et al.*, "Olfactory transmucosal SARS-CoV-2 invasion as a port of central nervous system entry in individuals with COVID-19," *Nature Neuroscience*, vol. 24, no. 2, pp. 168–175, Feb. 2021, DOI: 10.1038/s41593-020-00758-5.

[3]   V. Masson-Delmotte *et al.*, *Global Warming of 1.5°C An IPCC Special Report on the impacts of global warming of 1.5°C above pre-industrial levels and related global greenhouse gas emission pathways, in the context of strengthening the global response to the threat of climate change, sustainable development, and efforts to eradicate poverty Summary for Policymakers Technical Summary Frequently Asked Questions Glossary Edited by Science Officer Science Assistant Graphics Officer Working Group I Technical Support Unit*. 2019. [Online]. Available: www.environmentalgraphiti.org

[4]   "EXTERNAL SECTOR REPORT 2021 Divergent Recoveries and Global Imbalances INTERNATIONAL MONETARY FUND."

[5]   C. le Quéré *et al.*, "Temporary reduction in daily global CO2 emissions during the COVID-19 forced confinement," *Nature Climate Change*, vol. 10, no. 7, pp. 647–653, Jul. 2020, DOI: 10.1038/s41558-020-0797-x.

[6]   "SATURN V FLIGHT MANUAL SA 5O7."

[7]   "A SUSTAINABLE PATHWAY FOR THE EUROPEAN ENERGY TRANSITION HYDROGEN ROADMAP EUROPE", DOI: 10.2843/249013.

[8]   A. Wang *et al.*, "Analysing future demand, supply, and transport of hydrogen EUROPEAN HYDROGEN BACKBONE Executive summary," 2021. [Online]. Available: https://transparency.entsog.eu/

[9]   *The Hydrogen Economy*. Washington, D.C.: National Academies Press, 2004. DOI: 10.17226/10922.

[10]   "O 2 H 2 H 2 O."

[11]   "Hydrogen on the path to net-zero emissions."

[12]   G. Franchi, M. Capocelli, M. de Falco, V. Piemonte, and D. Barba, "Hydrogen production via steam reforming: A critical analysis of MR and RMM technologies," *Membranes*, vol. 10, no. 1, Jan. 2020, DOI: 10.3390/membranes10010010.

[13]   C. Antonini, K. Treyer, A. Streb, M. van der Spek, C. Bauer, and M. Mazzotti, "Hydrogen production from natural gas and biomethane with carbon capture and storage - A techno-environmental analysis," *Sustainable Energy and Fuels*, vol. 4, no. 6, pp. 2967–2986, Jun. 2020, DOI: 10.1039/d0se00222d.

[14]   Z. I. SG Adiya, V. Dupont, and T. Mahmud, "Chemical equilibrium analysis of hydrogen production from shale gas using sorption enhanced chemical looping steam reforming," *Fuel Processing Technology*, vol. 159, pp. 128–144, 2017, DOI: 10.1016/j.fuproc.2017.01.026.

[15]   Robert Rapier, "Estimating The Carbon Footprint Of Hydrogen Production," *https://www.forbes.com/sites/rrapier/2020/06/06/estimating-the-carbon-footprint-of-hydrogen-production/?sh=5af68d9024bd*.

[16]   M. Ishida and H. Jin, "A new advanced power-generation system using chemical-looping combustion," *Energy*, vol. 19, no. 4, pp. 415–422, Apr. 1994, DOI: 10.1016/0360-5442(94)90120-1.

[17]   "A Novel Chemical Looping Based Air Separation Technology for Oxy-Fuel Combustion of Coal, (2014)," in *Applications Guide for Determining the Yield Strength of In-Service Pipe by Hardness Evaluation: Final Report*, ASME Press, 2009. DOI: 10.1115/1.802915.ch1.

[18]   C. Arnaiz del Pozo, S. Cloete, J. H. Cloete, Á. Jiménez Álvaro, and S. Amini, "The potential of chemical looping combustion using the gas switching concept to eliminate the energy penalty of CO2 capture," *International Journal of Greenhouse Gas Control*, vol. 83, pp. 265–281, Apr. 2019, DOI: 10.1016/J.IJGGC.2019.01.018.

[19]   A. E. Farooqui *et al.*, "Assessment of kinetic model for ceria oxidation for chemical-looping CO 2 dissociation."

[20]   S. F. Cannone, A. Lanzini, and M. Santarelli, "A review on co2 capture technologies with focus on co2-enhanced methane recovery from hydrates," *Energies*, vol. 14, no. 2. MDPI AG, Jan. 02, 2021. DOI: 10.3390/en14020387.

[21]   "Cryogenic air separation."

[22]   S. K. Park, T. S. Kim, J. L. Sohn, and Y. D. Lee, "An integrated power generation system combining solid oxide fuel cell and oxy-fuel combustion for high performance and CO2 capture," *Applied Energy*, vol. 88, no. 4, pp. 1187–1196, 2011, DOI: 10.1016/j.apenergy.2010.10.037.

[23]   W. Sanz, H. Jericha, B. Bauer, and E. Göttlich, "Qualitative and quantitative comparison of two promising oxy-fuel power cycles for CO2 capture," *Journal of Engineering for Gas Turbines and Power*, vol. 130, no. 3, May 2008, DOI: 10.1115/1.2800350.

[24]   T. Kuramochi, H. Wu, A. Ramírez, A. Faaij, and W. Turkenburg, "Techno-economic prospects for CO2 capture from a Solid Oxide Fuel Cell-Combined Heat and Power plant. Preliminary results," in *Energy Procedia*, Feb. 2009, vol. 1, no. 1, pp. 3843–3850. DOI: 10.1016/j.egypro.2009.02.186.

[25]   D. McLarty and J. Brouwer, "Poly-generating closed cathode fuel cell with carbon capture," *Applied Energy*, vol. 131, pp. 108–116, Oct. 2014, DOI: 10.1016/j.apenergy.2014.06.011.

[26]   A. Franzoni, L. Magistri, A. Traverso, and A. F. Massardo, "Thermoeconomic analysis of pressurized hybrid SOFC systems with CO2 separation," *Energy*, vol. 33, no. 2, pp. 311–320, 2008, DOI: 10.1016/j.energy.2007.07.008.

[27]   J. Apt, A. Newcomer, L. B. Lave, S. Douglas, and L. Morris Dunn, "An Engineering-Economic Analysis of Syngas Storage Final Report," 2008. [Online]. Available: www.netl.doe.gov

[28]   A. Newcomer and J. Apt, "Storing syngas lower the carbon price for profitable coal gasification," *Environmental Science and Technology*, vol. 41, no. 23, pp. 7974–7979, Dec. 2007, DOI: 10.1021/es070956a.

[29]   M. Korpas, "Distributed Energy Systems with Wind Power and Energy Storage Preface."

[30]   C. Biliyok, R. Canepa, M. Wang, and H. Yeung, "Techno-Economic Analysis of a Natural Gas Combined Cycle Power Plant with CO2 Capture," *Computer-Aided Chemical Engineering*, vol. 32, pp. 187–192, Jan. 2013, DOI: 10.1016/B978-0-444-63234-0.50032-4.

[31]   "Fuel Cell Handbook (Seventh Edition)," 2004.

[32]   "KINETICS OF CONCENTRATION POLARIZATION INTRODUCTION 4.1."

[33]   C. Willich and J. Kallo, "Pressurized Solid Oxide Fuel Cells: Operational Behavior," 2011. [Online]. Available: https://www.researchgate.net/publication/225022210

[34]   "634181".

[35]   E. Audasso, F. R. Bianchi, and B. Bosio, "2D simulation for CH4internal reforming-SOFCs: An approach to study performance degradation and optimization," *Energies*, vol. 13, no. 15, Aug. 2020, DOI: 10.3390/en13164116.

[36]   S. Authayanun, T. Pornjarungsak, T. Prukpraipadung, D. Saebea, A. Arpornwichanop, and Y. Patcharavorachot, "SOFC running on steam reforming of biogas: External and internal reforming," *Chemical Engineering Transactions*, vol. 52, pp. 361–366, 2016, DOI: 10.3303/CET1652061.

[37]   K. Girona, J. Laurencin, J. Fouletier, and F. Lefebvre-Joud, "Carbon deposition in CH4/CO2 operated SOFC: Simulation and experimentation studies," *Journal of Power Sources*, vol. 210, Jul. 2012, doi: 10.1016/j.jpowsour.2011.12.005.

[38]   C. J. Laycock, J. Z. Staniforth, and R. M. Ormerod, "Biogas as a fuel for solid oxide fuel cells and synthesis gas production: effects of ceria-doping and hydrogen sulfide on the performance of nickel-based anode materials," *Dalton Transactions*, vol. 40, no. 20, 2011, DOI: 10.1039/c0dt01373k.

[39]   S. J. A. Livermore, J. W. Cotton, and R. M. Ormerod, "Fuel reforming and electrical performance studies in intermediate temperature ceria–gadolinia-based SOFCs," *Journal of Power Sources*, vol. 86, no. 1–2, pp. 411–416, Mar. 2000, DOI: 10.1016/S0378-7753(99)00493-0.

[40]   E. Dogdibegovic, Y. Fukuyama, and M. C. Tucker, "Ethanol internal reforming in solid oxide fuel cells: A path toward high-performance metal-supported cells for vehicular applications."

[41]   A. M. Gaddalla and M. E. Sommer, "Carbon dioxide reforming of methane on nickel catalysts," *Chemical Engineering Science*, vol. 44, no. 12, pp. 2825–2829, Jan. 1989, DOI: 10.1016/0009-2509(89)85092-4.

[42]   S. K. Park, T. S. Kim, J. L. Sohn, and Y. D. Lee, "An integrated power generation system combining solid oxide fuel cell and oxy-fuel combustion for high performance and CO2 capture," *Applied Energy*, vol. 88, no. 4, pp. 1187–1196, 2011, DOI: 10.1016/j.apenergy.2010.10.037.

[43]   T. Kuramochi, H. Wu, A. Ramírez, A. Faaij, and W. Turkenburg, "Techno-economic prospects for CO2 capture from a Solid Oxide Fuel Cell-Combined Heat and Power plant. Preliminary results," in *Energy Procedia*, Feb. 2009, vol. 1, no. 1, pp. 3843–3850. DOI: 10.1016/j.egypro.2009.02.186.

[44]   V. Spallina, P. Nocerino, M. C. Romano, M. van Sint Annaland, S. Campanari, and F. Gallucci, "Integration of solid oxide fuel cell (SOFC) and chemical looping combustion (CLC) for ultra-high efficiency power generation and CO2 production," *International Journal of Greenhouse Gas Control*, vol. 71, pp. 9–19, Apr. 2018, DOI: 10.1016/j.ijggc.2018.02.005.

[45]   D. J. Tashevski and D. M. Dimitrovski, "Optimization of binary co-generative thermal power plants with SOFC on solid fuel," in *Chemical Engineering Transactions*, 2013, vol. 34, pp. 31–36. DOI: 10.3303/CET1334006.

[46]   X. Zhang, Z. Chen, Z. Chen, and J. Li, "Exergy Analysis of a Novel Chemical Looping Hydrogen Generation System Integrated with SOFC," *Journal of Thermal Science*, vol. 30, no. 1, pp. 313–323, Jan. 2021, DOI: 10.1007/s11630-020-1404-1.

[47]   A. Musa, A. Agina, and M. Talbi, "Operating conditions on the performances of soft fuelled with methane," *Renewable Energy and Power Quality Journal*, vol. 1, no. 10, pp. 1608–1613, Apr. 2012, DOI: 10.24084/repqj10.776.

[48]   M. Welte, K. Warren, J. R. Scheffe, and A. Steinfeld, "Combined Ceria Reduction and Methane Reforming in a Solar-Driven Particle-Transport Reactor," *Industrial and Engineering Chemistry Research*, vol. 56, no. 37, pp. 10300–10308, Sep. 2017, DOI: 10.1021/acs.iecr.7b02738.

[49]   P. T. Krenzke and J. H. Davidson, "Thermodynamic analysis of syngas production via the solar thermochemical cerium oxide redox cycle with methane-driven reduction," *Energy and Fuels*, vol. 28, no. 6, pp. 4088–4095, Jun. 2014, DOI: 10.1021/ef500610n.

[50]   W. C. Chueh and S. M. Haile, "A thermochemical study of ceria: Exploiting an old material for new modes of energy conversion and CO2 mitigation," *Philosophical Transactions of the Royal Society A: Mathematical, Physical and Engineering Sciences*, vol. 368, no. 1923, pp. 3269–3294, Jul. 2010, DOI: 10.1098/rsta.2010.0114.

[51]   M. Welte, K. Warren, J. R. Scheffe, and A. Steinfeld, "Combined Ceria Reduction and Methane Reforming in a Solar-Driven Particle-Transport Reactor," *Industrial and Engineering Chemistry Research*, vol. 56, no. 37, pp. 10300–10308, Sep. 2017, DOI: 10.1021/acs.iecr.7b02738.

[52]   S. Abanades and G. Flamant, "Thermochemical hydrogen production from a two-step solar-driven water-splitting cycle based on cerium oxides," *Solar Energy*, vol. 80, no. 12, pp. 1611–1623, Dec. 2006, DOI: 10.1016/j.solener.2005.12.005.

[53]   K. J. Warren and J. R. Scheffe, "Kinetic insights into the reduction of ceria facilitated via the partial oxidation of methane," *Materials Today Energy*, vol. 9, pp. 39–48, Sep. 2018, DOI: 10.1016/j.mtener.2018.05.001.

[54]   S. Abanades and G. Flamant, "Thermochemical hydrogen production from a two-step solar-driven water-splitting cycle based on cerium oxides," *Solar Energy*, vol. 80, no. 12, Dec. 2006, DOI: 10.1016/j.solener.2005.12.005.

[55]   K. J. Warren *et al.*, "Theoretical and Experimental Investigation of Solar Methane Reforming through the Nonstoichiometric Ceria Redox Cycle," *Energy Technology*, vol. 5, no. 11, pp. 2138–2149, Nov. 2017, DOI: 10.1002/ente.201700083.

[56]   X. Zhang, Z. Chen, Z. Chen, and J. Li, "Exergy Analysis of a Novel Chemical Looping Hydrogen Generation System Integrated with SOFC," *Journal of Thermal Science*, vol. 30, no. 1, pp. 313–323, Jan. 2021, DOI: 10.1007/s11630-020-1404-1.

[57]   M. Ebrahimi and I. Moradpoor, "Combined solid oxide fuel cell, micro-gas turbine and organic Rankine cycle for power generation (SOFC–MGT–ORC)," *Energy Conversion and Management*, vol. 116, May 2016, DOI: 10.1016/j.enconman.2016.02.080.

[58]   J. Jia, Q. Li, M. Luo, L. Wei, and A. Abudula, "Effects of gas recycling on the performance of solid oxide fuel cell power systems," *Energy*, vol. 36, no. 2, pp. 1068–1075, Feb. 2011, DOI: 10.1016/J.ENERGY.2010.12.001.

[59]   K. Nakamura *et al.*, "Development of a Highly Efficient SOFC Module Using Two-stage Stacks and a Fuel Regeneration Process," *Fuel Cells*, vol. 17, no. 4, pp. 535–540, Aug. 2017, DOI: 10.1002/fuce.201600192.

[60]   W. Zhang, E. Croiset, P. L. Douglas, M. W. Fowler, and E. Entchev, "Simulation of a tubular solid oxide fuel cell stack using AspenPlusTM unit operation models," *Energy Conversion and Management*, vol. 46, no. 2, pp. 181–196, Jan. 2005, DOI: 10.1016/J.ENCONMAN.2004.03.002.

[61]   S. E. Veyo, "The Westinghouse solid oxide fuel cell program-a status report." doi: 10.1109/IECEC.1996.553868.

[62]   J. Hong, G. Chaudhry, J. G. Brisson, R. Field, M. Gazzino, and A. F. Ghoniem, "ANALYSIS OF OXY-FUEL COMBUSTION POWER CYCLE UTILIZING A PRESSURIZED COAL COMBUSTOR."

[63]   "SI Appendix General information and Assumption."

[64]   "CARBON DIOXIDE CAPTURE AND STORAGE."

[65]   M. Goel, "Carbon Capture and Storage Technology for Sustainable Energy," in *Paths to Sustainable Energy*, InTech, 2010. DOI: 10.5772/16172.

[66]   S. F. Cannone, A. Lanzini, and M. Santarelli, "A review on co2 capture technologies with focus on co2-enhanced methane recovery from hydrates," *Energies*, vol. 14, no. 2. MDPI AG, Jan. 02, 2021. DOI: 10.3390/en14020387.